Integration of GaN Thin Films with Dissimilar Substrate Materials by Wafer Bonding and Laser Lift-off

by

William Sam Wong

B.S. (University of California, Los Angeles) 1990

M.S. (University of California, San Diego) 1995

A dissertation in partial satisfaction of the

requirements for the degree of

Doctor of Philosophy

in

Engineering - Materials Science and Mineral Engineering

in the

GRADUATE DIVISION

of the

UNIVERSITY OF CALIFORNIA, BERKELEY

Committee in charge:

Professor Timothy D. Sands, Chair
Professor Nathan W. Cheung
Professor Eicke R. Weber

Fall 1999

The dissertation of William Sam Wong is approved:

12/8/99

Chair Date

12/9/99

Date

12/10/99

Date

University of California, Berkeley

Fall 1999

Integration of GaN Thin Films with Dissimilar Substrate Materials by Wafer Bonding and Laser Lift-off

Copyright 1999

by

William Sam Wong

Abstract

Integration of GaN Thin Films with Dissimilar Substrate Materials by Wafer Bonding and Laser Lift-off

by

William Sam Wong

Doctor of Philosophy in Materials Science and Mineral Engineering

University of California, Berkeley

Professor Timothy D. Sands, Chair

Enhancing integrated microsystem functionality requires the joining of dissimilar materials in which the integration process may be accomplished through a variety of techniques. These techniques include bonding of discrete elements, wafer bonding, lift-off and transfer, and direct thin-film deposition. In this dissertation, the development of a new integration tool, laser lift-off (LLO) will be presented. By combining the LLO process with wafer bonding techniques, the integration of GaN thin films onto dissimilar substrate materials was demonstrated.

Successful separation of GaN from GaN/sapphire structures was accomplished using a single 38 ns KrF excimer (248 nm) laser pulse directed through the transparent sapphire substrate. For fluences between 400-600 mJ/cm^2, the absorption at the GaN/sapphire interface induces a highly localized, rapid thermal decomposition of the GaN, yielding metallic Ga and N_2 gas. Heating the interface above the melting point of Ga (30°C) allows the separation of the GaN from the sapphire. Characterization of the GaN films after LLO by scanning electron microscopy, atomic force microscopy, x-ray

diffraction and photoluminescence showed that the separation process does not degrade the structural and optical qualities of the GaN films.

Thermal calculations were made using analytical solutions to the heat transfer equation, and confirmed with finite element analysis, to predict the laser fluence needed for LLO. These calculations showed the GaN decomposition temperature (~1000°C) was exceeded in a 100 nm thick GaN interfacial layer at an incident fluence of 600 mJ/cm^2, the experimentally observed lift-off fluence threshold. Thermoelastic stress analysis was also performed to predict a process window to minimize the possibility of GaN structural degradation during the LLO process.

By incorporating a low-temperature Pd-In bonding process with LLO, GaN thin films were successfully transferred from sapphire onto Si, GaAs, and polyimide substrates. The intermetallic compound $PdIn_3$ (T_m=664°C), formed from a Pd-In bilayer after a 200°C anneal, was used as the bonding interface. The integration process was completed after removing the sapphire substrate by LLO. By utilizing these process integration tools, the fabrication of a vertical InGaN blue light-emitting diode, pre-fabricated on sapphire and subsequently transferred onto Si, was demonstrated.

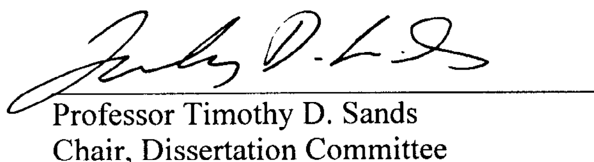

Professor Timothy D. Sands
Chair, Dissertation Committee

Table of Contents

Chapter 1 - Introduction *1*

Chapter 2 - Background *6*

2.1 - Large-area Crystal Growth **6**

2.2 - GaN Thin-film Growth **10**

2.2.1 - Buffer Layers 11

2.2.2 - Dissimilar Substrate Materials 12

2.3 - Doping Issues **13**

2.4 - GaN Decomposition **15**

Chapter 3 - Experimental *25*

3.1 - KrF Pulsed Excimer Laser Beam Profile **25**

3.2 - The Wafer-bonding Tool **27**

Chapter 4 - Wafer-bonding and Laser Lift-off *35*

4.1 - Integration by Direct Deposition: GaAs on Si **36**

4.2 - Integration by Lift-off and Transfer **37**

4.3 - GaN Thin-film Lift-off Processes **38**

4.4 - The Laser Lift-off Process **40**

Chapter 5 - Thermal Analysis of Laser-Target Interactions *49*

5.1 - Laser-target Interaction **50**

5.2 - Finite Element Analysis **55**

Chapter 6 - Thermoelastic Stress Analysis *66*

6.1 - Thermoelastic Stress: Analytical Solution **67**

6.2 - Thermoelastic Stress: Finite Element Analysis **70**

6.3 - Design Constraints for Laser Lift-off **71**

Chapter 7 - Fabrication of Thin-film GaN Membranes *81*

7.1 - Free-standing Thin-film GaN Membrane Fabrication **81**

7.2 - Free-standing Thin-film InGaN LED Membrane Fabrication **82**

7.3 - GaN Membrane Results **83**

7.4 - InGaN LED Membrane Results **84**

Chapter 8 - Low-temperature Pd-In Metal Bonding and LLO *94*

8.1 - Pd-In Bonding Process **95**

8.2 - Pd-In Bonding and Laser Lift-off **96**

8.3 - Post-processing of LLO GaN **99**

8.3.1 - Results and Discussion 99

8.4 - Fabrication of Vertical-structure Light-emitting Diodes...102
Chapter 9 - Conclusion...115
Chapter 10 - Appendix...118
10.1 - Thermoelastic Stress Wave Propagation..118
References 123

List of Figures

Figure 2–1: *Free energy of formation for GaN at 1 atmosphere.* 20
Figure 2–2: *Clinographic projection of the GaN structure.* 21
Figure 2–3: *Operating temperature and pressures for various GaN growth processes. (Ref. 9)* 22
Figure 2–4: *GaN decomposition rate as a function of temperature. (Ref. 9)* 23
Figure 2–5: *Pressure-temperature curve for GaN. Shaded region is area where GaN decomposes at 1250 K.* 24
Figure 3-1: *Schematic of the KrF pulsed excimer laser system.* 29
Figure 3-2: *Knife-edge measurement process to characterize laser beam profile for vertical profile (top) and horizontal profile (bottom).* 30
Figure 3-3: *Vertical energy profile of the KrF excimer laser used for LLO.* 31
Figure 3-4: *Horizontal laser beam profile of the KrF excimer laser used for LLO.* 32
Figure 3-5: *Energy intensity contour of the KrF pulsed excimer laser.* 33
Figure 3-6: *Wafer-bonding Tool* 34
Figure 4–1: *Epitaxial lift-off process.* 43
Figure 4–2: *Laser lift-off process.* 44
Figure 4–3: *Cross-sectional SEM micrograph showing a separated GaN film bonded to a Si substrate. The bonding material is epoxy. A 600 mJ/cm^2 laser fluence directed through the original sapphire substrate was used to separate the GaN from the sapphire.* 45
Figure 4–4: *A θ - 2θ coupled XRD spectra of GaN bonded to Si after lift-off from the sapphire substrate. The separation process was done at a laser fluence of 600 mJ/cm^2.* 46
Figure 4–5: *A ϕ-circle scan of the $10\bar{1}2$ GaN reflection shows that the GaN retains six-fold symmetry on the cubic Si substrate.* 47
Figure 4–6: *Comparison of GaN film quality by XRC of the 0002 GaN reflection for: (a) GaN on sapphire, and (b) after transfer from sapphire to a Si substrate. The FWHM of the 0002 GaN reflection remains unchanged after lift-off indicating that the film was separated and transferred without appreciable thermal or mechanical damage. A laser fluence of 600 mJ/cm^2 was used.* 48
Figure 5–1: *A simulated temperature profile for a single 38 ns, 400 mJ/cm^2 pulse from a KrF laser. The temperature rise, coupled with a large temperature gradient across the thickness of the GaN film, occurs in a highly localized heated area that is within 100 nm below the irradiated GaN/sapphire interface (referenced at 0 μm depth).* 58
Figure 5–2: *GaN surface morphology as a function of laser fluence.* 59
Figure 5–3: *Heat capacity for GaN as a function of temperature. (Ref. 103)* 60
Figure 5–4: *Coefficient of thermal expansion for GaN as a function of temperature. (Ref. 104)* 61
Figure 5–5: *Thermal conductivity for GaN as a function of temperature. (Ref. 104)* 62
Figure 5–6: *Temperature distribution of GaN thin film irradiated on the GaN surface for a fluence of 400 mJ/cm^2. The calculations were done using temperature-independent GaN properties.* 63

Figure 5–7: *Temperature distribution of GaN thin film irradiated on the GaN surface for a fluence of 400 mJ/cm^2. The calculations were done using temperature-dependent GaN properties.* *64*
Figure 5–8: *Temperature distribution of GaN thin film irradiated at the GaN/sapphire interface for a fluence of 600 mJ/cm^2. The calculations were done using temperature-dependent GaN properties.* *65*
Figure 6–1: *Thermoelastic stress development of KrF pulsed excimer surface irradiated GaN.* *75*
Figure 6–2: *Thermoelastic stress development of KrF pulsed excimer surface irradiated GaN.* *76*
Figure 6–3: *Schematic the buckling phenomena for a GaN thin film.* *77*
Figure 6–4: *Buckled GaN film showing a defect where fracture can occur.* *78*
Figure 6–5: *Substrate support thickness for increasing laser irradiated spot size. The predicted safe region for a GaN or Si support is given.* *79*
Figure 6–6: *SEM surface morphology of backside irradiated GaN/sapphire. The surface pattern are generated from the backside mask on the sapphire.* *80*
Figure 7–1: *Process flow for fabrication of InGaN LED membranes: 1) Starting material - pre-fabricated InGaN MQW LED/sapphire and Si supporting substrate, 2) Bond InGaN MQW LED/sapphire onto Si supporting substrate, 3) KrF laser irradiation of the sapphire/InGaN MQW LED/adhesive/sapphire structure through the transparent sapphire substrate, 4) Heat post-laser processed structure above melting point of Ga to release sapphire substrate, and 5) Immerse InGaN MQW LED/adhesive/Si structure in solvent to release LED membrane. The inset shows the pre-fabricated InGaN MQW well structure processed on the sapphire substrate.* *86*
Figure 7–2: *AFM scan of a 20 μm × 20 μm area of the former GaN interface. The scan shows a relatively smooth surface morphology with a measured surface roughness of approximately 24 nm (rms).* *87*
Figure 7–3: *SEM micrograph of a 3 μm thick free-standing GaN membrane.* *88*
Figure 7–4: *Low-temperature (4 K) PL spectra for GaN/sapphire and GaN membranes. The measured FWHM of the DX peaks after separation did not show appreciable broadening, indicating no detectable optical degradation of the GaN films. The measured red-shift of ~10 meV for the GaN membrane corresponds to a biaxial compressive stress relief of approximately 0.4 GPa after separation of the GaN from sapphire.* *89*
Figure 7–5: *Low-temperature (4 K) PL spectra for GaN/sapphire and GaN membranes* *90*
Figure 7–6: *DC current-voltage characteristics for a 20 μm × 500 μm InGaN multiple quantum well (MQW) LED membrane and LED on sapphire. The threshold voltage showed no change before and after LLO from the sapphire growth substrate.* *91*
Figure 7–7: *Pulsed (1% duty cycle) light output vs. current characteristic for a series of three InGaN LED membranes before and after sapphire substrate removal. The light output of the LED membranes was 4 mW at a 100 mA forward current, corresponding to an external quantum efficiency of ~1.3%. The slight attenuation of the power output for the LED membrane compared to the LED on sapphire is due in*

part to the light being measured through a quartz supporting substrate for the LED membrane...92
Figure 7–8: *Room-temperature emission spectra for the InGaN MQW LED before and after sapphire substrate separation measured at 10 mA dc forward current. The measured peak emission at 389 nm with a FWHM of 10 nm showed no measurable degradation in the emission spectra for the InGaN LED membrane compared to the LED on sapphire. 93*
Figure 8–1: *Pd-In phase diagram showing the $PdIn_3$ melting point at 664°C.............103*
Figure 8–2: *Pd-In wafer bonding process and LLO process for transferring GaN thin films. 104*
Figure 8–3: *X-ray diffraction pattern of Pd-In bi-layers deposited on a SiO_2 coated Si wafer. The as-deposited Pd-In layers show the dominant 002 In and 111 Pd peaks. After a 30-minute anneal at 200°C in a N_2 ambient the 411 and 321 $PdIn_3$ peaks have become dominant. The absence of the 111 Pd peak indicates consumption of the Pd layer to form $PdIn_3$ after 60 minutes. 105*
Figure 8–4: *Cross sectional SEM micrograph of a transferred GaN film onto a Si substrate. Pd-In metal bilayers were used as bonding material which formed the compound $PdIn_3$ after the low-temperature bonding process. Cleaving the Si substrate was performed to make the cleavage facets on the GaN...............................106*
Figure 8–5: *Theta-two-theta normal coupled scans of transferred GaN thin films onto GaAs, Si and polyimide substrates. The $PdIn_3$ 411 reflection from the metallic bond is shown along with the 0002 GaN reflection..107*
Figure 8–6: *X-ray rocking curve of GaN transferred onto polyimide. The full-width at half maximum of the 0002 GaN reflection broadened slightly from 0.18° to 0.20° indicating the structural quality of the transferred film did not degrade significantly after bonding and LLO. 108*
Figure 8–7: *SEM micrograph of pattern transferred GaN onto a Si substrate............109*
Figure 8–8: *Low-temperature (4K) PL of GaN on sapphire and GaN transferred onto Si. The broadening of the GaN/Si DX peak FWHM compared to the as-grown GaN/sapphire is due to the localized defects at the exposed GaN/sapphire interface. ..110*
Figure 8–9: *C-RBS results for the as-grown GaN on sapphire and after removal of 1.5 μm of GaN by ion milling with a 1 kV Ar ion beam. The spectrum shows the GaN to be of high quality with a minimum yield of approximately 3% at the surface of the film. The defective interfacial region thickness was measured to be approximately 350 nm. 111*
Figure 8–10: *Backscattering yield as a function of depth for as-separated GaN on Si and after ion-beam processing. The c-RBS results show that after removal of 400 nm of GaN by ion milling, the backscattering yield returned to the initial χ-minimum values of the original GaN/sapphire surface..112*
Figure 8–11: *Low-temperature PL of the GaN thin film after ion milling. The DX peak FWHM was comparable to that from the original GaN surface after removing 400 nm of the former interface. A slight red-shift is due to release of the compressive stress after removing the sapphire substrate. The relative DX peak intensities have been normalized to better show the change in the FWHM and red shift. The relative peak intensities of the original surface and ion milled interface were within 5% of each other. 113*

Figure 8–12: *Vertical-structure InGaN blue-LED...114*
Figure 10–1: *Schematic of an incident wave incident onto an interface between materials a and b..122*

List of Tables

Table 2–1: *Thermodynamic data for GaN (from Ref. 20)*..*17*
Table 2–2: *Melting points and decomposition temperatures of the III-V nitrides.* *18*
Table 2–3: *Materials properties of the III-V nitrides and selected substrates. (Ref. 66)*..*19*

Acknowledgements

For their guidance and support, I am indebted to my advisors, Professors Tim Sands and Nathan Cheung. Their insights and inspirations created a very productive and successful research environment throughout my graduate career at Berkeley. I would also like to thank Professor Eicke Weber for his invaluable input towards my research and for serving on my dissertation committee.

For their expertise in characterization, I wish to thank Kin Man Yu for providing the channeling RBS data and Joachim Krüger for helping in the photoluminescence measurements. I wish to also acknowledge the UC Berkeley Integrated Materials Laboratory where many of the experiments were performed. Additionally, acknowledgements are given to the Blue Laser Group at the Xerox Palo Alto Research Center for providing the InGaN LED devices presented in Chapters 7 and 8.

I also wish to acknowledge my co-workers and friends for making my stay at Berkeley enjoyable. Thanks goes to former Plasmalab members: Bill En, Erin Jones, Sundar Kumar Iyer, James Chan, and Barry Linder who helped me assimilate as a graduate student at Cal when I first joined the group. Thanks also to Loucas Tsakalakos, Alberto Salleo, and Nate Quitoriano of the Sands group for their contributions to the wafer bonding and laser process. I also want to thank Changhan Yun, Yonah Cho, Adam Wengrow, and Larry Schloss for their invaluable assistance and support during the last three years.

Finally, I wish to thank my parents and my sister, Joann Marion Wong, for their support throughout my life. Although they never really understood what I did in graduate school, their support and encouragement was always a source of motivation for me.

Chapter 1 - Introduction

The III-V nitrides have recently been the focus of intense research activity spurred by the rapid development of gallium nitride (GaN)-based optoelectronic applications. The direct wide-bandgap GaN compound, E_g=3.4 eV, when alloyed with In or Al offers a range of optical emission from the red to the ultraviolet (UV). Thus, the binary (GaN, AlN, and InN), ternary (AlGaN, InGaN, and InAlN) and quaternary (InAlGaN) systems have promising applications in the optoelectronic industry, in particular blue/UV light-emitting diodes (LEDs) and laser diodes (LDs). In addition, GaN is a very favorable materials system for high-temperature and high-power electronic devices given its large direct bandgap. Although progress in the high-power electronics arena lags that of the optoelectronics, GaN-based heterojunction bipolor transistor and field-effect transistor technologies are also developing at a rapid pace.[1]

Competing against the III-V nitrides are the silicon carbide (SiC) system and the II-VI compounds. The II-VI materials, in particular ZnSe, suffer from reliability and efficiency problems compared to the III-V nitride system.[2] Although the ZnSe-based LEDs and LDs showed early promise for blue/UV emission, they languished from short lifetimes caused by inherent crystal defects and low brightness, which hampered their commercialization.[3] SiC, on the other hand, has shown promise as a material for high brightness LED and LD applications.[4,5] Although SiC-based LEDs have been available for quite some time, the indirect bandgap of this material has restricted its optoelectronic performance. In addition, the high cost of SiC substrates makes the SiC-based devices cost prohibitive for large-scale commercialization. Due, in part to the lack of a more

competitive and low-cost alternative for blue light emission, the SiC and ZnSe systems had been in the forefront for blue/UV optoelectronic applications.

The swift development of the GaN-based optoelectronic industry has caused an expeditious change in the materials used for blue-light emission. The GaN system has matured rapidly in the last ten years, becoming the material of choice for blue LEDs and LDs.[6,7] GaN based high-brightness blue LEDs, and more recently, blue LDs have become commercially available. Despite the advancements in the GaN field, the primary impediment to this compound is its thermal decomposition at relatively low temperatures to produce metallic Ga and N_2 gas.[8,9] As a result, large area GaN substrates are still difficult to fabricate, necessitating heteroepitaxial growth of GaN thin films onto dissimilar substrates such as sapphire or SiC.[10,11] The GaN crystal structure, combined with the high GaN growth temperatures make deposition of high-quality material directly onto common semiconductor substrates such as Si or GaAs very difficult.

The most commonly used growth substrate, sapphire, still imposes constraints on the GaN film quality due to the lattice and thermal-expansion coefficient mismatch between the sapphire and GaN.[12] The disparate properties of these two materials result in a high density of extended defects, such as dislocations and stacking faults, at the GaN thin film/substrate interface.[12,13]

Due to the low thermal and electrical conductivity constraints imposed by the sapphire substrates, many groups have attempted to integrate GaN with other more conductive materials. A more electrically conductive substrate would allow backside ohmic contacts to GaN-based devices unattainable with a sapphire substrate. For devices processed on sapphire, all contacts must be made from the topside. This configuration

complicates contact and packaging schemes, resulting in a spreading-resistance penalty and increased operating voltages.[14] The poor thermal conductivity of sapphire, compared to Si or SiC, also prevents efficient dissipation of heat generated by high-current devices, such as LDs and high-power transistors, consequently inhibiting device performance.[15]

The integration of GaN with other substrates could take advantage of the complimentary functionality of different materials systems. Several techniques may be used to perform the integration process including direct deposition, bonding of discrete elements, flip-chip bonding, wafer bonding or lift-off and layer transfer. Of these techniques, a combination of wafer bonding and thin-film lift-off offers the greatest flexibility of joining dissimilar materials. The development of such a process would allow joining the III-nitride optoelectronics with substrates such as Si, glass, or polymers unattainable by direct deposition. Consequently, a monolithic integration process would lower the cost and size per unit for a given microsystem.

In this dissertation, the methodology for the integration of GaN thin films with dissimilar substrate materials is presented. The approach towards this integration employs a wafer bonding and thin-film lift-off technique. The bonding and lift-off process involves adhesion of a heterostructure still on its growth substrate to a final micromachined, patterned, and metallized substrate. To allow maximum flexibility for a wide range of materials combinations, the following requirements were prescribed in order to best demonstrate the integration methodology:

1) A bonding layer that has low resistance to shear stress at temperatures below 200°C such that sub-micron surface asperities and particulates do not prevent full surface contact.

2) A bonding layer that is both adherent to the heterostructure and the final "receptor" substrate.

3) A bonding process that is performed at low-temperature (≤ 200°C) that does not leave behind a component or phase with a melting point below 200°C.

4) A resulting bond that has low electrical resistance.

5) A bonding layer that is thinner than the heterostructure to be transferred, such that its properties do not dominate those of the transferred thin film.

6) A lift-off process which does not adversely effect the properties of the transferred film.

The following sections will discuss and demonstrate a newly developed integration process that employs a KrF pulsed excimer laser (248 nm) to separate GaN thin films from their growth sapphire substrates. The laser light, when directed through the transparent sapphire, decomposes a thin layer of the GaN at the interface allowing the film to separate.[16,17] Using this laser lift-off (LLO) process, in conjunction with a low-temperature transient liquid-phase metal bonding process, will allow the above criteria to be met.

An overview of the GaN thin-film/substrate issues will first be presented along with considerations to the direct heteroepitaxial growth of GaN on different substrate materials. Next, a methodology for removing the sapphire substrate constraint will then be discussed followed by experimental results. A discussion of the laser target interaction with analytical and numerical calculations will be used to understand the experimental results obtained. The integration of GaN thin films with dissimilar substrate materials is then demonstrated and discussed using a low-temperature Pd-In metal bonding process to

integrate GaN with Si, GaAs and polymer substrates. Furthermore, the efficacy of the LLO process on functional GaN-based optoelectronic devices will be shown.

Chapter 2 - Background

The drive for a stable and reproducible blue-ultraviolet light source has been the catalyst for incredible advancements in the growth and processing of the III-V nitrides. During the early development of this system, high-quality GaN thin films had been difficult to obtain due, in part, to the lack of a lattice-matched substrate. In addition, the study of bulk high-quality free-standing GaN single crystals has been slowed due to the extremely high processing temperatures and pressures involved in fabricating such crystals. With the increased study of the nitrides, researchers have been able to develop growth processes to produce high-quality GaN thin films for device applications. The fabrication of large-area bulk crystals has also been refined over the past two years motivated by the need to obtain a GaN substrate.

2.1 - Large-area Crystal Growth

The requirements for producing GaN thin films or bulk crystals include high growth temperatures, activated nitrogen species or high nitrogen background pressures necessary to overcome the large kinetic barriers of solid phase formation.[9] The high melting temperature of GaN (T_m ~ 2800 K) and decomposition pressure at melting (~ 40 kbar)[18] prevents the growth of bulk crystals from stoichiometric melts by conventional processes such as Czochralski or Bridgman methods. Recent advances and novel techniques have been developed to grow relatively large single crystal GaN at temperatures below the GaN melting point.[19]

The stability of the GaN compound may be illustrated by considering the temperature dependence of the Gibbs free energy. From the data obtained from the free

energy of the reactants and products, the stability of the GaN system may be inferred from the derived phase diagrams. First, consider a binary reaction of a metal, *M* with nitrogen gas, N_2. Such a reaction can be written as:

$$M(l) + \tfrac{1}{2} N_2(g) = MN(s) \qquad [2.1–1]$$

The following free energy difference as a function of temperature and pressure can then be given as:

$$\Delta G^{P,T} = G^{P,T}_{MN(s)} - G^{P,T}_{M(l)} - \tfrac{1}{2} G^{P,T}_{N_2(g)} \qquad [2.1–2]$$

For a given temperature there exists a specific nitrogen pressure, P_{N_2}, which when the ambient nitrogen is higher than this pressure will result in a spontaneous formation of *MN*(*s*). Likewise, an ambient pressure lower than P_{N_2} will result in a spontaneous decomposition of *MN*(*s*) into *M*(*l*) and $N_2(g)$. Similarly, for a given pressure there exists a specific equilibrium temperature below which MN(s) will spontaneously form and above which *MN*(*s*) will decompose into *M*(*l*) and $N_2(g)$.

At equilibrium, under constant pressure and temperature conditions, the Gibbs free energy change is zero. By using this criterion, the determination of the stable thermodynamic phases for GaN can be found. From these results, the associated phase diagrams can then be calculated and used to illustrate the stable products as a function of the independent variables, temperature and pressure.

The temperature dependence of the state variables such as enthalpy (*H*), thermal entropy (S_{th}) and free energy (*G*) are all determined from the heat capacity, C_p. The heat capacity is usually described over a specified range of temperatures by a power-law expression:

$$C_p = a + bT + cT^{-2} + dT^2 \qquad [2.1–3]$$

From the heat capacity, the temperature dependence of the state variables are then given as:

$$H_0^T = H^+ + aT + \frac{bT^2}{2} - cT^{-1} + \frac{d}{3}T^3 \qquad [2.1–4]$$

$$S_0^T = S^+ + a\,lnT + bT - \frac{c}{T^2} + \frac{d}{2}T^2 \qquad [2.1–5]$$

$$G_0^T = H_0^T - TS_0^T = \left(a - S^+\right)T - aT\,lnT - \frac{bT^2}{2} - \frac{c}{2T} - \frac{d}{6}T^3 + H^+ \qquad [2.1–6]$$

where H^+, S^+, a, b, c, and d are given in Table 2–1.

The free energy of reaction may now be evaluated for the binary reaction. An equilibrium constant $K (= e^{-\Delta G_{T,P}/RT})$ can be used to obtain the thermodynamic properties. It is often useful to express the equilibrium constant as a function of the activities to generalize the formulas as much as possible. In using this approach, the phases that do not have properties of the ideal gases, pure solids or ideal solutions may be more easily evaluated. For equation 2.1–1 the free energy change can be written as:

$$\Delta G^{T,P} = G_{MN(s)}^{T,P} - G_{M(l)}^{T,P} - \frac{1}{2}G_{N_2(g)}^{T,P} = -RT\,ln\,K \qquad [2.1–7]$$

where, $K = \dfrac{a_{MN(s)}}{a_{M(l)}a_{N_2(g)}^{1/2}}$.

The activity of pure liquids and pure solids is unity in the standard state. For ideal gases, the activity is P/P_0 where P_0 is the reference pressure. Neglecting the changes due to

pressure in the free energy of solids and liquids, the free energy change at arbitrary temperature and pressure becomes:

$$\Delta G^{T,P} = G^{T}_{MN(s)} - G^{T}_{M(l)} - \tfrac{1}{2}\left(G^{T}_{N_2(g)} + RT\,ln\,P_{N_2(g)}\right) \qquad [2.1\text{–}8]$$

where P is in bars. Using equation 2.1–8, the free energy change and equilibrium pressure can be plotted. Table 2–1 gives the thermodynamic properties of the relevant phases for GaN from several sources[20] and Figure 2–1 is a plot calculated using these values.

Given the thermodynamic constraints for GaN synthesis, it is easy to understand the difficulty in growing large-volume single crystals. Figure 2–1 shows the free energy change in an activated nitrogen ambient for the GaN solid phase compared to a molecular nitrogen ambient. In order to extend the stability range of GaN, high N_2 pressures or activated N species are required for growth due to the relatively inert N_2 molecule. Early attempts at growing bulk GaN single crystals have met with limited success and crystal size (typically in the order of a few millimeters). Johnson *et al.*[21] first grew small GaN crystals by flowing undiluted ammonia over gallium. Zetterstrom[22] later was able to increase the crystal size to 1-2 mm platelets by heating pre-synthesized GaN in an ammonia ambient at temperatures between 1150-1180°C and Karpinski *et al.*[23] have fabricated bulk GaN single crystals using high nitrogen ambient pressures. The latter have reported a nitrogen pressure of 20 kbar at a temperature of 1600°C as the best conditions for GaN crystallization from a melt. Given the unusually high temperatures and pressures for bulk GaN crystal growth, many groups have pursued the heteroepitaxial thin film approach to obtain high-quality GaN single crystals.

2.2 - GaN Thin-film Growth

The literature contains an exhaustive list of different substrate materials that have been examined for GaN growth. Substrates such as sapphire,[24] GaAs,[25] Si, [26,27] MgO,[28] SiC,[29] and ZnO[30] have all been tried with varying degrees of success. Currently the preferred substrate is sapphire due to its compatibility with GaN in crystal orientation and its ability to withstand the high-temperature growth conditions.

The typical GaN crystal structure is wurtzite based on a hexagonal Bravais lattice. Along the c-axis of the lattice the stacking sequence for GaN is …$Ga_AN_AGa_BN_BGa_AN_AGa_BN_BGa_CN_C$… The Ga atom sits at positions (0, 0, 0) and (2/3, 1/3, 1/2) while the N atoms are at (0, 0, u) and at (2/3, 1/2, 1/2 +u) where u ~ 3/8. The hexagonal wurtzite structure is shown in Figure 2–2 for GaN. Table 2–3 gives the lattice parameters and thermal expansion coefficient for GaN, its alloys and various growth substrates.

The most commonly used GaN thin film growth technique is metal-organic chemical vapor deposition (MOCVD). The MOCVD process allows for relatively high growth rates along with superior thin-film uniformity, high yield and throughput and in the case of GaN, high growth temperatures. GaN and its related compounds can crystallize in both the zincblende and wurtzite structure with the latter being more stable. In general, most of the device applications and characterization of GaN crystals have been performed using the wurtzite structure.

Figure 2–6 shows the typical growth conditions for several processes and their relation to thermodynamically stable GaN. From the figure, it is seen that chemical vapor deposition (CVD) is the only process that forms GaN under equilibrium conditions. Other

techniques such as plasma/ion-assisted molecular beam epitaxy (MBE) and electron cyclotron resonance assisted metal-organic CVD grow GaN in the unstable region. It has been reported that the high gas pressures and growth temperatures associated with the MOCVD technique overcome the inherent kinetic barrier of epitaxial growth while still maintaining the thermodynamically stable conditions.[9] The plasma-assisted MBE and CVD process enable GaN formation in a metastable region by supplying a higher flux of activated N species compared to the rate of sublimation of the GaN during growth. Figure 2–7 shows the measured rate of sublimation as a function of temperature.[8] The rate of sublimation of the GaN thin film was attributed to overcoming a kinetic barrier of decomposition.

2.2.1 - Buffer Layers

The heteroepitaxial growth of GaN thin films typically uses various techniques to minimize the generated defects during deposition. These approaches focus primarily on optimizing a buffer layer between the main GaN epilayer and the sapphire substrate. These techniques include a low-temperature GaN buffer layer, AlN or AlGaN buffer layer or lateral epitaxial overgrowth from a seed window opening, typically defined by a SiO_2 mask, over the GaN buffer layer. The approaches have resulted in reducing the density of extended defects in the GaN film from 10^{12} cm^{-2} to 10^{8} cm^{-2}, which is adequate for GaN-based optoelectronic device operation.

AlN buffer layers,[31] and later low-temperature GaN buffer layers[32] of thickness ranging between 50-100 nm, were recognized as a way to relieve the stress and associated defects in GaN thin films grown on large lattice-mismatched substrates. The buffer layer acted as a template to supply nucleation sites for growth of the GaN epilayer.

This buffer relieves some of the large lattice mismatch that is detrimental to achieving high-quality films. The layer also effectively absorbs the stress created by the lattice and thermal expansion coefficient mismatch through the generation of extended defects such as dislocations and stacking faults. The creation of these defects helps eliminate the significant stress build up within the main GaN epilayer.

Recently, the density of threading dislocations have been reduced even further using an epitaxial-lateral-overgrowth (ELOG) process.[33,34] The technique was successful in reducing the threading dislocation density down to the order of 10^7 cm^{-2} by implementing SiO_2 mask windows to selectively limit the propagation of the threading dislocations. Many researchers have followed this process to produce superior diode devices with improved luminescent qualities.[35,36] The process has also been used to make free-standing GaN substrates by either etching away the SiO_2 masks or mechanically polishing the sapphire substrate away.[37]

2.2.2 - Dissimilar Substrate Materials

Despite the rapid improvements in the growth and materials quality of GaN on sapphire, a variety of other substrate materials has also been investigated. In the early 1990's, many researchers explored the growth of GaN on GaAs substrates in order to obtain the metastable zincblende phase of GaN.[25,38,39] Other substrates, which were used in order to achieve the zincblende GaN phase include Si,[40,41] SiC,[42,43] and MgO[44]. With the exception of SiC, the interest in using these substrates has slowly decreased. The primary reason for the decline in interest in the zincblende substrates is the inherent difficulty in growing high quality GaN in the cubic phase. In addition, the high growth temperature involved usually precludes the use of materials with low decomposition

temperatures such as GaAs. Due to the reactivity of nitrogen with Si, amorphous Si_3N_4 layers typically form before the GaN deposition, preventing high-quality GaN films on Si substrates.[45,46]

Currently, the SiC materials system is challenging the GaN/sapphire system for dominance in both the optoelectronic and electronic arena.[4,5,47] SiC offers a higher electrical and thermal conductivity compared to sapphire and is available in the hexagonal crystal structure. Despite these advantages, SiC suffers from being substantially more expensive compared to sapphire. The prohibitive cost of using SiC has limited its usefulness and availability to only a small number of groups.

2.3 - Doping Issues

An additional obstacle to the fabrication of effective optoelectronic and electronic GaN-based devices was the inability to achieve p-type films. GaN thin films are inherently n-type due largely to contamination from oxygen or silicon impurities or nitrogen vacancies.[48] In 1989, Amano *et al.*[49] first reported the successful fabrication of p-type Mg-doped GaN thin films grown on sapphire substrates using an AlN buffer layer. The key for p-type activation in GaN was the use of low-energy electron-beam irradiation (LEEBI) treatment after growth. This technique yielded a dopant concentration of 10^{17} cm^{-3} and a sheet resistivity of 12 Ω-cm.[50] Nakamura and co-workers[51] duplicated the process two years later with GaN grown on a low-temperature GaN buffer layer. The activation of the Mg dopants was accomplished again using the LEEBI process. These films had a dopant concentration of 7×10^{18} cm^{-3} and film resistivity as low as 0.2 Ω-cm. Nakamura *et al.* later duplicated these results using nitrogen-ambient or vacuum-ambient

thermal annealing.[51] An annealing temperature of 700°C was effective in converting as grown Mg-dope GaN films into low-resistivity p-type GaN.

In a study investigating the mechanism for Mg-dopant activation in GaN, Nakamura and co-workers also observed the conversion to p-type GaN material was only accomplished in a hydrogen-free ambient. For this study, samples annealed in a NH_3 ambient consistently showed high electrical resistivity and low hole concentration while samples annealed in a vacuum or nitrogen ambient resulted in highly p-type low resistivity GaN. Interestingly, the p-type material was converted back to highly resistive GaN when the same samples were annealed in NH_3 at 700°C. Similar trends were observed in the photoluminescence of the GaN depending on the annealing gas ambient. Nakamura concluded from these results that the hydrogen dissociated from the ammonia at temperatures above 400°C and diffused into the GaN from the surface passivating the Mg dopants in the film.[52,53] As a result of the H-passivation, p-type GaN could be converted back to highly resistive material while a thermal anneal in a nitrogen ambient removed the hydrogen from the GaN, returning the film to p-type conductivity.

Other doping processes have also been investigated. Ion implantation was first used by Pankove *et al.*[54,55] in the mid-1970's. In their work, they noted that Mg is the shallowest p-type dopant in GaN. It was not until the mid-1990s that Pearton and co-workers first reported electrically active n- and p-dopants in GaN from ion implantation. In their work, Si was used as the n-type dopant and Mg, in conjunction with P, was used to achieve p-type material. Rapid thermal annealing at 1100°C was used to activate the implanted dopants. The same group subsequently reported that O and Ca could also be used as donor and acceptors, respectively, in GaN. Chan *et al.*[56] reported similar results

for Si and Mg implanted GaN which improved optical and electrical properties with increasing annealing temperatures.

2.4 - GaN Decomposition

The bonding energies of the III-V nitrides are relatively high compared to other III-V compounds. The bonding energy for AlN, GaN and InN are 11.52, 8.92, and 7.72 eV/molecule, respectively.[57] These high bond energies result in the higher melting temperatures and good thermal stability of the AlN and GaN compounds compared to other compound semiconductors. Table 2–2 shows the melting point and decomposition pressures for AlN, GaN, and InN. Given the strong triple bond of the N_2 molecule (4.38 eV/atom) the free energy of the GaN constituents (Ga + $\frac{1}{2}N_2$) decreases and approaches the free energy of the solid. Given the free energy of the constituents decreases with temperature faster than the GaN solid, GaN will become unstable at high temperatures.

Groh *et al.*[58] has reported the activation energy for GaN decomposition to be 3.25 eV/atom. They also observed the presence of Ga droplets during decomposition in vacuum suggesting the GaN undergoes an incongruent sublimation. A similar analysis by Munir and Searcy[8] also obtained a similar activation energy of ~3.18 eV/atom but in contrast to the Groh report, there was no observable Ga droplet formation. Later reports suggest the GaN decomposition process is strongly affected by the choice of substrate material and ambient conditions.

In a report by Sun *et al.*[59] the thermal decomposition of MOCVD grown GaN on r-plane sapphire was found to occur at a temperature of 1000°C in a hydrogen ambient. They reported that the surface of the GaN thin film was totally decomposed leaving only a residual Ga droplet surface. Surprisingly, GaN thin films grown on 6H-SiC showed no

indication of thermal decomposition. Similar results for GaN on SiC substrates was also reported by Lin *et al.*[60] The phenomena was attributed to differences in the surface polarities on each separate substrate material.[59] In the case of GaN on sapphire, the Ga^{3+} terminated GaN surface reacts with the hydrogen ambient ($GaN+\frac{3}{2}H_2 \rightarrow Ga+NH_3$) while the N terminated GaN surface of GaN/SiC combines with the ambient H atoms to form N-H. The N-H molecule is energetically more stable than Ga-H resulting in a more stable GaN surface.[61] Surface decomposition of the GaN films was not observed for either sapphire or SiC growth substrates when the films were annealed in a nitrogen ambient.

By using the data from Table 2–1, a pressure-temperature (P-T) curve of the GaN system can be generated. Figure 2–8 shows the calculated P-T curve for GaN. The plot indicates decomposition of the $GaN \rightarrow 2Ga(l)+N_2(g)$ will occur at a critical temperature of ~1000°C at atmospheric pressure. The shaded region shows the predicted decomposition realm of GaN at the critical temperature, which correlates to the experimental data obtained by various groups.[58-60]

Phase	***a (J/K mol)***	***b (J/K mol)***	***c (J/K mol)***	***d (J/K mol)***	***H^+ (J/mol)***	***S^+ (J/mol)***	***T-range***
GaN(s)	38.0740	8.996E-03			-1.214E+05	-189.9080	
GaN(s)	45.3631	6.500E-03	1.910E-01		-1.635E+05	-206.225	
GaN(s)	39.5930	3.565E-03	1.910E-01		-1.635E+05	-206.225	T<700K
GaN(s)	41.7770	1.272E-03	-1.190E-01		-1.649E+05	-219.244	T>700K
Ga(l)	24.3840	2.293E-03	3.100E+05		-7.550E+02	-78.636	T<700K
Ga(l)	26.5680				-2.164E+03	-91.655	T>700K
Ga(g)	24.8660	-1.381E-03	2.510E+05		2.641E+05	29.07900	
N_2(g)	30.4180	2.544E-03	-2.380E+05		-9.982E+03	16.20300	
N(g)	20.8780	1.460E-04	3.800E+04	5.400E-08	4.666E+05	34.59900	

Table 2–1: Thermodynamic data for GaN (from Ref. 20)

Material	**Melting Temperature (K)** *theoretical*	**Nitrogen Decomposition Pressure (kbar)** *extrapolated*	**Nitrogen Decomposition Pressure (kbar)** *experimental*	**Comments**
AlN	3500	0.2	>0.1	Ref. 62 and 63
GaN	2800	45	>40	Ref. 62, 64, and 65
InN	2200	60	>35	Ref. 66

Table 2–2: Melting points and decomposition temperatures of the III-V nitrides.

Material	Lattice Parameter (nm)	Thermal Conductivity (W/cm K)	Thermal Expansion Coefficient ($\times 10^6$/K)	Bandgap (eV)
w-GaN	a=0.3189 c=0.5185	1.3	a=5.59 c=3.17	3.39
w-AlN	a=0.3112 c=0.4982	2.0	a=4.2 c=5.3	6.2
w-In	a=0.3548 c=0.5760	4.9	a=4.2 c=5.3	1.89
6H-SiC	a=0.308 c=1.512	4.9	a=4.2 c=4.68	2.996
Sapphire	a=0.4758 c=1.299	0.5	a=7.5 c=8.5	6.2
ZnO	a=3.252 c=5.213	0.24	a=2.9 c=4.75	3.37
c-GaN	a=0.4521			3.2-3.3
c-AlN	a=0.4380			5.11
c-InN	a=0.4980			2.2
Si	a=0.54301	1.5	a=3.59	1.1
GaAs	a=0.5653	0.5	a=6.0	1.519
β-SiC	a=0.436	4.9	a=4.8	2.2
GaP	a=0.54512	1.1	a=4.65	2.272
MgO	a=0.4126	4.1	a=10.5	
InP	a=0.58693	0.68	a=4.5	1.34

Table 2–3: Materials properties of the III-V nitrides and selected substrates. (Ref. 67)

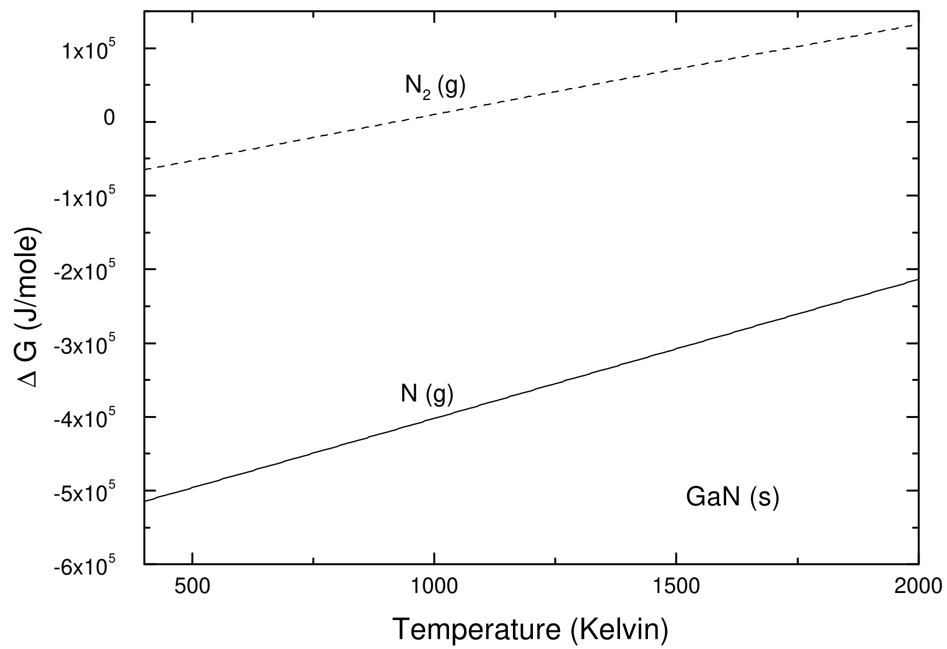

Figure 2–1: Free energy of formation for GaN at 1 atmosphere.

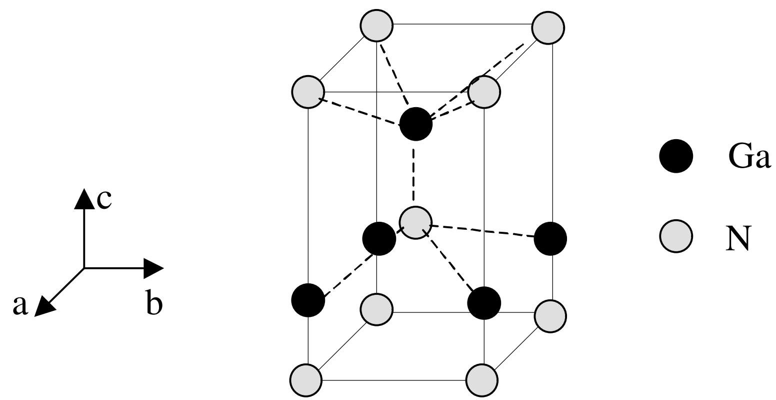

Figure 2–2: Clinographic projection of the GaN structure.

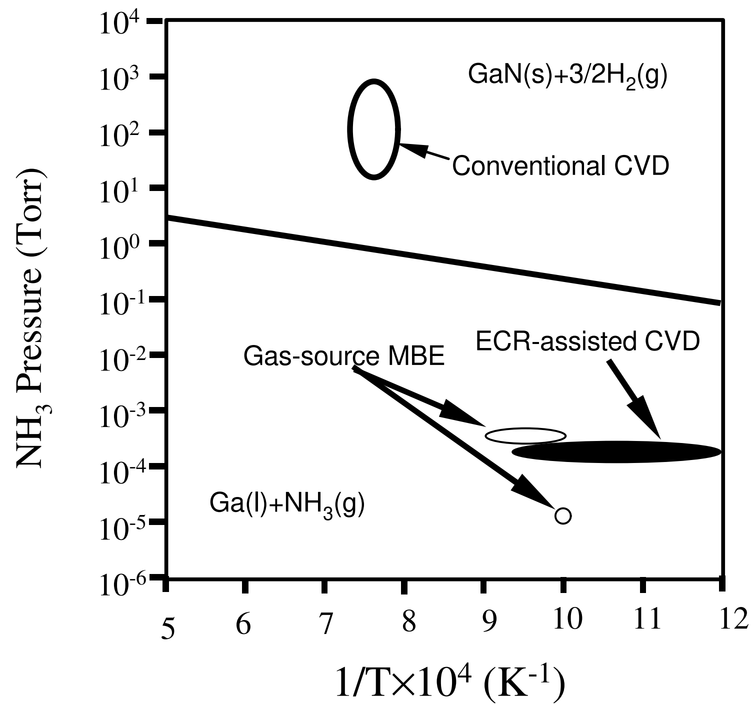

Figure 2–3: Operating temperature and pressures for various GaN growth processes. (Ref. 9)

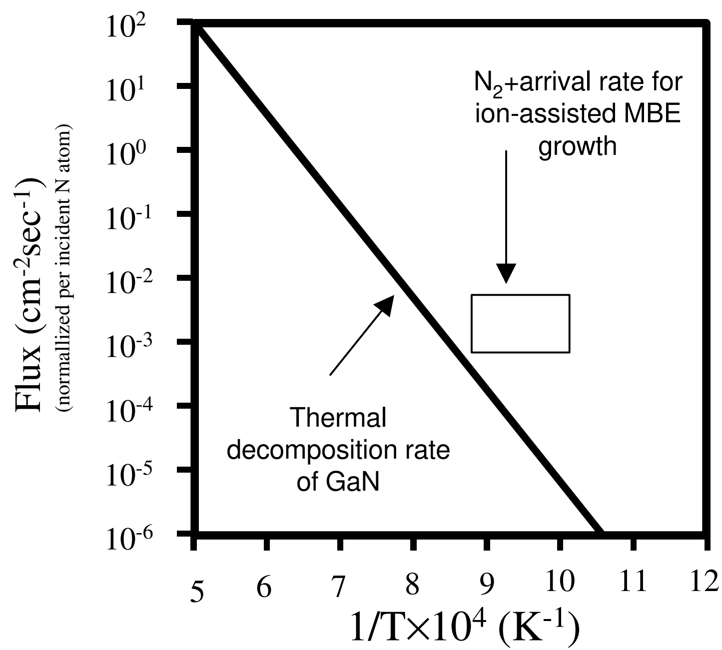

Figure 2–4: GaN decomposition rate as a function of temperature. (Ref. 9)

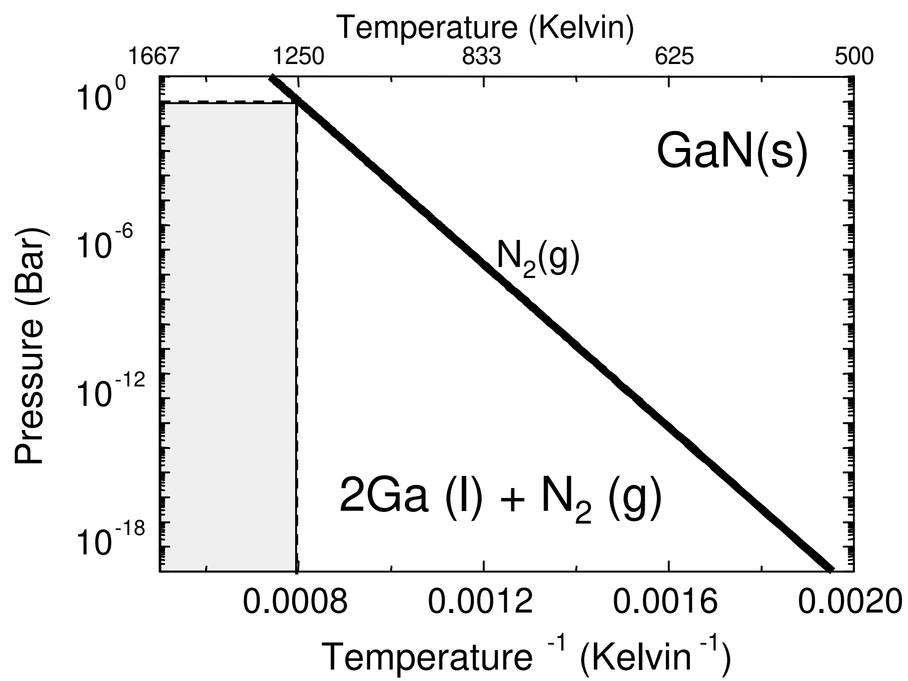

Figure 2–5: Pressure-temperature curve for GaN. Shaded region is area where GaN decomposes at 1250 K.

Chapter 3 - Experimental

All laser processing was performed in air using a Lambda Physik Lextra 200 KrF pulsed excimer laser (38 ns pulse width) with the incident beam directed through the sapphire substrate. The energy density of the incident laser light was varied between 100 and 600 mJ/cm^2 by defocusing the laser beam with a fused silica plano-convex lens having a 350 mm focal length. The laser processing equipment is shown schematically on Figure 3–1. The beam-energy output from the KrF pulsed excimer laser is approximately 1 Joule per pulse at a wavelength of 248 nm. Before each experiment, the output beam power was calibrated with a portable calorimeter with the beam measured at the sample target position. The output energy from the laser is adjusted by varying the high voltage discharge in the range of 16 to 24 kV.

3.1 - KrF Pulsed Excimer Laser Beam Profile

The experimental setup for the laser was borrowed from a system primarily used for pulsed laser deposition. As a result, the spatial beam profile of the laser output was not homogenized as would be expected for a set up to perform areal laser processing. In order to use the laser arrangement effectively, the spatial characterization of the beam was investigated. Due to the intrinsic non-uniformity in the output beam profile, typically found in a gas laser, local high-intensity regions or "hot-spots" may develop within the irradiation area. These hot spots ordinarily are ignored in PLD, but for the LLO process a given process window is desired for the decomposition of the GaN. At higher fluences above the process threshold, the violent ejection of the sapphire substrate, due to the GaN decomposition, can cause the mechanical fracture of the GaN thin film. By compensating

for a known high-intensity region, the output energy can be adjusted to minimize the probability of film fracture due to excessive laser fluence.

The laser beam profile of the KrF laser was characterized using a simple knife-edge technique. An aperture with a razor blade edge was first placed across the entire beam spot. As the aperture was opened in either the vertical or the horizontal direction, a change in the incident energy as a function of the aperture opening was recorded. The energy density of the beam is then given by:

$$\xi = \frac{E}{aC} = \frac{E}{A} \qquad [1]$$

where E is the incident laser energy, a is the exposed area of irradiation and C is the constant dimension in either the x- or y-direction. Figure 3–2 shows the axis orientation and experimental configuration for measuring the beam profile. The change in energy density is given by:

$$\Delta\xi = \frac{E}{\delta aC} = \frac{E}{\Delta A}. \qquad [2]$$

The energy gradient as a function of the aperture area opening can be used to determine the change in energy within a given area in the beam spot. The slope or energy gradient, $E/\delta a$, is proportional to the energy density at a particular region in the beam spot. A constant slope along the entire direction of the irradiated area would indicate a homogeneous spatial energy distribution. A decrease or increase in the slope would indicate a cold or hot spot, respectively.

Figure 3–3 shows a plot of the beam profile along the vertical axis of the KrF pulsed excimer laser used for LLO. The energy gradient was measured to have a

Gaussian profile to ~ 8 mm from the leading edge. A second flat-top region is found to extend approximately 2.3 cm across the vertical position of the beam. The flat-top area has a measured gradient of ~14.1 mJ/cm. Along the far edge of the beam (vertical position > 3.0 cm) the beam profile is found to drop off again in a Gaussian profile. For these measurements, an incident beam energy of ~525 mJ (aperture fully opened) was used.

In the horizontal axis, three separate regions were found in the beam profile (Figure 3–4). The first region begins from the lower edge of the beam and extends approximately 5 cm. The measured profile was again fitted to a Gaussian tail. A second region with a measured slope of 26.9 mJ/cm extends approximately 2 cm within the horizontal beam spot. At the end of this region, the energy gradient decreases again with a fitted Gaussian profile. The measured energy change along this vertical direction is expected to be the dominant "hot" area given the slope along that direction nearly twice the other measured regions. Consequently, the predicted high-intensity zone should be a region slightly offset from center spanning the width of the beam.

Figure 3–5 shows the superposition of the energy profiles from the vertical and horizontal measurements. The energy contour was obtained by integrating the area under the energy-gradient profiles in Figures 3–3 and 3–4. The offset "hot" zone is predicted to be the high intensity region that will anchor the upper limit of the output energy for the LLO process.

3.2 - The Wafer-Bonding Tool

The wafer-bonding process was performed using a modified heater plate capable of a maximum annealing temperature of 350°C. The plate is equipped with two 300 Watt

resistive heaters and a manual screw-down press for pressure bonding. Samples were mounted below the manual press and a bonding pressure of ~3 MPa was applied to join wafers at 200°C. The temperature of the hot-plate was controlled using a solid-state relay switch controlled by a variable frequency generator. The wafer-bonding tool is able to bond wafers up to four inches in diameter. Figure 3–6 shows a schematic of the wafer-bonding set-up. The entire tool was enclosed in a nitrogen-purged Plexiglas™ case. The nitrogen ambient was used to minimize oxidation of the bonding metals during the 200°C anneal.

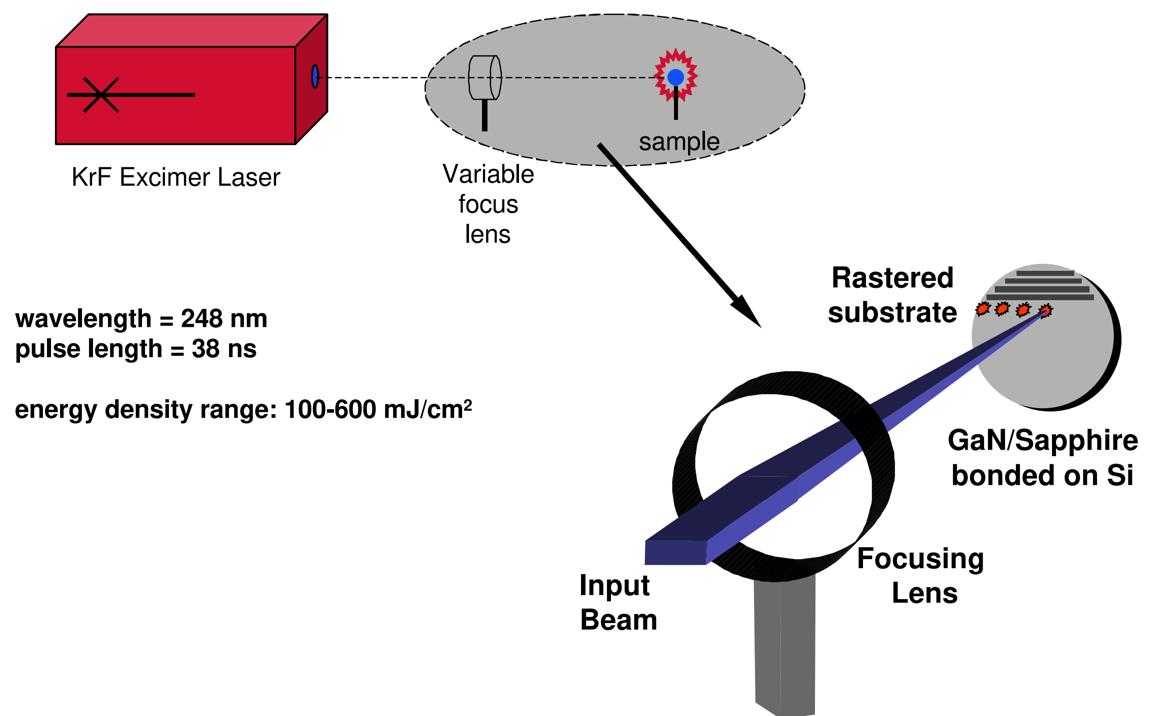

Figure 3-1: Schematic of the KrF pulsed excimer laser system.

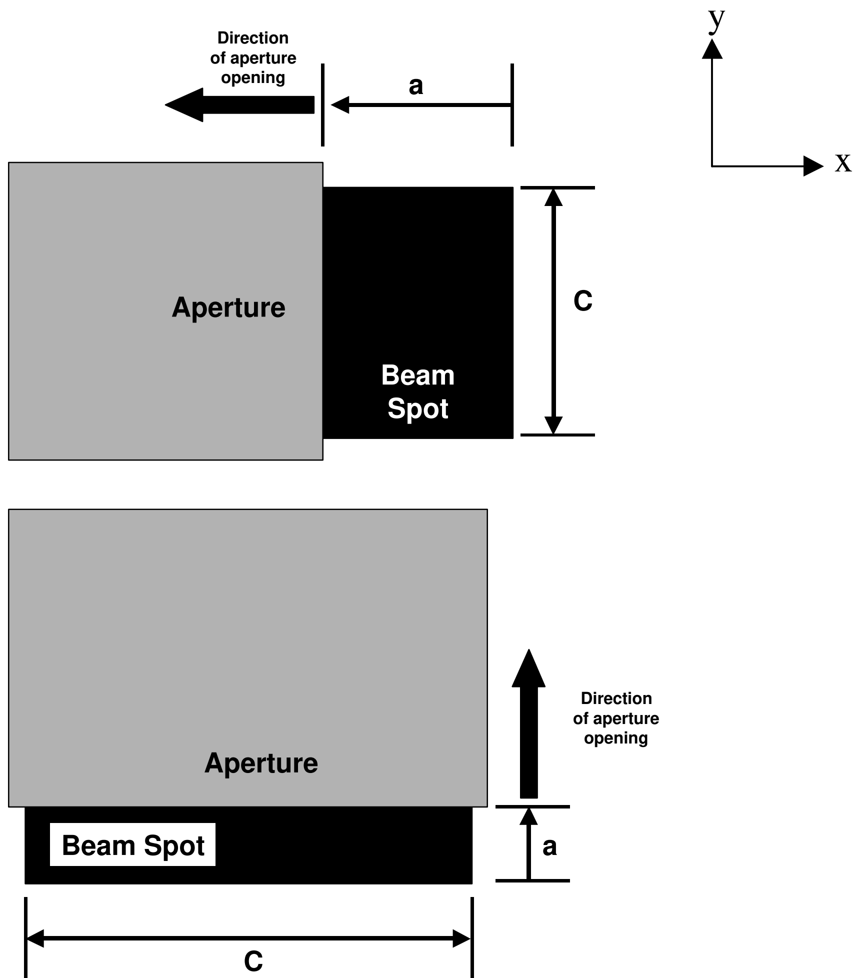

Figure 3-2: Knife-edge measurement process to characterize laser beam profile for vertical profile (top) and horizontal profile (bottom).

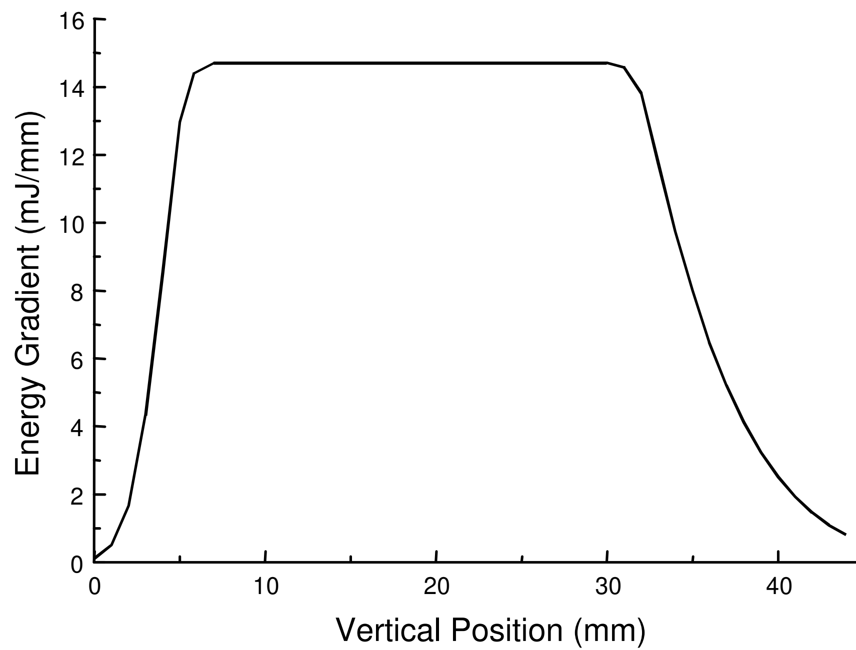

Figure 3-3: Vertical energy profile of the KrF excimer laser used for LLO.

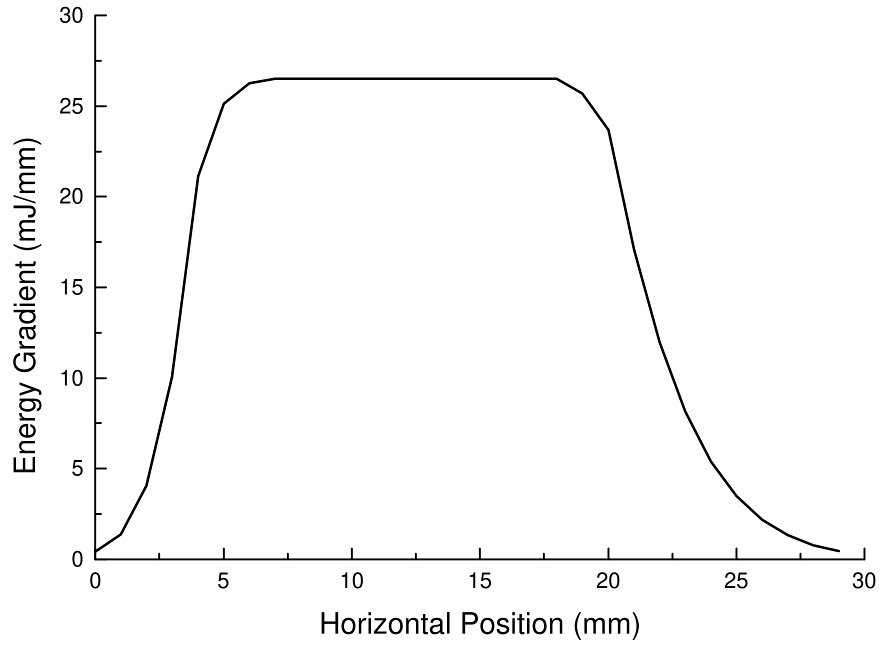

Figure 3-4: Horizontal laser beam profile of the KrF excimer laser used for LLO.

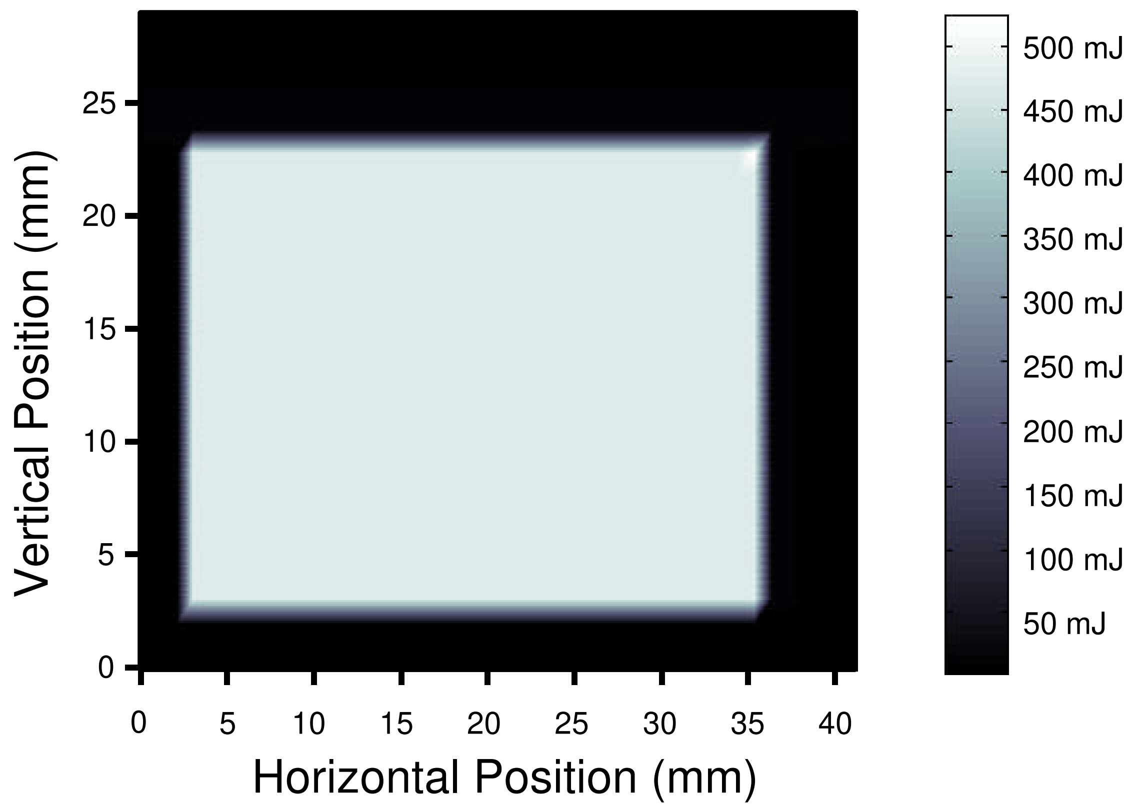

Figure 3-5: Energy intensity contour of the KrF pulsed excimer laser.

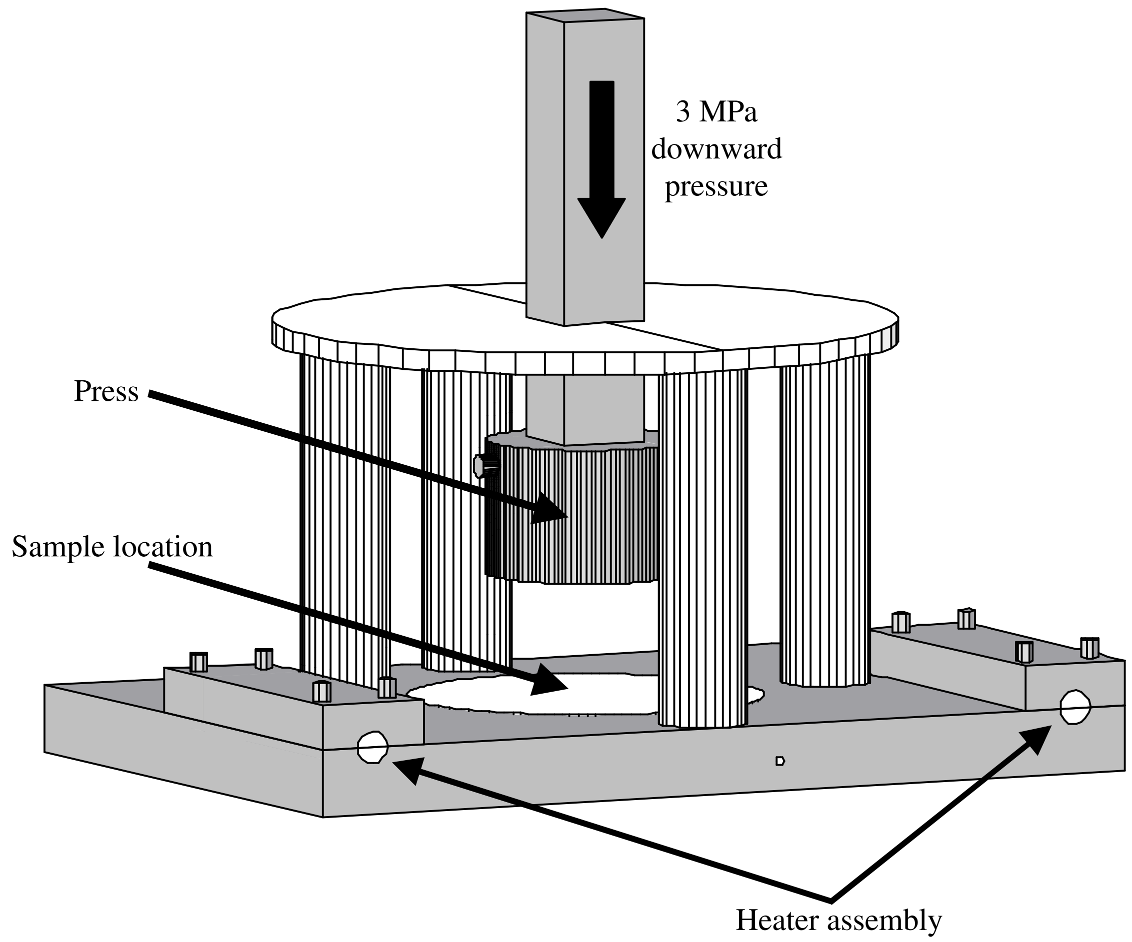

Figure 3-6: Wafer-bonding Tool

Chapter 4 - Wafer-bonding and Laser Lift-off

Despite the lack of a lattice-matched substrate and high defect density, GaN thin-film quality has improved extremely quickly due to the rapid development of the GaN growth techniques. Within the last ten years, progress in the III-V nitrides has taken the GaN system from a novel materials group for blue emission to the leading compound semiconductor for blue light-emitting diodes and laser diodes. The current progress may be further extended by combining the III-V nitrides with Si, polymers and other III-V materials such as GaAs or GaP.

Many approaches to monolithic integration have been proposed and demonstrated to join dissimilar systems onto one platform. For example, in the early and mid-1980's, a large interest in integrating GaAs thin films with Si substrates was motivated by combining the optoelectronic functionality of GaAs with the processing power of complimentary metal-oxide-semiconductor Si integrated circuit (IC) technology. The union of GaAs devices with Si substrates would have created new possibilities for high-speed intrachip communications. Motivated by the possibilities of an integrated GaAs/Si microsystem on a chip, several groups attempted, with moderate success, to perform the integration process by direct heteroepitaxial growth of GaAs onto Si.

Many of the problems and obstacles researchers faced fifteen years ago parallel those being faced by researchers currently working on the GaN materials system. The rewards to be had with the integration of GaN with low-cost substrate materials such as Si, glass, or polymers are far reaching. The integration process could pave the way for

advanced, high-resolution color displays; micro-emitter-detector arrays for environmental sampling; or low-cost, low-power high-brightness room lighting.

4.1 - Integration by Direct Deposition: GaAs on Si

The integration of two dissimilar materials is most easily accomplished by direct deposition. For GaAs and Si, this process was first demonstrated by a GaAs-based device fabricated on Si as a shallow-homojunction solar cell.[68] Subsequently GaAs-based LEDs,[69] LDs,[70] and metal-semiconductor field-effect transistors[71] were reported. Due to the 4% lattice and 67% thermal expansion coefficient mismatch between the zincblende structure GaAs and the diamond structure Si, the GaAs thin films normally suffered from a high density of defects at the thin-film/substrate interface. To reduce the defect density introduced during the heteroepitaxial growth and improve the GaAs film quality, a thin intermediate buffer layer, an idea borrowed by most GaN thin-film growers, was first deposited onto the Si substrate.[72]

More complicated growth techniques, such as a two-step process using an intermediate Ge/SiO_2 layer, were subsequently employed.[73] As the understanding of the GaAs/Si growth process improved, the growth techniques were later refined and the need for the SiO_2 intermediate layer was soon eliminated. The first successful fabrication of device-quality material for GaAs-based LEDs on Ge-coated Si substrates was demonstrated using organometallic vapor-phase deposition.[74] Soon after, the first demonstrations of device-quality GaAs thin films grown directly on Si were accomplished by molecular-beam epitaxy.[75]

Eliminating the Ge buffer layer in the GaAs/Si system was an improvement over the previously described methods since both the substrate pre-growth preparation and the

possibility of Ge autodoping during the GaAs growth was removed. Despite the simpler growth process and improved film quality, the integration of GaAs with Si during direct deposition was still hampered by the defects introduced by the heteroepitaxy. Consequently, the device performance of these films, in particular the minority-carrier devices, was inferior to the GaAs material homoepitaxially grown on GaAs substrates.

4.2 - Integration by Lift-off and Transfer

A less direct integration method, but a more flexible process, is thin-film lift-off and transfer to join dissimilar materials. A lift-off and transfer process allows integrating the highest quality materials available, pre-fabricated in separate process steps, to create one wholly-optimized system. The final product, created by bonding and lift-off onto the desired platform, is completed by removing the transferred film from its original growth substrate. This integration method has been demonstrated by several methods. One technique for thin-film lift-off is the use of a thin sacrificial layer between the growth substrate and the desired thin film. The method has been described and demonstrated for the $Al_xGa_{1-x}As$ system using an AlAs release layer grown on a GaAs substrate.[76-78]

The epitaxial lift-off (ELO) process takes advantage of the extreme etch selectivity between $Al_xGa_{1-x}As$ and AlAs in a hydrofluoric (HF) acid.[79] In this materials system, the selectivity for etching has been measured to be $> 10^7$ between the AlAs and $Al_xGa_{1-x}As$ ($x < 0.4$). Crack-free GaAs thin films of thickness down to 80 nm have been successfully lifted off by the ELO process. A wax layer was used to support the free-standing films after delamination. An essential feature in the ELO process was the fact that the supporting wax bonder was under tension during the lift-off while the GaAs thin film was under compression. This configuration then ensures the mechanical lifting of the

GaAs film as it was being undercut by the acid solution; in particular it allows the dissolved H_2 gas in the HF solution to diffuse from the etching zone. The process is shown in Figure 4–1.

Device characterization of the ELO released films demonstrated the device performance was not degraded by the lift-off process.[80] Although the results were encouraging, the ELO process was limited by its inability to delaminate large areas. The process has been restricted to sample sizes of only ~ 0.8 cm × 2.5 cm while taking approximately 24 hours to complete. Such a technique is unacceptable for large volume throughput expected in a manufacturing environment. As such, the ELO process is an excellent demonstration of using a lift-off and transfer method for materials integration. On the one hand, it has overcome the poor materials quality inherent in heteroepitaxial growth but is severely limited by small process areas and lengthy process times.

4.3 - GaN Thin-film Lift-off Processes

At present, the lack of a large-area GaN substrate precludes homoepitaxial deposition of GaN thin films in which the substrate of choice for high-quality thin films is currently sapphire. Despite the high density of defects associated with GaN, thin films grown on sapphire the device performance of this system has been remarkably good. In terms of LED and LD performance, GaN and its alloys with Al and In are fairly insensitive to defect densities ranging from 10^8-10^{10} cm^2.[81]

The integration of GaN with cheaper and readily available substrates such as Si, in analogy with the GaAs and Si system, by direct deposition has not yielded the high material quality commonly achieved with GaN on sapphire. Similar to the case of integrating GaAs onto Si, thin-film lift-off techniques, in conjunction with wafer bonding

processes, may be a more applicable approach to integrate GaN with other dissimilar materials, thus eliminating the sapphire substrate constraint. In this way, the high-quality material obtained from the growth of GaN on sapphire may be used in other systems where it is often difficult or impossible to obtain. The sapphire may be eliminated by various techniques including chemo-mechanical removal of the substrate,[82] wet chemical etching of a sacrificial layer,[30] or pulsed-laser processing.[16,17,83] The relative hardness of sapphire and the lack of an effective wet-chemical etch for GaN or materials compatible with GaN, have precluded the use of the former techniques as efficient and viable lift-off processes.

A LLO process, first demonstrated by Kelly *et al.*,[83] with the incident beam directed through the transparent sapphire can be used to rapidly and effectively separate GaN thin films from its growth substrates. A two-step LLO process,[16] described in this dissertation and shown schematically in Figure 4–2, has also been developed independently from the work by Kelly. The process has allowed the flexibility of integrating large-area GaN films with other materials systems of choice, depending on the desired application.

Since these first demonstrations, many groups have also used LLO to separate GaN thin films from sapphire substrates. The lift-off of a functioning pn-diode using LLO from sapphire onto a different substrate was first demonstrated by Kelly *et al.*[84] Other groups soon reported the transfer of GaN-based LEDs, prefabricated on sapphire, onto copper[85-87] and Si[88] substrates. LLO has also been demonstrated on other thin-film materials systems such as $(Pb,La)(Zr,Ti)O_3$,[89] $Pb(Zr,Ti)O_3$,[90] and ZnO[91] in which the laser source was a XeCl[86,87] or KrF[85,88-91] pulsed-excimer laser, or the third harmonic of a

excimer laser to separate films deposited onto MgO substrates.[89] The following section describes a simple investigation of the two-step LLO process,[16] demonstrating the efficacy of this bandgap-selective technique using a KrF pulsed-excimer laser. Characterization of the GaN thin film before and after laser processing will show no detectable degradation of GaN crystal quality after the lift-off and transfer process.

4.4 - The Laser Lift-off Process

GaN thin films of thickness 3 μm on a single-sided polished sapphire substrate were used as the starting material. A boron doped, p-type Si (001) wafer was bonded to the surface of the GaN thin film using epoxy, forming a sapphire/GaN/epoxy/Si structure. Prior to the wafer bonding, the backside of the sapphire substrate was polished using diamond paper. Attenuation of the KrF excimer laser beam through the 0.5 mm thick sapphire substrate is approximately 20-30% at 248nm.[92]

Initial irradiation of the bonded structure at fluences up to 200 mJ/cm^2 did not reveal any changes in the GaN/sapphire interface upon visual inspection. By increasing the laser fluence to 300 mJ/cm^2, a distinct change in the appearance of the interfacial region from transparent to a metallic silvery color was noted. This observation suggested that the GaN at the GaN/sapphire interface was beginning to decompose into metallic gallium. However, the substrate remained firmly attached to the film even after several pulses at 300 mJ/cm^2.

At fluences greater than or equal to 400 mJ/cm^2, successful lift-off and transfer of the GaN film from the sapphire to the Si substrate was accomplished after a single laser pulse. Separation of the film from its sapphire substrate resulted after warming the

sample on a hot plate to a temperature above the Ga melting point (T_m = 30°C). GaN films up to 3 mm×4 mm were successfully transferred onto 5 mm×5 mm Si substrates.

Characterization of the bonded GaN on Si was performed by x-ray diffraction (XRD) and scanning electron microscopy (SEM). The cross-sectional SEM image in Figure 4–3 shows a GaN/epoxy/Si structure after separation from the sapphire substrate. The transferred GaN thin film was smooth and intact with a thickness of 2.5-3 microns.

Using an optimal 600 mJ/cm^2 fluence, Figure 4–4 shows a θ-2θ coupled XRD spectrum for the GaN on Si after lift-off from sapphire. The 0002 GaN and 004 Si reflections are evident. The ϕ-circle scan in Figure 4–5 shows the six-fold symmetry of the GaN thin film on Si indicating that the GaN retains its original wurtzite crystal structure after transferred to the cubic Si substrate.

Analysis of the GaN film by x-ray rocking curve (XRC) measurement dramatically displays the effectiveness of this laser processing technique. Figure 4–6(a) is an XRC spectrum of the GaN 0002 reflection for the as-deposited GaN on sapphire before lift-off. The plot indicates relatively high-quality GaN as shown by the peak full-width at half maximum (FWHM) of approximately 0.1°. Figure 4–6(b) shows a rocking curve of the same film after lift-off using a laser fluence of 600 mJ/cm^2; the FWHM of the 0002 GaN reflection is unchanged from the value measured prior to lift-off. If the film had suffered thermal or mechanical damage (*e.g.* microcracking or buckling) during separation then the rocking-curve width would have increased, reflecting a greater mosaic spread. The XRD data combined with the film thickness measured by cross-sectional SEM indicate that the interfacial decomposed layer is very thin compared to the film

thickness, as would be expected for an absorption depth that is estimated to be less than 75 nm at a wavelength of 248 nm.[92]

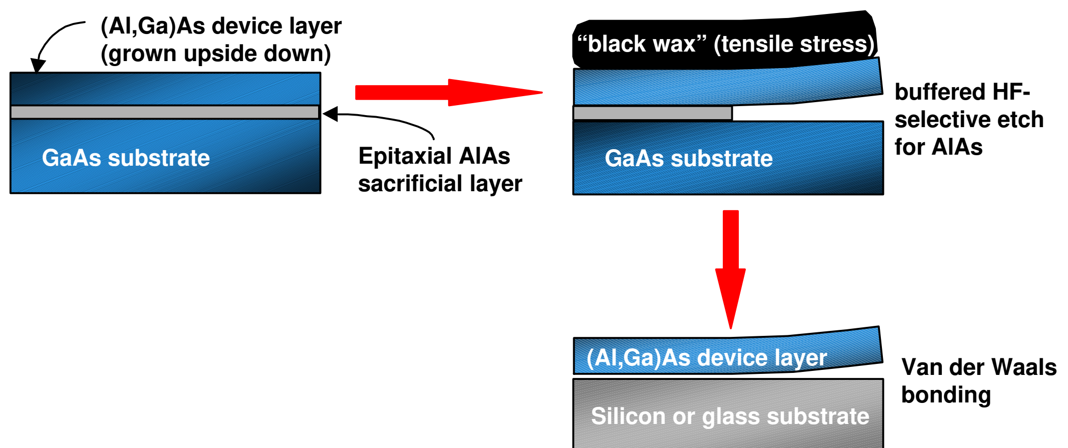

Figure 4–1: Epitaxial lift-off process.

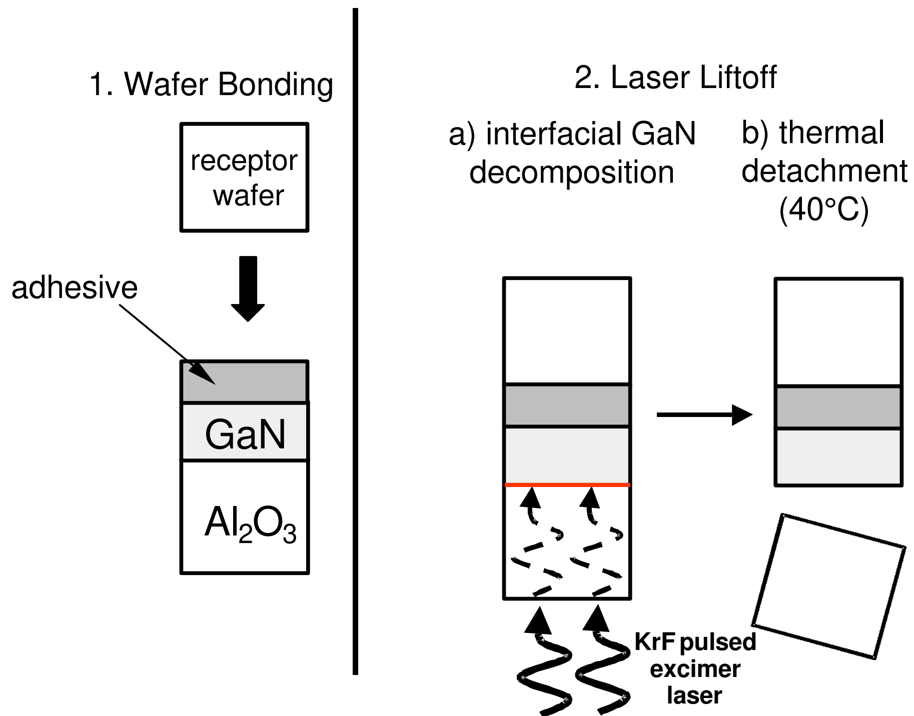

Figure 4–2: Laser lift-off process.

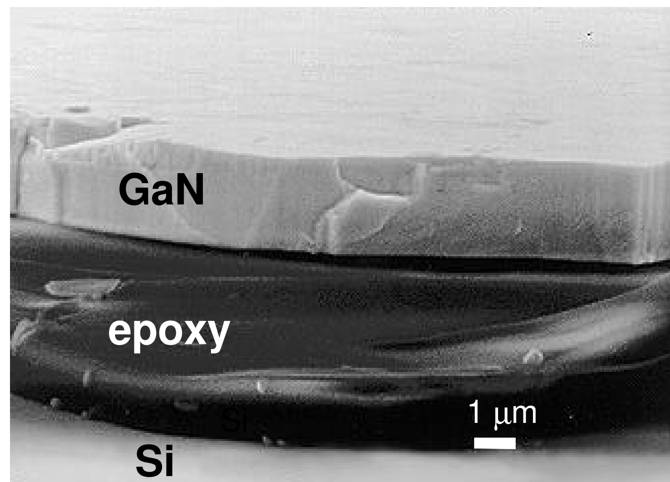

Figure 4–3: Cross-sectional SEM micrograph showing a separated GaN film bonded to a Si substrate. The bonding material is epoxy. A 600 mJ/cm^2 laser fluence directed through the original sapphire substrate was used to separate the GaN from the sapphire.

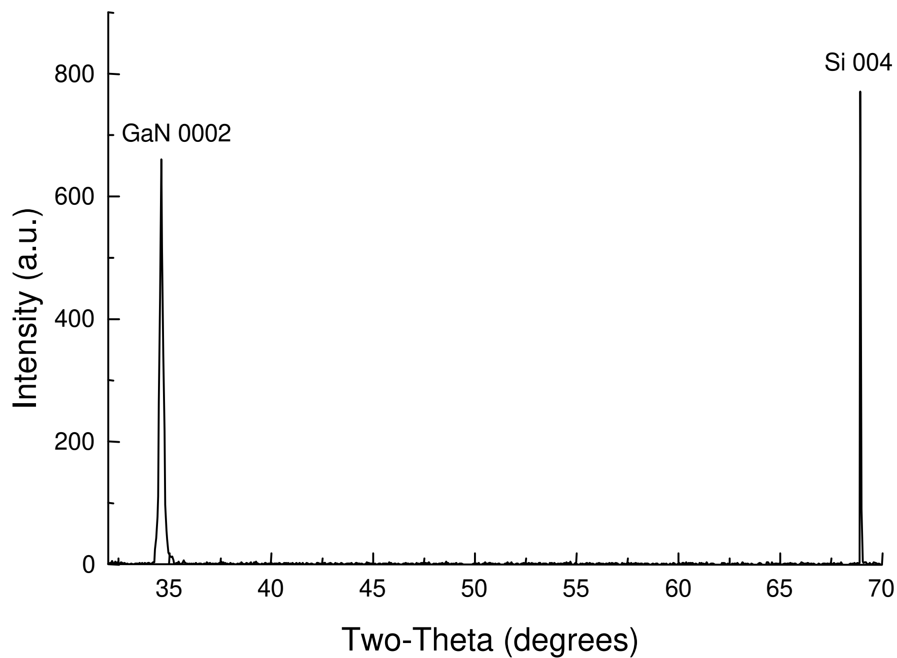

Figure 4–4: A θ - 2θ coupled XRD spectra of GaN bonded to Si after lift-off from the sapphire substrate. The separation process was done at a laser fluence of 600 mJ/cm^2.

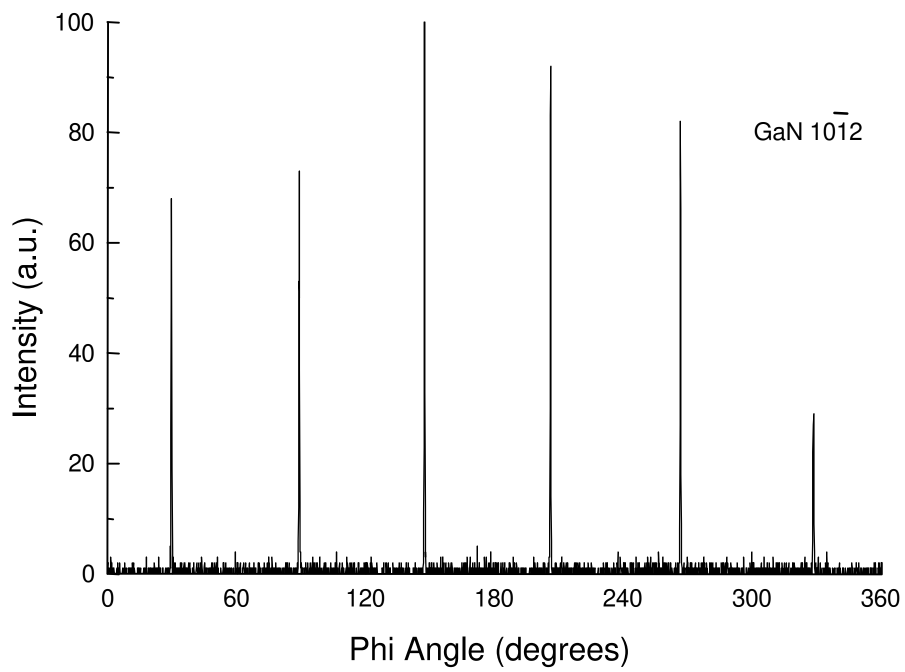

Figure 4–5: A ϕ-circle scan of the $10\bar{1}2$ GaN reflection shows that the GaN retains six-fold symmetry on the cubic Si substrate.

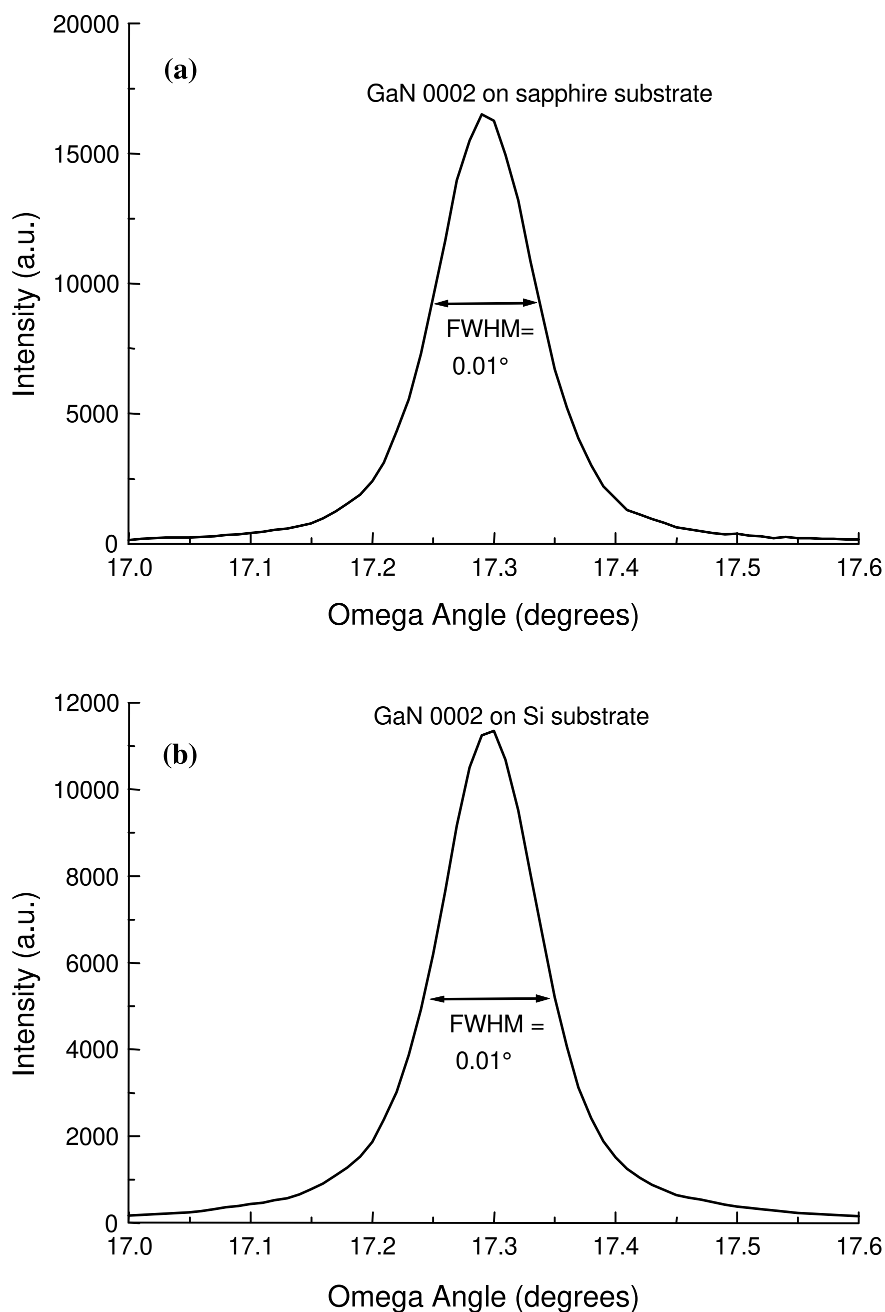

Figure 4–6: Comparison of GaN film quality by XRC of the 0002 GaN reflection for: (a) GaN on sapphire, and (b) after transfer from sapphire to a Si substrate. The FWHM of the 0002 GaN reflection remains unchanged after lift-off indicating that the film was separated and transferred without appreciable thermal or mechanical damage. A laser fluence of 600 mJ/cm^2 was used.

Chapter 5 - Thermal Analysis of Laser-Target Interactions

The heat treatment of materials serves many purposes in the processing of semiconductors. The applications and examples of thermal annealing include dopant activation, dopant diffusion, compound formation, oxide-layer growth, and wafer bonding. The conventional heat treatment typically involves furnace annealing of bulk materials under equilibrium conditions. Laser processing, on the other hand, has the advantage of providing localized heating in both the temporal and spatial domain. The amount of heating can be controlled by choosing the appropriate laser wavelength, beam energy and exposure duration. For example, a spatially localized heating effect may be obtained by choosing a short laser pulse with a wavelength at which the material to be heated has a large absorption coefficient. In this way, well-defined volumes of material may be heated to above the melting or decomposition temperature of a material while allowing the remainder of the target specimen to remain at near-ambient temperatures. In addition, laser emission wavelengths can be tuned so that one material transmits while another absorbs, thus enabling selective processing at a buried interface.

In this section, the interaction of laser light with GaN thin films will be explored. Specifically, the temperature distributions of a laser irradiated GaN thin film will be investigated for the case of a KrF pulsed excimer laser (248 nm, 38 ns pulse-width). An analysis by both analytical and numerical solutions to the one-dimensional heat equation will be given. In the case of the numerical solution, temperature distributions for temperature dependent and temperature independent parameters will be discussed.

5.1 - Laser-target Interaction

During the irradiation of a semiconductor by laser light, energy is typically transported by hot carriers before being given up to the lattice. When the lattice finally absorbs this energy, heat flow begins within the material. The mathematical representation of heat conduction in a solid assumes that a heat flux, Φ, develops across a plane and is proportional to the local temperature gradient:

$$\Phi(z_0) = -\kappa\left(\frac{dT}{dz}\right)_{z_0} \qquad [5.1\text{–}1]$$

where κ is the thermal conductivity of the material. If we consider a slab bounded by two planes at position z and $z+\Delta z$, then the energy balance for the slab in terms of a volumetric heat capacity C_p/V is: [93]

$$\Delta t\left[\Phi(z) - \Phi(z+\Delta z)\right] = \Delta T\,\frac{C_p}{V}\,\Delta z \qquad [5.1\text{–}2]$$

where ΔT is the change in temperature as a result of the heat flux across the two boundaries. As $\Delta z \rightarrow 0$, the term on the left-hand side of equation 5.1–2 becomes $\left(\frac{\partial \Phi}{\partial z}\right)\Delta z \Delta t$. Using equation 5.1–1, the heat flow equation can then be written in its standard form: [94]

$$\frac{\partial}{\partial z}\left(\kappa\frac{\partial T}{\partial z}\right) = \frac{C_p}{V}\frac{\partial T}{\partial t}. \qquad [5.1\text{–}3]$$

To successfully transfer a thin film from the growth substrate after wafer bonding, the LLO process must not adversely affect the properties of the transferred thin film. For the GaN/sapphire system, a temperature in excess of 1000°C is required at the interface

in order to induce decomposition.[8,9] Yet, the temperature at the interface between the GaN and the bonding layer should not exceed 200°C to maintain maximum flexibility in choice of the bonding material and the receptor substrate. For the case when heat is produced by irradiation from a laser with a particular power density, the heat equation is rewritten as:[93]

$$\frac{\partial T}{\partial t} = \frac{\alpha}{\rho C_p} I(z,t) + \frac{1}{\rho C_p} \frac{\partial}{\partial z}\left(\kappa \frac{\partial T}{\partial t} \right). \qquad [5.1\text{–}4]$$

In this equation, $I(z,t)$ is the power density [mJ/cm^2] of the incident laser light at a depth z and time t. The variables T, ρ, C_p, κ, and α are the temperature, density, specific heat, thermal conductivity and optical absorption coefficient, respectively, for GaN or sapphire. Assuming the thin film is a homogeneous absorbing medium, the incident power density can be written as:

$$I(z,t)=I_0(t)(1-R)e^{-\alpha z}, \qquad [5.1\text{–}5]$$

where $I_0(t)$ is the output laser power density and R is the reflectivity.

For high intensity irradiation (~10^8 W/cm^2), a large density of carriers will build up before the lattice is appreciably heated.[95] Collisions between carriers will establish thermal equilibrium within a time scale of 10^{-14} sec. After the pulse ends, the hot carriers will recombine, typically within 10^{-9} s.[96] These high intensities may bring about a plasma formation at the irradiated surface but for these first-order calculations a generated plasma is ignored.

The heat equation can then be solved analytically assuming a one-dimensional heat flow, the thermal and optical parameters are invariant with temperature, the GaN film is of a semi-infinite thickness ($z = 0$ to $z = L$ for $L = \infty$), and no phase change occurs

during the laser pulse. These conditions are then met by satisfying the following boundary conditions: $\frac{\partial T}{\partial z} = 0$ for $z = 0$ and $z = L$ at all times t. If the incident beam irradiates the target surface at $z = 0$ then the heat-flow equation can be written as:[93]

$$\frac{\partial T}{\partial t} = K_d \nabla^2 T + \frac{\alpha I_a (x, y, t) V}{C_p} e^{-\alpha z} \qquad [5.1\text{–}6]$$

where the thermal diffusivity is $K_d = \kappa/\rho C_p$, and I_a is the absorbed irradiation. The Green's function technique[97] is used to obtain the analytical solution to the heat equation. This solution can be solved for two limiting cases: 1) the laser light has a short penetration depth into the target (surface source) and 2) the laser light has a finite penetration depth (penetrating source).

In the case of a uniform surface source ($\alpha^{-1} << 2\sqrt{K_d t}$), where the laser source is assumed to have a constant power and fluence I_0 (switched on at $t = 0$ and off at $t = \tau_0$) the solution is given as:[98]

$$T(z,t) = \left[\frac{2I_0\sqrt{K_d t}}{\kappa}\right] \sum_{n=-\infty}^{\infty} ierfc\left[\frac{2nL - z}{2\sqrt{K_d t}}\right](1 - R) \qquad [5.1\text{–}7]$$

For the particular case of a semi-infinite solid ($L = \infty$), the temperature at the irradiated surface is:

$$T(0,t) = I_a \frac{2\sqrt{K_d t}}{\kappa\sqrt{\pi}}(1 - R) \qquad [5.1\text{–}8]$$

In the case where the absorption depth, α^{-1}, is large compared to the heat diffusion length, $2\sqrt{K_d t}$, adiabatic heating takes place and the solution for a uniform penetrating source is:[98]

$$T(z,t) = \frac{I_0}{4\kappa} \int_0^{2\sqrt{K_d t}} exp\left[-\left(\frac{\alpha\beta}{2} \right)^2 \right] Y_2 d\beta \qquad [5.1\text{–}9]$$

where $Y_2 = \sum_{n=-\infty}^{\infty} exp[\alpha(2nL - z)] \times \left[erfc\left(\frac{(2n+1)L - z}{\beta} + \frac{\alpha\beta}{2} \right) - erfc\left(\frac{2nL - z}{\beta} + \frac{\alpha\beta}{2} \right) \right]$ and

$\beta = 2\sqrt{\kappa|t - t'|}$.

The closed form solution for the semi-infinite solid is: [93]

$$T(z,t) = \frac{I_0}{\kappa} \left\{ \begin{array}{l} 2\sqrt{K_d t} \cdot ierfc\left(\frac{z}{2\sqrt{K_d t}} \right) - \left(\frac{1}{\alpha} \right) e^{-\alpha z} + \left(\frac{1}{2\alpha} e^{\alpha^2 K_d t} \right) \\ \times \left[e^{-\alpha z} erfc \frac{2\alpha\sqrt{K_d t}}{2} - \frac{z}{2\sqrt{K_d t}} \right] + e^{2\alpha\sqrt{Dt}} erfc\left(\alpha\sqrt{K_d t} + \frac{z}{2\sqrt{K_d t}} \right) \end{array} \right\} . [5.1\text{–}10]$$

For the temperature at the surface of the irradiated target the solution is:

$$T(0,t) = \frac{I_0}{\kappa} \left\{ \frac{2\sqrt{K_d t}}{\sqrt{\pi}} - \frac{1}{\alpha}\left[1 - e^{\alpha^{2Dt}} erfc(\alpha K_d t) \right] \right\}. \qquad [5.1\text{–}11]$$

At the end of the pulse duration, $t = \tau_0$, the target specimen will begin to cool. The temperature profile for the time $t > \tau_0$: [93]

$$T(z,t) = P_a \int_0^t g_{us} dt' =$$

$$\left(2\frac{I_a}{\kappa} \right) \sqrt{\kappa t} \cdot ierfc\left(\frac{z}{2\sqrt{\kappa t}} \right) - [t > \tau_0] \sqrt{\kappa(t - \tau_0)} \cdot ierfc\left[\frac{z}{2\sqrt{\kappa(t - \tau_0)}} \right] \qquad [5.1\text{–}12]$$

By combining equations 5.1–7 or 5.1–9 (for heating) and 5.1–12 (for cooling) the temperature contour of an irradiated target can be calculated as a function of time and depth. For the case of GaN the absorption coefficient is given to be ~ 4.4×10^5 at a wavelength of 248 nm with a calculated thermal diffusion length of approximately 1.5

μm.[99] For these thermal properties, the laser irradiation of GaN can be modeled as a surface heating source using equation 5.1–7 and 5.1–12.

For a single 38 ns pulse from a KrF laser, equations 5.1–7 and 5.1–12 reveal an approximately 400 mJ/cm^2 is needed to raise the surface of the GaN film to the decomposition temperature of 900°C-1000°C. The values for ρ, C_p, κ, R and α used in the calculations were 6.11 g/cm^3, 9.745 cal/mol-K, 1.3 W/cm-K, 0.3 and 4.4×10^5 cm^{-1}, respectively.[20,99,100] A simulated temperature profile for a single 38 ns, 400 mJ/cm^2 pulse from a KrF laser as a function of time and depth is shown in Figure 5–1. This figure shows the temperature rise, coupled with a large temperature gradient across the thickness of the GaN film, occurs in a highly localized heated area that is within 100 nm below the irradiated GaN/sapphire interface. This selective localized heating allows for the formation of a thin interfacial layer to yield separation of the GaN film from the sapphire substrate.

Experimental data was used to confirm the findings of the analytical solution. GaN (thickness = 1.5 μm) on sapphire samples were irradiated using a 38 ns pulse from the KrF (248 nm) pulsed-excimer laser. Figure 5–2 shows the surface morphology of the GaN surface as analyzed by scanning electron microscopy. For a laser fluence of 200 mJ/cm^2 the GaN surface was found to be smooth and featureless as expected from the thermal simulations. As the energy density was raised to 400 mJ/cm^2, which was predicted to raise the GaN surface to the decomposition temperature, small surface features were found on the GaN. At a fluence of 600 mJ/cm^2 the surface was noticeably rougher with an increased droplet size and formation density. Examination of the larger droplets by energy dispersive x-ray analysis verified the features were Ga rich in

composition. The results suggest that a fluence in excess of 400 mJ/cm^2 is needed to decompose the GaN surface into Ga metal and N_2 gas with a resulting Ga rich droplet formation on the thin film surface.

5.2 - Finite Element Analysis

The analytical modeling approach assumes temperature independent properties. To test this assumption, finite element analysis (FEA) utilizing temperature-dependent properties were performed. The commercially available FEA application COSMOS/M® was used to solve the heat equation [5.1–4] using a 1001 node mesh with 900 elements.[102] In the calculations, the temperature-independent values of R and α used for GaN in the calculations were 0.3 and 4.4×10^5 cm^{-1}, respectively,[20,100] while temperature-dependent values for C_p, ρ, and κ were obtained from references 103 and 104 (Figures 5–3-5–5). Materials parameters for sapphire were obtained from references 105 and 106. The interface was subjected to a 38 ns flat-top pulse profile to model the actual laser pulse with absorption of the irradiation occurring at the sapphire/GaN interface. The COSMOS/M® program calculated the temperature distribution every 0.1 ns up to an ending time of 50 ns.

First, FEA calculations were compared to the analytical results (Figure 5–1). Figure 5–6 shows the temperature distribution for temperature-independent GaN materials properties. The two calculations agree rather well with a similar peak temperature at the surface. The temperature gradient below the GaN surface is slightly less than that obtained from the analytical solution but the same trend is found in both models.

Figure 5–7 displays the temperature contour for a fluence of 400 mJ/cm^2 using the FEA calculation with temperature-dependent GaN properties. Again, for a single 38 ns pulse from a KrF laser (248 nm), the solution to equation 5.1–4 reveals that a 400 mJ/cm^2 laser fluence is needed to raise the surface of the GaN film to its decomposition temperature of ~900-1000°C. The difference in the profile near the surface is not changed significantly although the profile of the 1000°C region was found to be shallower due to the decrease in the thermal conductivity in GaN with increasing temperature. As expected, this effect would cause more localized heating of the GaN.

A model was next created to predict the needed fluence to cause the decomposition of GaN at a sapphire substrate interface for a GaN/sapphire structure. The information obtained from such a model would help to determine the actual fluence that is needed to perform the LLO process. The simulation showed that in order to raise the interface temperature to 1000°C a 600 mJ/cm^2 pulse from a KrF laser is needed. The simulated temperature as a function of time and depth is shown in Figure 5–8. As seen previously with the irradiation of the GaN surface, the temperature rise is due to the localized heat generated at the GaN/sapphire interface. A non-negligible temperature rise of the sapphire substrate during the laser irradiation is also found from the calculations.

The analytical and FEA calculations assumed no phase changes during the irradiation. It should be noted that at the threshold temperature, the GaN decomposition would transform the interface into a Ga rich region. The thermal model does not account for the enhanced reflectivity due to the Ga formation or generation of a plasma[107] during irradiation. Although the formation of Ga metal would increase the thermal conductivity, the reflectivity will also increase and effectively diminish the light absorption at the

interface. Consequently, the expected temperature rise should decrease due to a phase change or plasma generation.

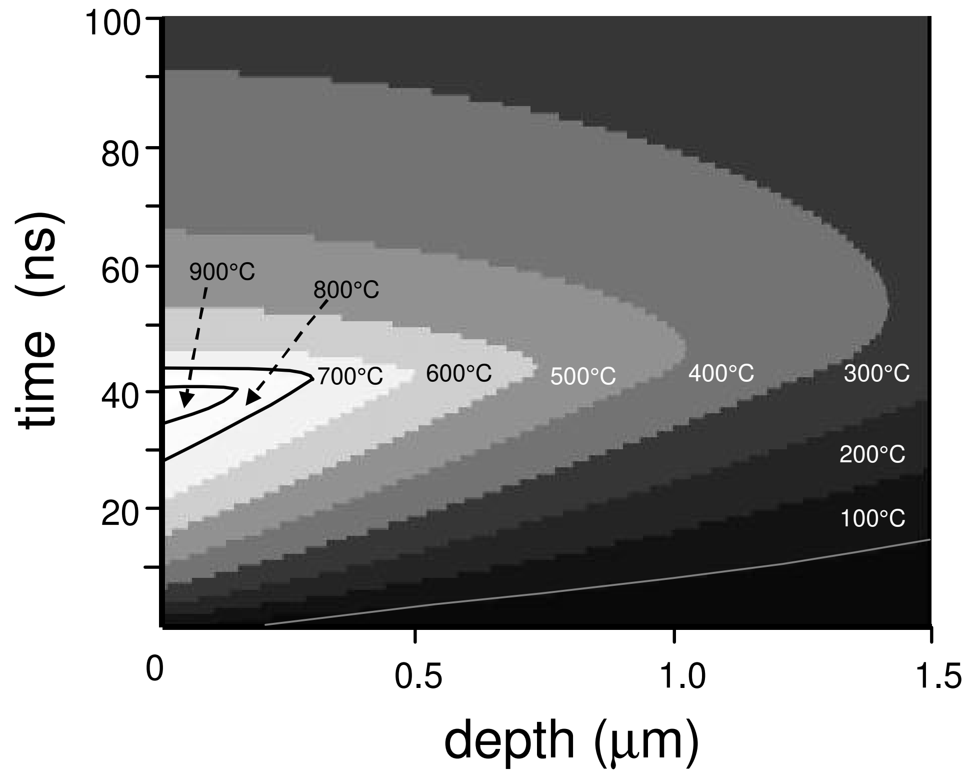

Figure 5–1: A simulated temperature profile for a single 38 ns, 400 mJ/cm^2 pulse from a KrF laser. The temperature rise, coupled with a large temperature gradient across the thickness of the GaN film, occurs in a highly localized heated area that is within 100 nm below the irradiated GaN/sapphire interface (referenced at 0 μm depth).

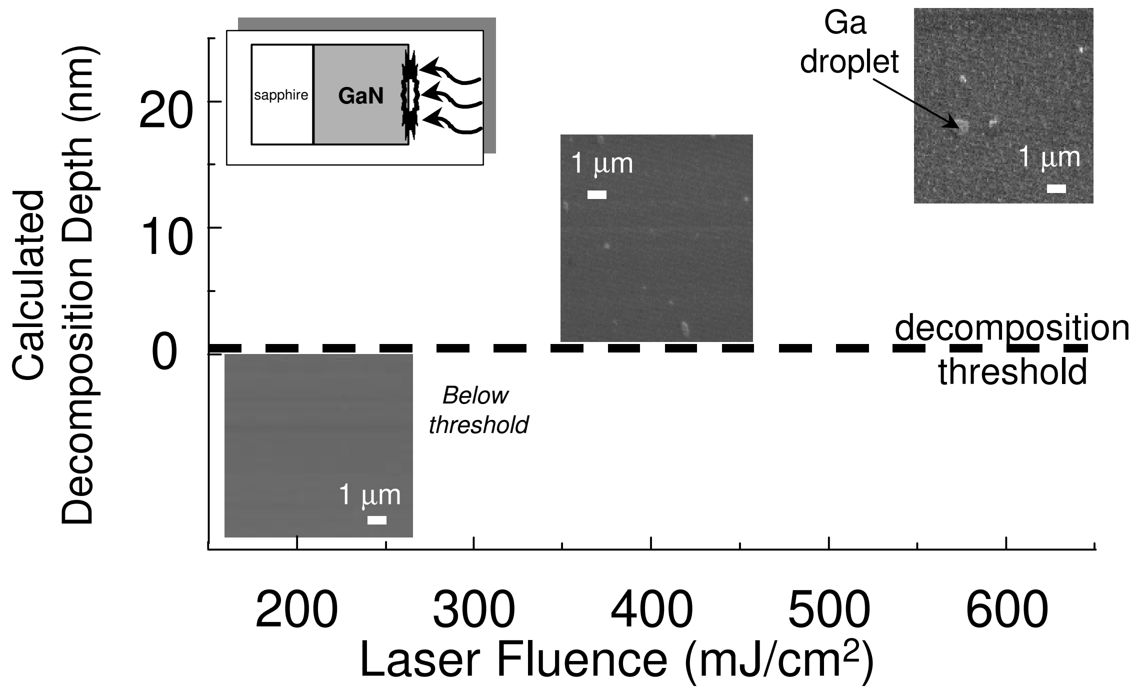

Figure 5–2: GaN surface morphology as a function of laser fluence.

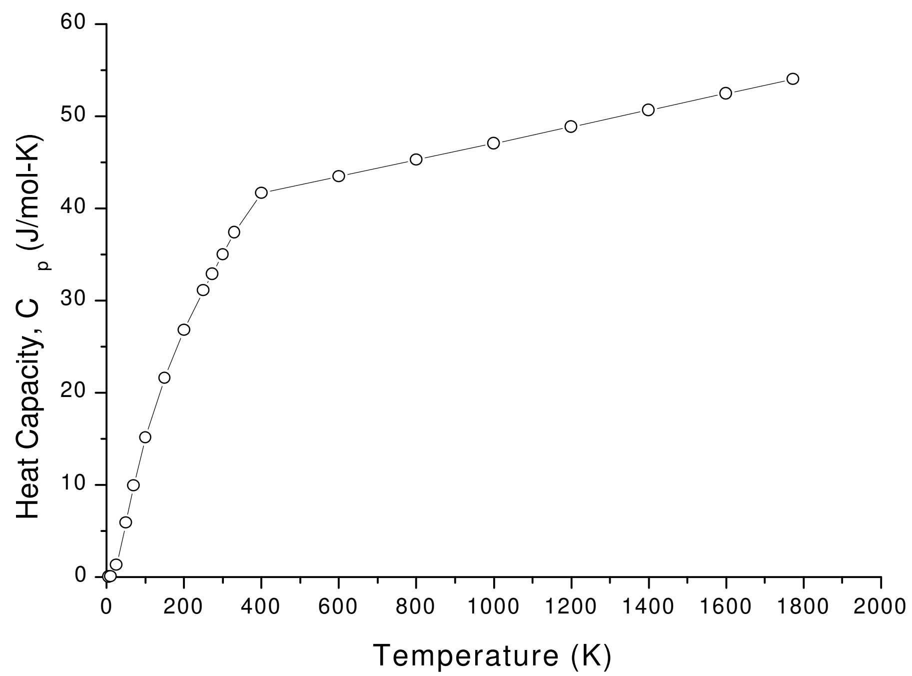

Figure 5–3: Heat capacity for GaN as a function of temperature. (Ref. 103)

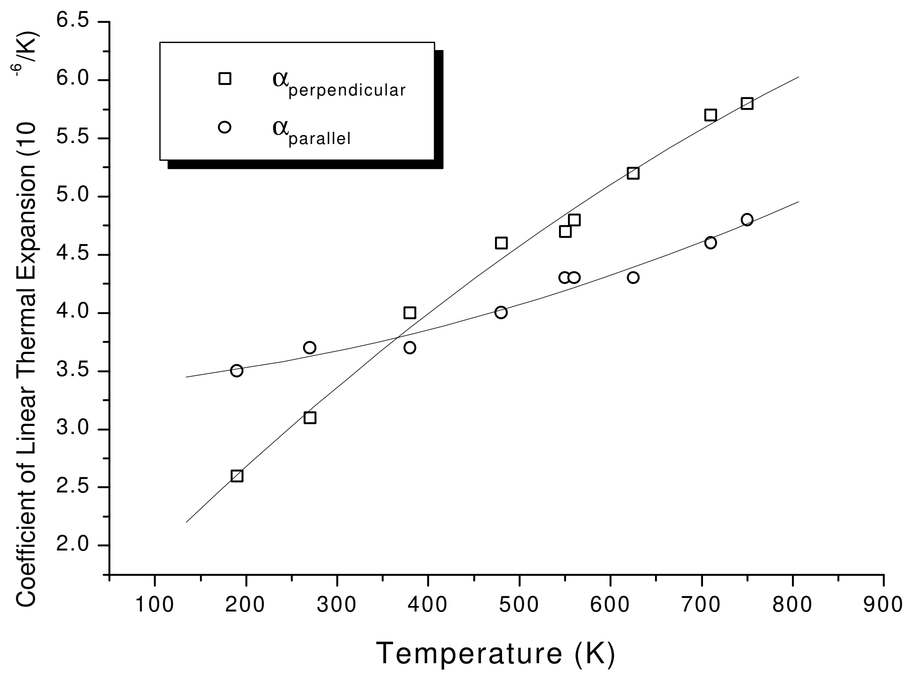

Figure 5–4: Coefficient of thermal expansion for GaN as a function of temperature. (Ref. 104)

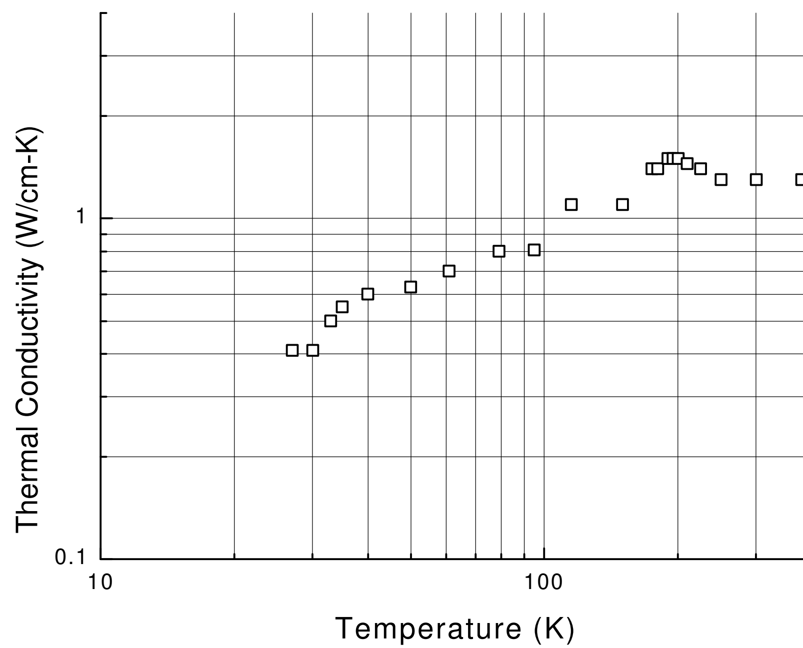

Figure 5–5: Thermal conductivity for GaN as a function of temperature. (Ref. 104)

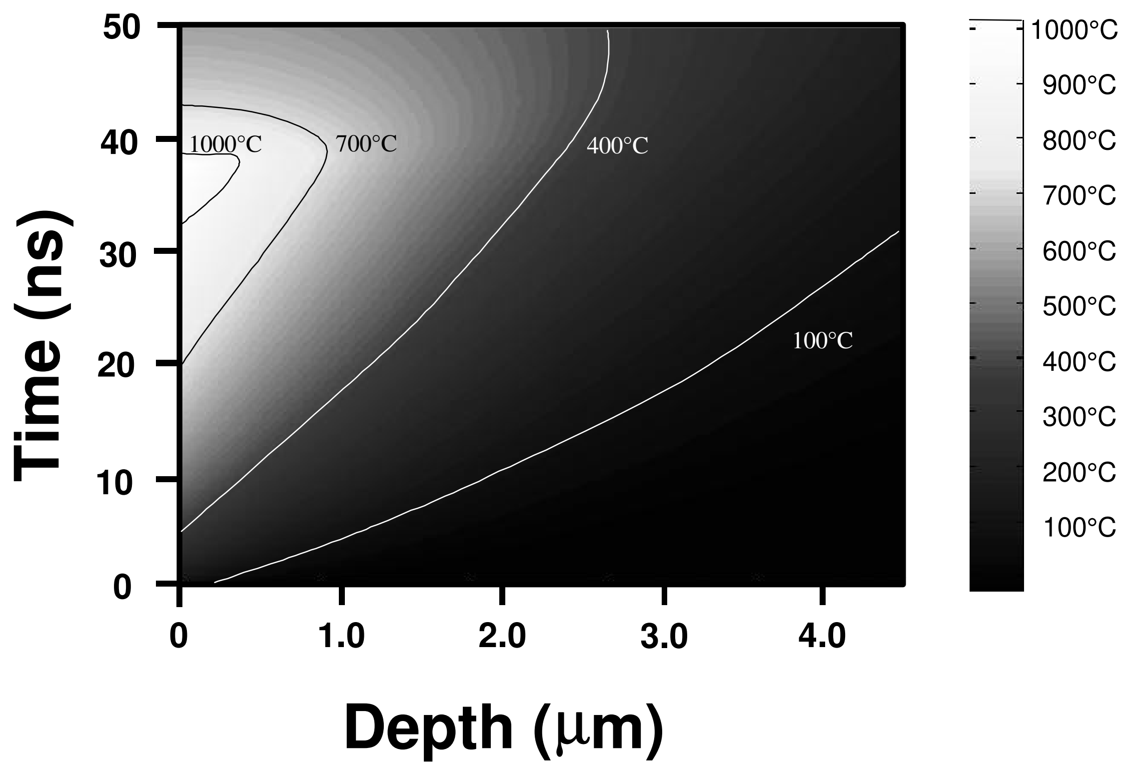

Figure 5–6: Temperature distribution of GaN thin film irradiated on the GaN surface for a fluence of 400 mJ/cm^2. The calculations were done using temperature-independent GaN properties.

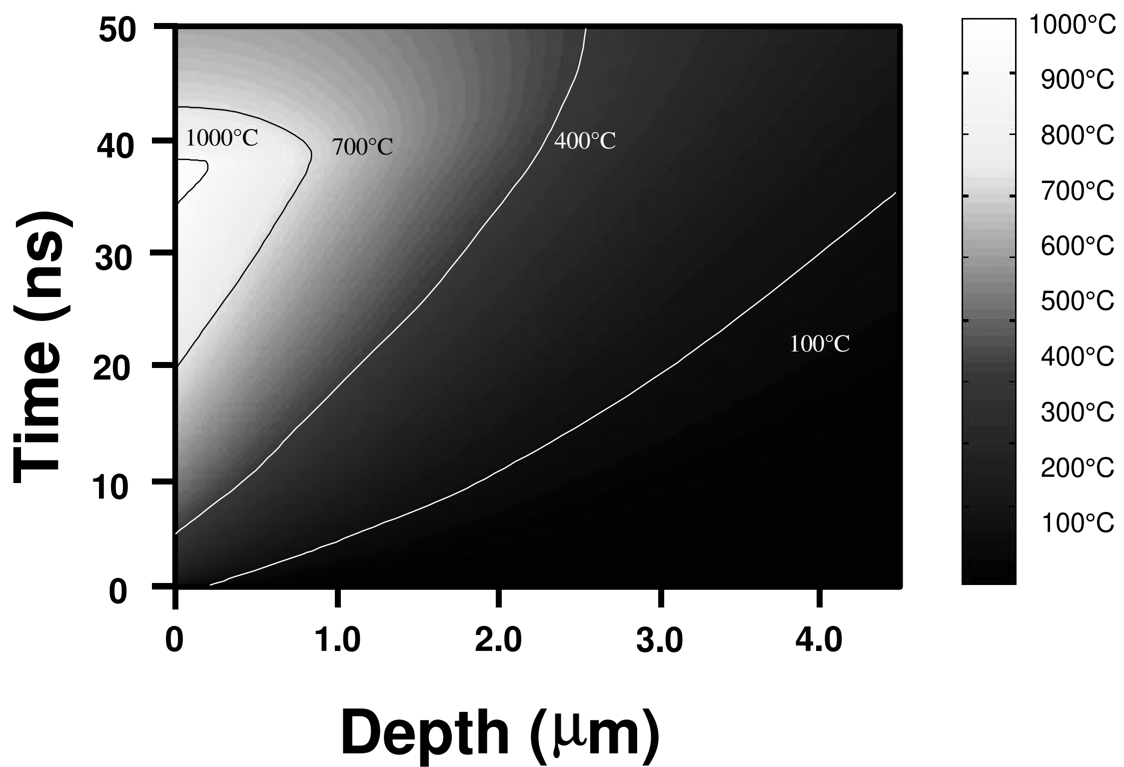

Figure 5–7: Temperature distribution of GaN thin film irradiated on the GaN surface for a fluence of 400 mJ/cm^2. The calculations were done using temperature-dependent GaN properties.

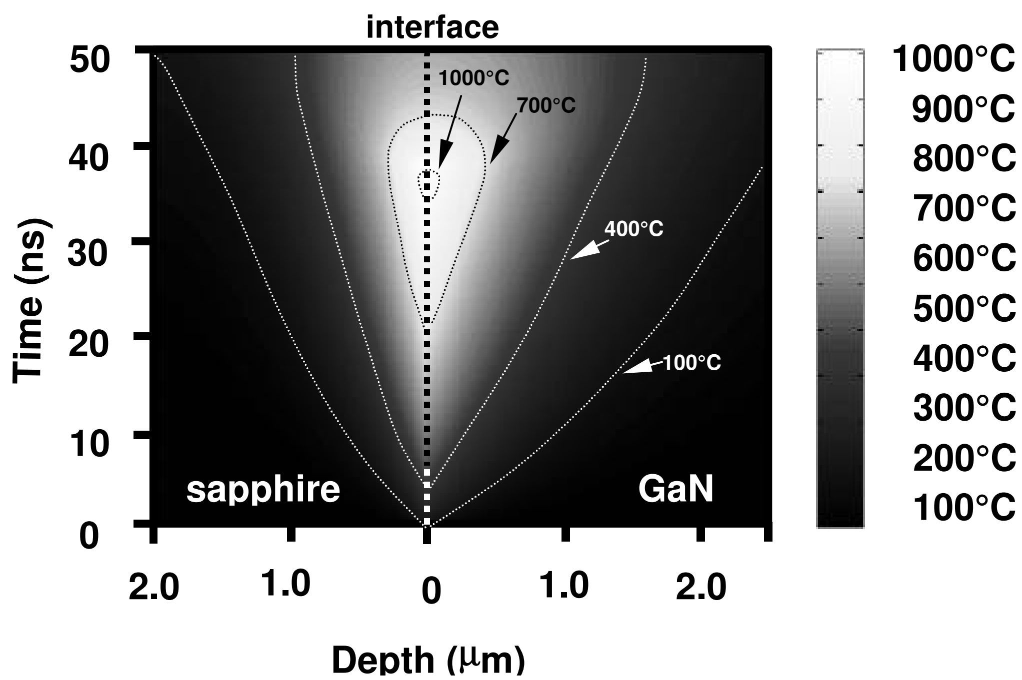

Figure 5–8: Temperature distribution of GaN thin film irradiated at the GaN/sapphire interface for a fluence of 600 mJ/cm^2. The calculations were done using temperature-dependent GaN properties.

Chapter 6 - Thermoelastic Stress Analysis

In order for a laser processing technique to be successfully implemented, it must not degrade the quality of the material being processed. For the laser lift-off and transfer technique to be viable, the laser process should not introduce thermoelastic stresses that may fracture the target material. For the GaN thin-film system, an analysis of the inplane stresses developed during the 38 ns pulsed laser irradiation will be presented. The induced in-plane stress will be compared with the fracture strength of the GaN material as well as the stress introduced due to the decomposition of the GaN and the formation of N_2 gas. The pressure introduced by the N_2 gas may cause the film to fracture at the interface of the GaN/sapphire interface. After the initial thermoelastic analysis, a design criterion will be presented to predict the required GaN thickness in order to minimize the effect of the thermoelastic stress and possible mechanical fracture.

The heating during laser irradiation introduces a non-uniform temperature distribution causing the development of thermoelastic stresses. For the case of the GaN LLO process, the thermoelastic stress is largely due to a non-uniform temperature profile as revealed in the thermal analysis. Consider first a mesh of elements of equal size in an unconstrained continuous body. If the body is heated uniformly with a uniform temperature rise, the elements will expand in equal proportions in space and no stress will develop. For a non-uniform temperature rise, each element will experience a proportional amount of expansion dependent on the temperature of that particular element. In order for the elements to remain a continuous body, each element will be distorted according to the temperature distribution resulting in a developed strain and associated stress within the body.

6.1 - Thermoelastic Stress: Analytical Solution

In a Cartesian orthogonal coordinate system x, y, z, assuming an elastic isotropic medium, the total strains are related to the stresses by Hooke's Law of linear isothermal elasticity:[108,109]

$$\left.\begin{aligned} \varepsilon_{xx} &= \frac{1}{E}\left[\sigma_{xx} - \upsilon\left(\sigma_{yy} + \sigma_{zz}\right)\right] + \alpha T \\ \varepsilon_{yy} &= \frac{1}{E}\left[\sigma_{yy} - \upsilon\left(\sigma_{zz} + \sigma_{xx}\right)\right] + \alpha T \\ \varepsilon_{zz} &= \frac{1}{E}\left[\sigma_{zz} - \upsilon\left(\sigma_{xx} + \sigma_{yy}\right)\right] + \alpha T \end{aligned}\right\} \qquad [6.1\text{–}1]$$

$$\varepsilon_{xy} = \frac{1}{2G}\sigma_{xy} \qquad \varepsilon_{yz} = \frac{1}{2G}\sigma_{yz} \qquad \varepsilon_{xz} = \frac{1}{2G}\sigma_{xz} \qquad [6.1\text{–}2]$$

The shear modulus, G, is related to the Young's modulus, E, and Poisson's ratio ν by:[109]

$$G = \frac{E}{2(1+\upsilon)}$$

and the bulk modulus, k, is related to Poisson's ratio and Young's modulus by: [109]

$$k = \frac{E}{3(1-2\upsilon)}. \qquad [6.1\text{–}3]$$

The stresses can also be expressed in terms of the strains by the following equations: [109]

$$\left.\begin{aligned} \sigma_{xx} &= \lambda e + 2\mu\varepsilon_{xx} - (3\lambda + 2\mu)\alpha T \\ \sigma_{yy} &= \lambda e + 2\mu\varepsilon_{yy} - (3\lambda + 2\mu)\alpha T \\ \sigma_{zz} &= \lambda e + 2\mu\varepsilon_{zz} - (3\lambda + 2\mu)\alpha T \end{aligned}\right\} \qquad [6.1\text{–}4]$$

$$\sigma_{xy} = 2\mu\varepsilon_{xy} \qquad \sigma_{yz} = 2\mu\varepsilon_{yz} \qquad \sigma_{xz} = 2\mu\varepsilon_{xz}$$

where λ and μ are the Lamé constants and are related to E and ν by:

$$\lambda = \frac{\upsilon E}{(1+\upsilon)(1-2\upsilon)} \qquad \mu = \frac{E}{2(1+\upsilon)} = G$$

The above equations are the mathematical descriptions of the stress-strain relationships for a given material. The equations can then be solved by imposing the equations of equilibrium and the strain-displacement relations. The equations of equilibrium in Cartesian coordinates are:[110]

$$\left.\begin{aligned}\frac{\partial\sigma_{xx}}{\partial x}+\frac{\partial\sigma_{xy}}{\partial y}+\frac{\partial\sigma_{xz}}{\partial z}+X=0\\ \frac{\partial\sigma_{xy}}{\partial x}+\frac{\partial\sigma_{yy}}{\partial y}+\frac{\partial\sigma_{yz}}{\partial z}+Y=0\\ \frac{\partial\sigma_{xz}}{\partial x}+\frac{\partial\sigma_{yz}}{\partial y}+\frac{\partial\sigma_{zz}}{\partial z}+Z=0\end{aligned}\right\} \qquad [6.1\text{–}5]$$

where X, Y, Z are the body forces components in the x, y, and z directions, respectively. For the surface heating of a GaN thin film, the system can be modeled as a free flat plate with a temperature variation normal to the surface with the body forces equal to 0. Thus, the strain-displacement relations in rectangular coordinates are:[111]

$$\varepsilon_{xx}=\frac{\partial u}{\partial x} \qquad \varepsilon_{yy}=\frac{\partial v}{\partial y} \qquad \varepsilon_{zz}=\frac{\partial w}{\partial z}$$

$$\varepsilon_{xy}=\frac{1}{2}\gamma_{xy}=\frac{1}{2}\left(\frac{\partial u}{\partial y}+\frac{\partial v}{\partial x}\right)$$

$$\varepsilon_{yz}=\frac{1}{2}\gamma_{yz}=\frac{1}{2}\left(\frac{\partial v}{\partial z}+\frac{\partial w}{\partial y}\right) \qquad [6.1\text{–}6]$$

$$\varepsilon_{zx}=\frac{1}{2}\gamma_{zx}=\frac{1}{2}\left(\frac{\partial w}{\partial x}+\frac{\partial u}{\partial z}\right)$$

with u, v, w being the components of the displacement vector in the x, y, z directions, respectively.

For the case in which the effect of stress is due solely to the temperature effects the following boundary conditions apply:[111]

$$\left.\begin{aligned}\sigma_{xx}n_x+\sigma_{xy}n_y+\sigma_{xz}n_z&=0\\\sigma_{xy}n_x+\sigma_{yy}n_y+\sigma_{yz}n_z&=0\\\sigma_{xz}n_x+\sigma_{yz}n_y+\sigma_{zz}n_z&=0\end{aligned}\right\} \qquad [6.1\text{–}7]$$

where n_x, n_y, n_z are the direction cosines normal to a principal plane in the x, y, z direction respectively.

Lastly, the compatibility equations can be expressed in terms of the stress components and have been shown to be:[112]

$$\left.\begin{aligned}(1+\upsilon)\nabla^2\sigma_{xx}+\frac{\partial^2\Theta}{\partial x^2}+\alpha E\left(\frac{1+\upsilon}{1-\upsilon}\nabla^2 T+\frac{\partial^2 T}{\partial x^2}\right)&=0\\(1+\upsilon)\nabla^2\sigma_{yy}+\frac{\partial^2\Theta}{\partial y^2}+\alpha E\left(\frac{1+\upsilon}{1-\upsilon}\nabla^2 T+\frac{\partial^2 T}{\partial y^2}\right)&=0\\(1+\upsilon)\nabla^2\sigma_{zz}+\frac{\partial^2\Theta}{\partial z^2}+\alpha E\left(\frac{1+\upsilon}{1-\upsilon}\nabla^2 T+\frac{\partial^2 T}{\partial z^2}\right)&=0\\(1+\upsilon)\nabla^2\sigma_{xz}+\frac{\partial^2\Theta}{\partial x\partial z}+\alpha E\frac{\partial^2 T}{\partial x\partial z}&=0\\(1+\upsilon)\nabla^2\sigma_{yx}+\frac{\partial^2\Theta}{\partial x\partial y}+\alpha E\frac{\partial^2 T}{\partial x\partial y}&=0\\(1+\upsilon)\nabla^2\sigma_{yz}+\frac{\partial^2\Theta}{\partial y\partial z}+\alpha E\frac{\partial^2 T}{\partial y\partial z}&=0\end{aligned}\right\} \qquad [6.1\text{–}8]$$

where $\Theta = \sigma_{xx}+\sigma_{yy}+\sigma_{zz}$.

The problem of a free flat plate, in this case the plate being GaN, can be solved using the equations of equilibrium, the equations of compatibility and the above boundary conditions. For a free plate with a temperature variation through the thickness, the stress components in the x- and y-directions are a function of the thickness of the film:

$$\sigma_{xx}=\sigma_{yy}=f(z) \qquad \text{and} \qquad \sigma_{zz}=\sigma_{xz}=\sigma_{yz}=\sigma_{zy}=0$$

where the shear stress components are set to zero.

The solution for this problem can be been shown to be:[113]

$$\sigma_{xx} = \sigma_{yy} = \frac{1}{1-\nu}\left\{-\alpha ET + \frac{1}{2h}N_T + \frac{3z}{2h^3}M_T\right\} \text{ and } \sigma_{zz} = \sigma_{xy} = \sigma_{yz} = \sigma_{zx} = 0 \qquad [6.1\text{–}9]$$

where $N_T = \alpha E\int_{-h}^{h} Tdz$ and $M_T = \alpha E\int_{-h}^{h} Tzdz$.

For the specific case in which the temperature of an exposed surface is suddenly raised to T_a, the maximum stress occurs at $t=\tau_0$ and is represented as:[114]

$$(\sigma_{xx})_{max} = -\frac{\alpha ET_a}{1-\upsilon}. \qquad [6.1\text{–}10]$$

For GaN in which E = 295 GPa,[115] $\alpha = 3.66 \times 10^{-6}$, and $\nu = 0.23$,[116] the maximum stress calculated at 1300 K is a compressive stress of ~ 1.6 GPa.

6.2 - Thermoelastic Stress: Finite Element Analysis

A more thorough examination of the stress distribution during the laser irradiation will now be presented. The analysis follows the calculations done previously in determining the temperature distribution an incident beam onto the GaN and GaN/sapphire configuration. For the thermoelastic calculations, the same parameters used in the thermal profile calculations were used in addition to the temperature dependence of the Young's modulus and thermal expansion coefficient on temperature for sapphire. The COSMOS/M® FEA program was again used to calculate the thermoelastic inplane stresses at time steps of 19, 24, 29, 38, and 50 ns.

A preliminary calculation for the thermoelastic stress developed for a 400 mJ/cm^2 pulse on the surface of a GaN thin film was performed using the FEA method. Setting the maximum temperature at the surface of the GaN film to 1200°C resulted in a calculated compressive stress of 1.7 GPa, in excellent agreement with the analytical result. Using a 38 ns flat-top pulse for the laser temporal profile and the temperature distribution

obtained in the previous chapter (Figure 5–7) a maximum compressive stress of ~2.6 GPa is obtained. Figure 6–1 shows the in-plane stress profile as a function of depth away from the GaN surface. The magnitude of the stress is found to increase with irradiation time and is a maximum at $t = \tau_0 = 38$ ns. At the end of the laser irradiation, the maximum inplane compressive stress was found to shift below the surface of the GaN thin film. The shift corresponds to the thermoelastic stress wave generated by the rapid heating and cooling from the laser pulse.

Figure 6–2 shows the plot of the in-plane stresses that develop for a 600 mJ/cm^2 incident laser fluence at the GaN/sapphire interface. The figure shows a snapshot of the stress development again as a function of time for τ = 19, 24, 29, 38, and 50 ns. As the time of irradiation increases, it was found that the compressive stress at the interface reaches a maximum of ~ 7.6 GPa at τ = 38 ns coinciding with the peak temperature rise. Similar to the calculated temperature contour, the stress profile is also localized to the GaN/sapphire interface and approaches zero stress at a depth of ~ 2 μm away from the interface.

6.3 - Design Constraints for Laser Lift-off

One concern in the laser processing is the inadvertent delamination of the GaN from the sapphire due to the GaN decomposition and laser induced in-plane compressive stress. At the onset of decomposition, the formation of nitrogen gas within the interface is predicted from thermodynamics. The presence of the trapped gas will cause a small separation between the film and substrate to develop. At a given critical stress, the film may buckle and release from the substrate as shown schematically in Figure 6–3 which can lead to mechanical failure of the thin film. The critical stress for delamination can be

determined by modeling the delaminated region as a clamped circular plate. Whether this compressive stress will cause delamination of the GaN film during the LLO process will be examined next.

Due to the decomposition of the GaN interface, the biaxial compression introduced during the laser processing can cause the deformation and possible delamination of the GaN film from the sapphire substrate. If a maximum compressive stress of 7.6 GPa is considered from the FEA analysis then the plastic deformation of the GaN thin film should not occur since the yield strength of GaN is 15 GPa.[115] On the other hand, if the generation of N_2 inclusions is considered then the pressure formed from these inclusions or "bubbles" may be large enough to cause the film to fracture. This blistering effect has been observed in hydrogen implanted Si during thermal annealing.[117]

In a simple first order estimation and neglecting plasma formation, the pressure build-up from N_2 bubble generation at the GaN/sapphire interface from GaN decomposition may be modeled using the ideal gas law. For a laser spot size radius of 1.5 mm, the decomposition of GaN at 1000°C will generate a bubble pressure of ~ 85 MPa assuming a 20 nm GaN absorption depth decomposes. This pressure is less than the value predicted by the thermoelastic stress developed during LLO.

Another path to fracture, resulting from mode I deformation,[118] may be due to a crack opening at the film surface under a tensile stress applied in the normal direction. The tensile stress is caused by the deformation due to buckling (Figure 6–3). The critical defect dimension, a, for fracture can be solved from the basic equation for fracture toughness:

$$K_{Ic} = \sigma\sqrt{\pi a} \qquad [6.3\text{–}1]$$

where K_{Ic} is the GaN plane-strain fracture toughness. An applied compressive stress, σ = 1 GPa, is taken from Figure 6–2. This value was used instead of the peak thermoelastic stress by assuming the flaw is on the surface of the GaN and the applied stress is the thermoelastic stress near this surface. The assumption is valid since the peak thermoelastic stress is highly localized at the GaN/sapphire interface and the crack feature is assumed << the thickness of the film, *t*.

For K_{Ic} = 0.8 MPa$\sqrt{m}$,[119] a critical flaw size of ~20 nm would cause fracture along the direction normal to the film for an applied stress of 1 GPa. This failure will occur if the film is given a chance to buckle when the GaN decomposes during the LLO process. The addition of a "stiffener" layer would help to constrain the film from buckling in the normal direction and prevent possible mechanical failure. It has been shown that the application of a "stiffener" or constraining substrate will prevent blistering effects for ion-cut Si layer transfer.[120]

The buckling of a thin film will cause a release of internal energy with the advancement of the interface crack. A critical stress, S_{cr}, for buckling can be model as a flat circular plate and shown to be: [121, 122]

$$S_{cr} = \left[\frac{KE}{12\left(1-\upsilon^2\right)}\right]\left(\frac{a}{t}\right)^2 \qquad [6.3\text{–}2]$$

where *K* is 14.68 for a clamped-circular plate.

A plot of the GaN film thickness as a function of the laser spot size from equation 6.3–2 is shown in Figure 6–5. Assuming the entire area irradiated during LLO decomposes, for a typical laser beam spot size diameter of 3 mm, a GaN thickness of ~ 20 µm is needed in order to prevent buckling. For a thickness less than 20 µm the GaN

film is predicted to buckle and possibly fracture. If a different supporting layer such as Si is used instead of GaN then a different process curve is found. Assuming the mechanical properties of the bond interface is similar to that of single crystal Si, the model may be modified using a Si support. By using the mechanical properties of Si in equation 6.3–4, the predicted supporting substrate thickness is greater than GaN due to the smaller Young's modulus of Si. Thus, a standard Si wafer (thickness 0.5 mm) can be used as a support to transfer entire 2-inch diameter GaN thin films from sapphire onto Si in a single laser pulse.

Figure 6–6 shows a SEM micrograph of the GaN surface of a 1 μm thick film. The GaN delaminated from the sapphire at the irradiated region while the area adjacent to the exposed area remained intact. The patterned features were transferred onto the GaN surface from a mask printed on the backside of the sapphire substrate (inset). When a supporting substrate with a thickness great enough to prevent fracture is used, as described in the LLO process, the films have separated from the sapphire intact without cracking during the laser process. The information obtained from the predicted temperature rise, the thermoelastic stress and support layer thickness can then be combined to design a process to separate GaN thin films from sapphire growth substrates.

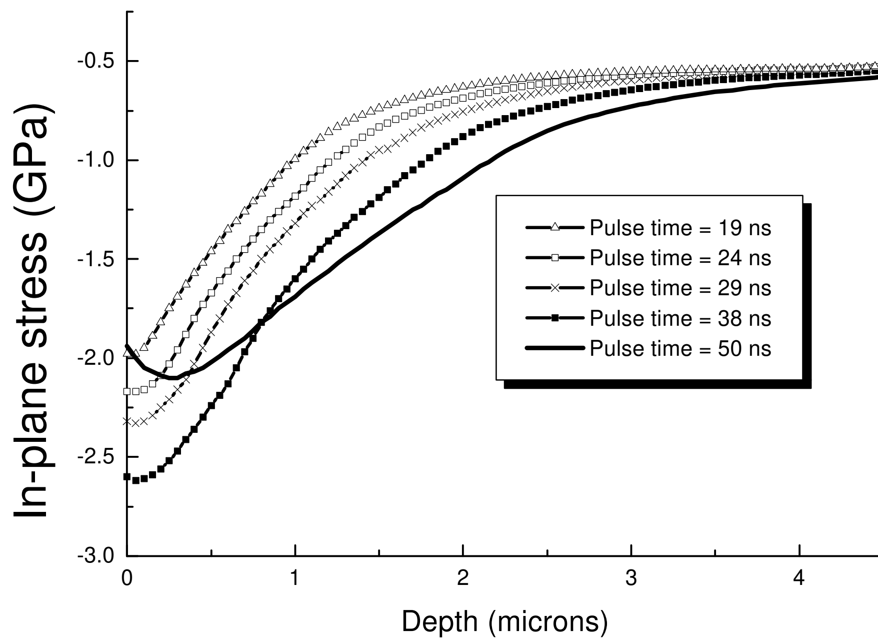

Figure 6–1: Thermoelastic stress development of KrF pulsed excimer surface irradiated GaN.

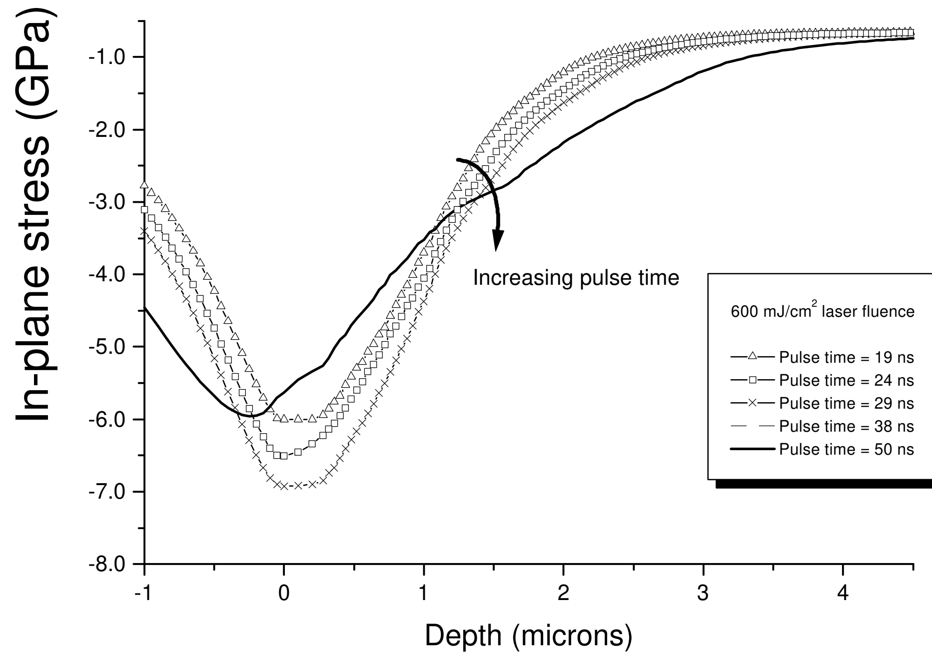

Figure 6–2: Thermoelastic stress development of KrF pulsed excimer surface irradiated GaN.

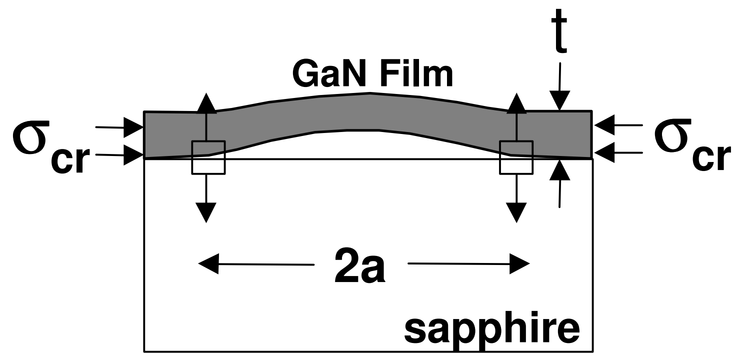

Figure 6–3: Schematic the buckling phenomena for a GaN thin film.

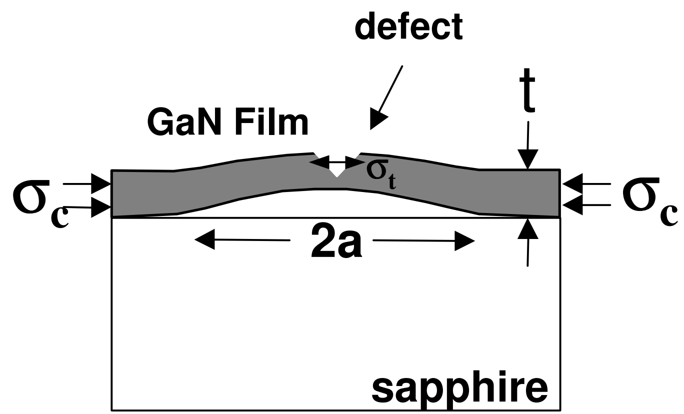

Figure 6–4: Buckled GaN film showing a defect where fracture can occur.

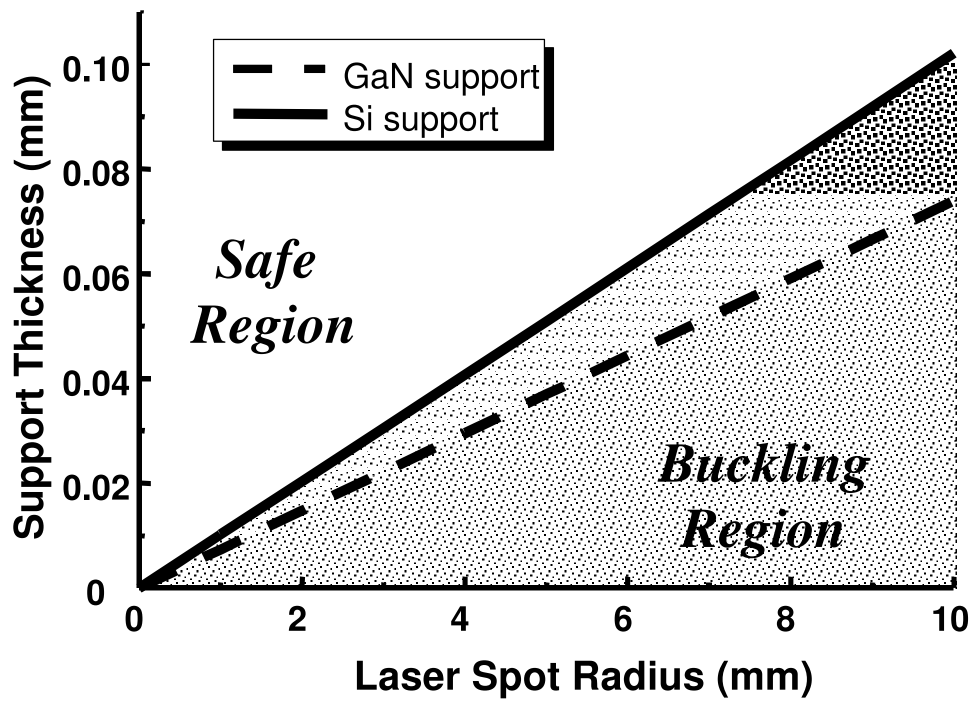

Figure 6–5: Substrate support thickness for increasing laser irradiated spot size. The predicted safe region for a GaN or Si support is given.

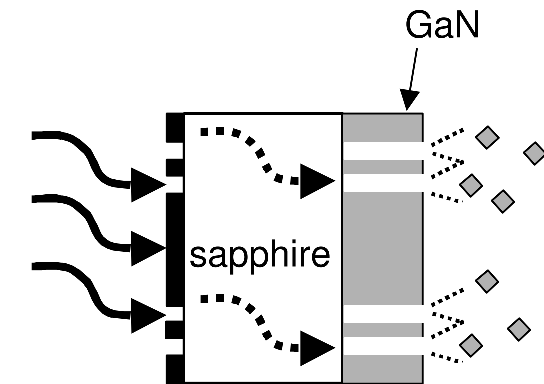

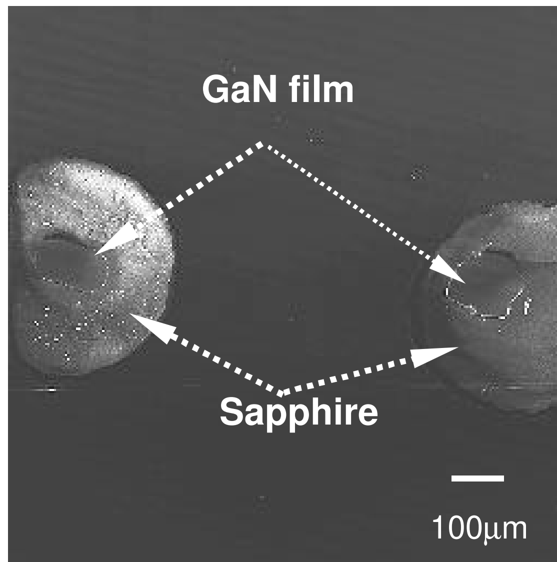

Figure 6–6: SEM surface morphology of backside irradiated GaN/sapphire. The surface pattern are generated from the backside mask on the sapphire.

Chapter 7 - Fabrication of Thin-film GaN Membranes

Following the initial prescription described in the integration methodology outlined in the introduction: a lift-off process for layer transfer of a thin film must not adversely effect the properties of the transferred film. One such way to test this criterion for LLO is to create free-standing GaN membranes. The characterization of the membranes can still give structural, optical and electrical information that may be directly compared to the film before laser processing, without the effect of the original growth substrate.

In addition, the removal of the supporting substrate by LLO, required in a thin-film layer transfer process, eliminates the influence of a dissimilar substrate during characterization. Free-standing GaN membranes can then be examined to determine the effect of the sapphire constraint on the GaN materials properties.[123,124] The following chapter describes the fabrication of GaN-based free-standing membranes and the effect of the LLO process on the structural, optical and electrical characteristics of GaN thin films and GaN-based device structures before and after lift-off.

7.1 - Free-standing Thin-film GaN Membrane Fabrication

The bonding process used to created free-standing membranes was similar to the process described previously. A Si (001) wafer was bonded to the surface of the GaN thin film using a low-melting temperature wax forming a sapphire/GaN/wax/Si structure. The LLO process, followed by a 40°C anneal, was used to remove the sapphire. Free-standing GaN membranes were then fabricated by dissolving the wax bond in acetone allowing the GaN to float off the supporting Si substrate. The GaN was then transferred onto a

supporting frame to allow for characterization by photoluminescence (PL) on either surface of the 5 mm × 5 mm membranes.

7.2 - Free-standing Thin-film InGaN LED Membrane Fabrication

For the fabrication of InGaN-based LEDs, InGaN multiple quantum well (MQW) structures were grown by organometallic chemical vapor deposition (OMCVD) on c-face sapphire substrates. First, a 4 μm thick Si-doped GaN layer was deposited followed by five $In_{0.1}Ga_{0.9}N$ quantum wells with a well width of 3.5 nm and a barrier width of 7 nm. A 700 nm thick Mg-doped GaN layer was subsequently grown on top of the MQW active region. After OMCVD growth, mesas were formed by etching into the Si-doped GaN layer using chemically assisted ion beam etching (CAIBE).[125] Finally Ti/Au metal contacts were deposited on the p-doped GaN:Mg layer and on the exposed n-doped GaN:Si layer for the lateral electrical connection.[126]

The pre-processed InGaN MQW LED structures were then bonded onto the surface of a boron doped, p-type Si (001) wafer using an ethyl cyanoacrylate (C_6-H_7-NO_2)-based adhesive, forming a sapphire/LED/adhesive/Si structure. Liftoff and transfer of the LED structures from sapphire onto the receptor Si substrate was accomplished using a single 600 mJ/cm^2 laser pulse directed through the transparent sapphire substrate. Following the laser irradiation, a low-temperature (T = 40°C) anneal completed the separation process by melting the Ga-rich interface. By using this two-step process, films up to 1 cm^2 in area were successfully transferred by rastering a 0.03 cm^2 beam spot across the entire sample. After liftoff and transfer of the LED device onto the supporting Si substrate, the LED/adhesive/Si structure was immersed in acetone to dissolve the

adhesive bond and release the LED, creating a free-standing membrane. The process flow for creating free-standing membranes and LED structure is shown in Figure 7–1.

7.3 - GaN Membrane Results

Similar to the transferred GaN onto Si using epoxy bonding, the XRC analysis for the transferred GaN thin films had no measurable structural degradation. The measured full-width at half maximum (FWHM) of the GaN 0002 reflection showed no broadening after separation from the sapphire substrate indicating the film had not suffered mechanical damage during the laser processing. The surface morphology of the exposed GaN interface was characterized by AFM. Figure 7–2 shows an AFM scan of a 20 μm × 20 μm area of the former GaN interface. The scan shows a relatively smooth surface morphology with a measured surface roughness of approximately 24 nm (rms).

Characterization of the optical quality for the separated GaN films was performed using low-temperature (4 K) PL. For these measurements, 3 μm thick GaN membranes were measured and compared to the same GaN formerly on sapphire. Figure 7–3 shows a SEM micrograph of a typical free-standing GaN membrane. Figure 7–4 shows the donor-bound exciton (DX) peak of the GaN films before and after separation from the sapphire substrate. The measured FWHM of the DX peaks after separation did not show appreciable broadening indicating no detectable optical degradation of the GaN films.

A DX peak red-shift was observed for the GaN membrane compared to the GaN on sapphire. This shift can be interpreted as a release of the compressive biaxial stress on the GaN film, introduced during the growth process,[127] when the substrate constraint is removed. The measured red-shift of ~10 meV for the GaN membrane after separation corresponds to a biaxial compressive stress of approximately 0.4 GPa. The resulting peak

position of the free-standing membrane matches well with that of stress-free GaN thin films grown on bulk GaN substrates.[127]

Similar analysis of the exposed former interface shows a largely attenuated DX peak compared to the original GaN on sapphire (Figure 7–5). The lower peak intensity is attributed to the high density of defects commonly found at the GaN/sapphire interface due to the lattice and thermal expansion coefficient mismatch. It is possible however, as will be discussed later, to remove the exposed interfacial defects and improve the luminescence quality of the GaN film.

7.4 - InGaN LED Membrane Results

As a further test of the LLO process, the effects of the laser process on the LED electrical and electroluminescence characteristics were analyzed. First, the Ga metal on the exposed device backside was removed with HCl and the membranes were then transferred onto a quartz substrate. The transfer allowed the membranes to be turned over and rigidly supported for probing of the original front-side metal contact pads.

Current-voltage (I-V) measurements before and after separation from the sapphire substrate were made to determine the effect of the LLO on the diode junction. Figure 7–6 shows the I-V characteristics for a 20 μm × 500 μm InGaN MQW LED measured from the top n- and p-contact pads. The measurement reveals no discernable change after separating the InGaN LED from sapphire compared to an adjoining device fabricated on the same substrate. Had the device experienced micro-cracking due to a thermal shock, or excessive heating during the laser process, the LED membrane would have shown poor diode behavior or a higher turn-on voltage.

Figure 7–7 exhibits the pulsed (1 μs pulse-width with a 10 kHz repetition frequency) light output vs. current characteristic for a series of three InGaN MQW LEDs before and after sapphire substrate removal. The light output, measured through the quartz substrate using a calibrated Si p-i-n-detector, after LLO was approximately 4 mW at 100 mA. Above 5 mA, the output shows a nearly linear rise with an external quantum efficiency, $\eta_E \sim 1.3\%$. Compared to the light output of the LED devices on sapphire ($\eta_E \sim 1.7\%$) the external quantum efficiency was slightly reduced after liftoff. This discrepancy may be due to differences in the light out-coupling efficiency, or to residual absorption or light scattering from the decomposed surface layer at the former GaN/sapphire interface. Figure 7–8 shows the room-temperature emission spectra of the InGaN MQW LEDs measured at a 10 mA dc forward current before and after laser liftoff. The peak emission wavelength for the InGaN LED membrane was at 389 nm with a spectral full-width at half maximum (FWHM) of 10 nm. Neither the emission wavelength nor the spectral width changed after substrate removal indicating the optical properties of the InGaN heterostructure did not degrade following the LLO process. Low-temperature measurements were not performed to confirm the absence of residual-stress relief since the devices showed no degradation due to the LLO. The InGaN MQW LED room-temperature emission spectra effectively demonstrate the potential for using LLO to create free-standing GaN-based thin-film devices

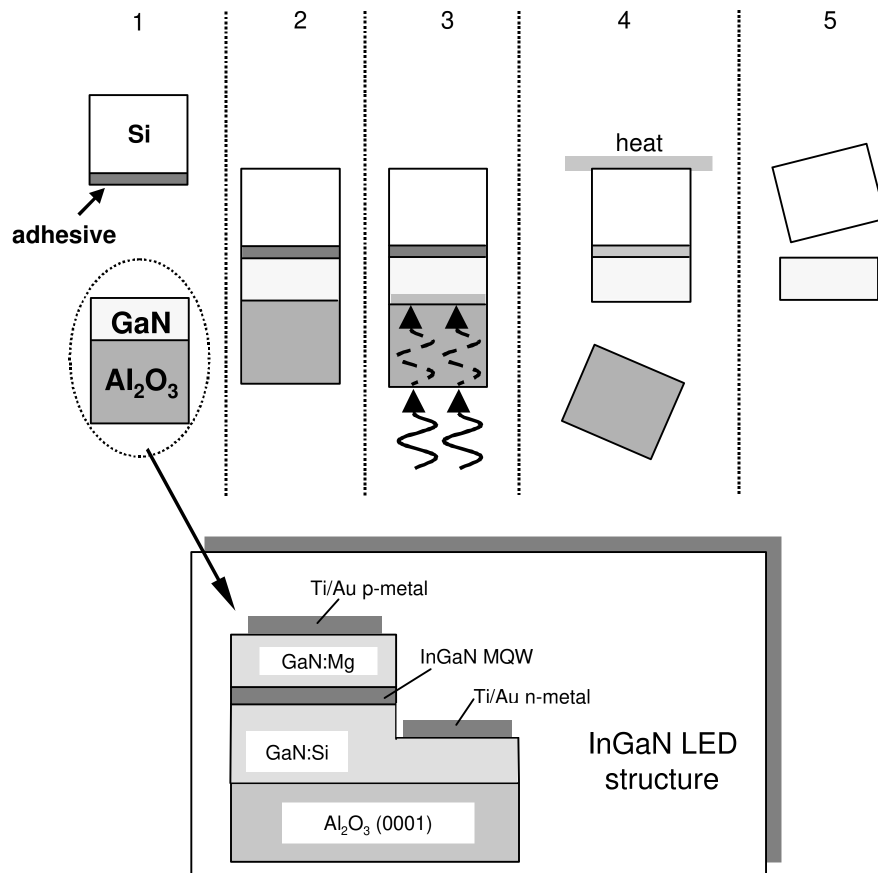

Figure 7–1: Process flow for fabrication of InGaN LED membranes: 1) Starting material - pre-fabricated InGaN MQW LED/sapphire and Si supporting substrate, 2) Bond InGaN MQW LED/sapphire onto Si supporting substrate, 3) KrF laser irradiation of the sapphire/InGaN MQW LED/adhesive/sapphire structure through the transparent sapphire substrate, 4) Heat post-laser processed structure above melting point of Ga to release sapphire substrate, and 5) Immerse InGaN MQW LED/adhesive/Si structure in solvent to release LED membrane. The inset shows the pre-fabricated InGaN MQW well structure processed on the sapphire substrate.

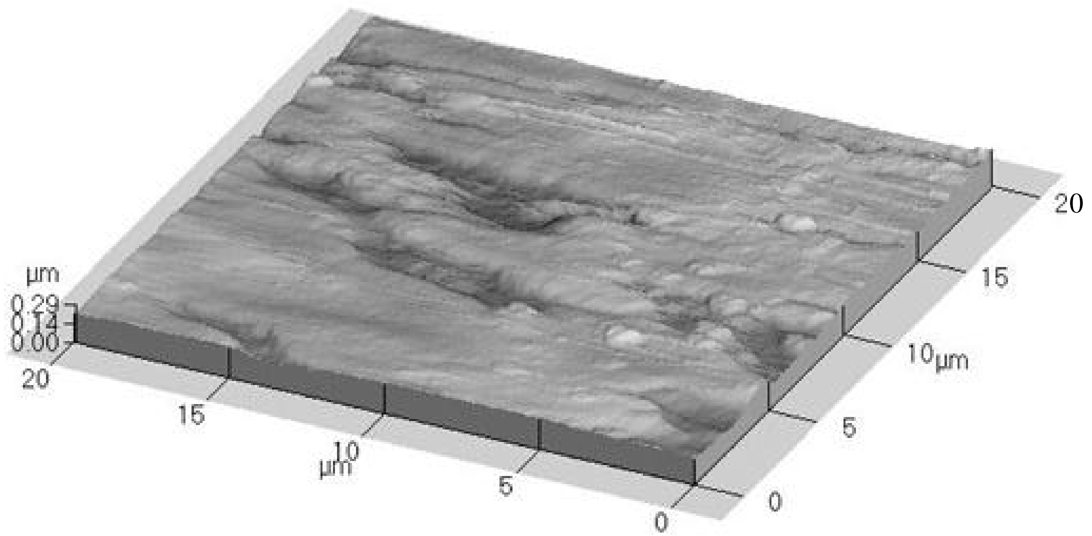

Figure 7–2: AFM scan of a 20 µm × 20 µm area of the former GaN interface. The scan shows a relatively smooth surface morphology with a measured surface roughness of approximately 24 nm (rms).

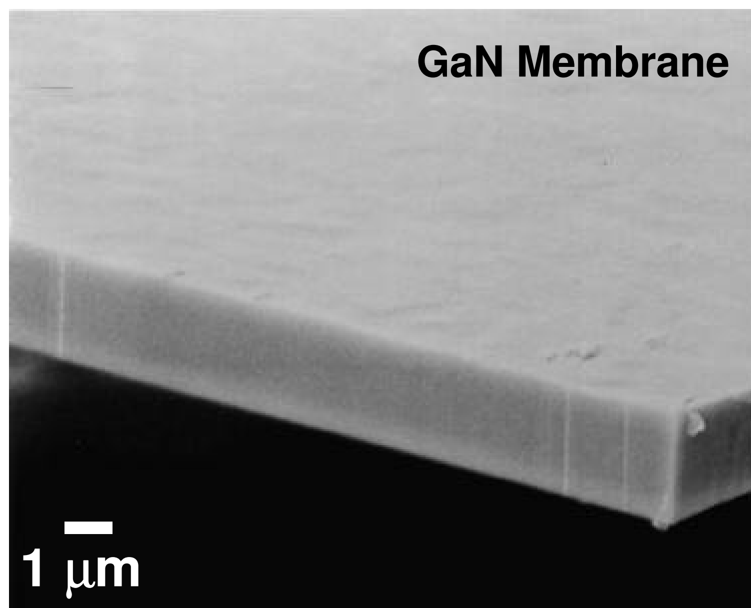

Figure 7–3: SEM micrograph of a 3 μm thick free-standing GaN membrane.

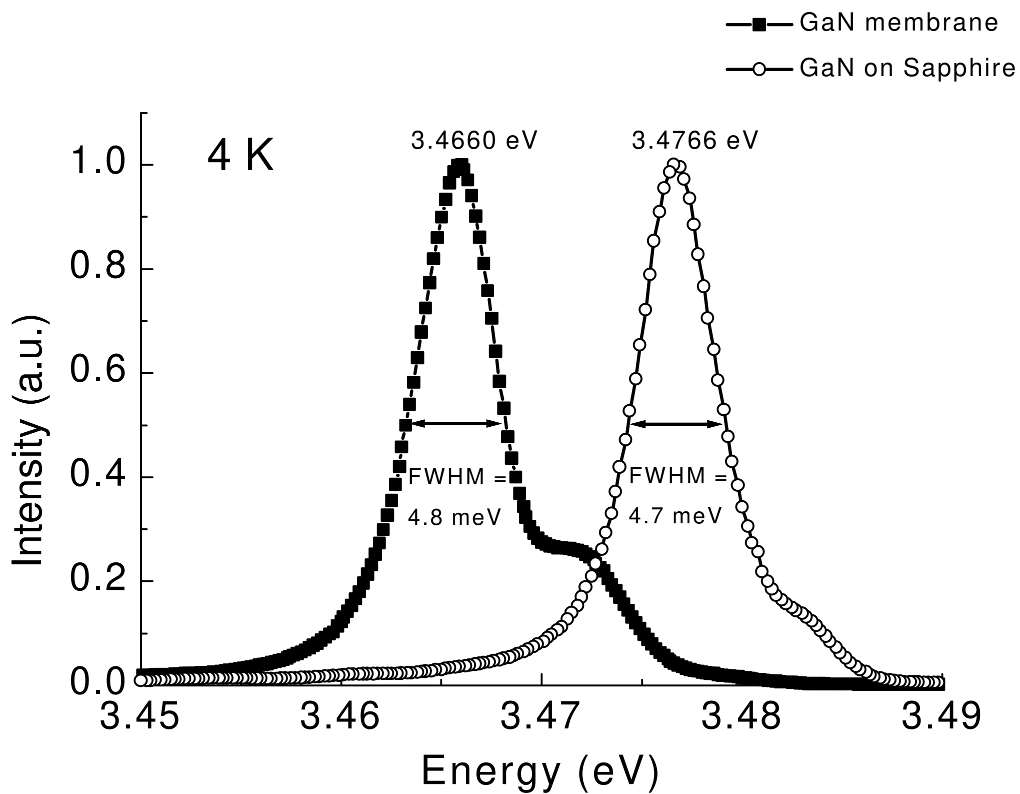

Figure 7–4: Low-temperature (4 K) PL spectra for GaN/sapphire and GaN membranes. The measured FWHM of the DX peaks after separation did not show appreciable broadening, indicating no detectable optical degradation of the GaN films. The measured red-shift of ~10 meV for the GaN membrane corresponds to a biaxial compressive stress relief of approximately 0.4 GPa after separation of the GaN from sapphire.

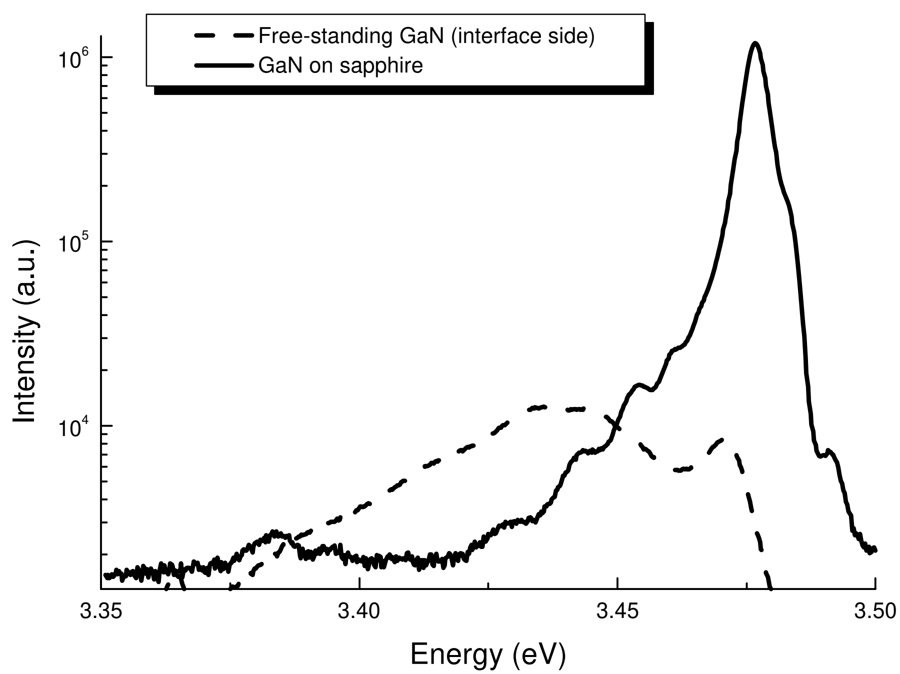

Figure 7–5: Low-temperature (4 K) PL spectra for GaN/sapphire and GaN membranes

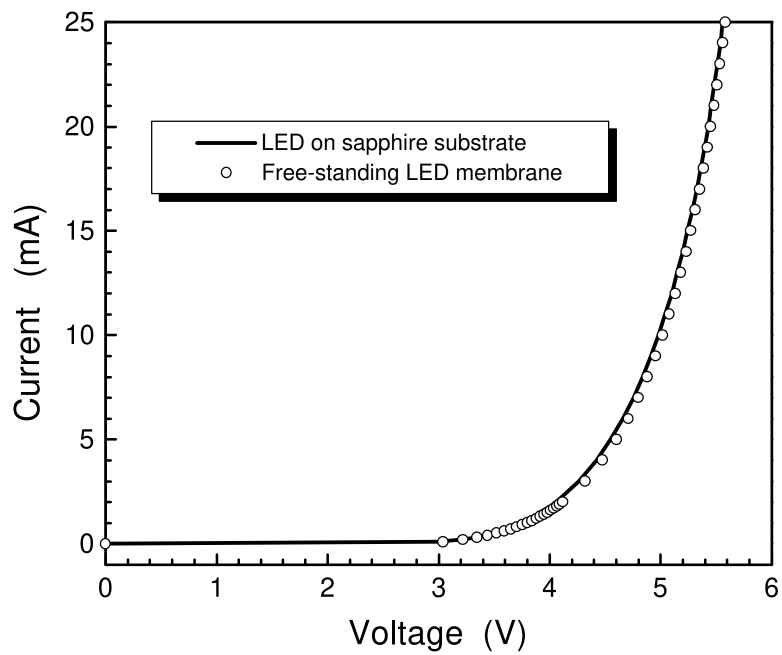

Figure 7–6: DC current-voltage characteristics for a 20 μm × 500 μm InGaN multiple quantum well (MQW) LED membrane and LED on sapphire. The threshold voltage showed no change before and after LLO from the sapphire growth substrate.

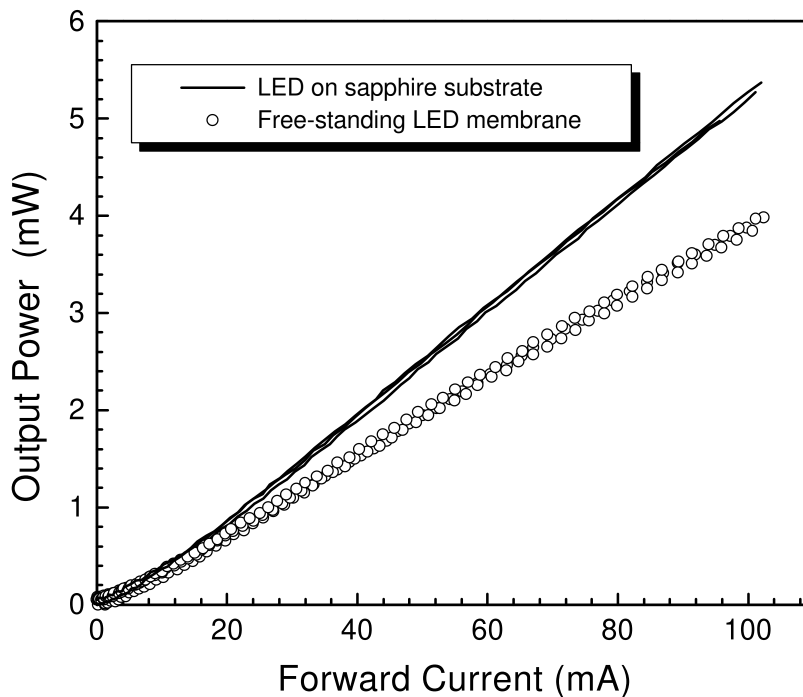

Figure 7–7: Pulsed (1% duty cycle) light output vs. current characteristic for a series of three InGaN LED membranes before and after sapphire substrate removal. The light output of the LED membranes was 4 mW at a 100 mA forward current, corresponding to an external quantum efficiency of ~1.3%. The slight attenuation of the power output for the LED membrane compared to the LED on sapphire is due in part to the light being measured through a quartz supporting substrate for the LED membrane.

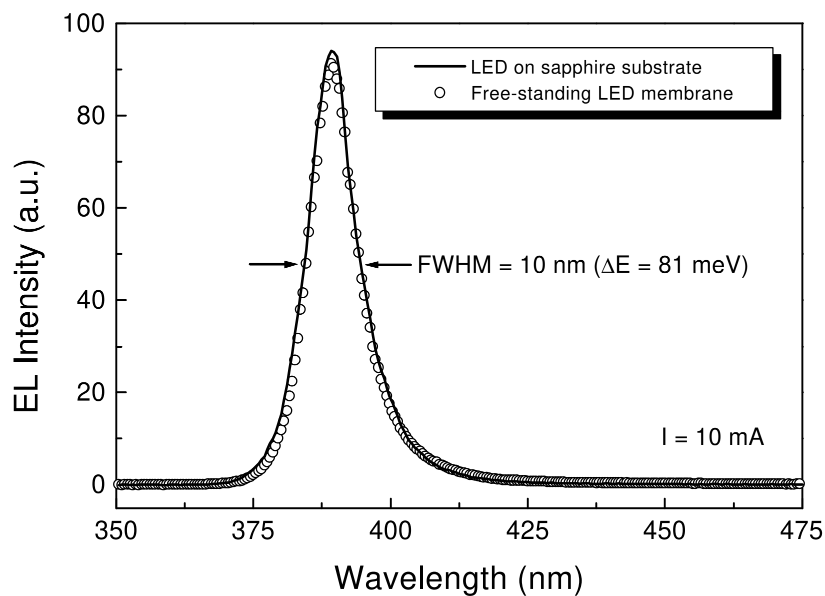

Figure 7–8: Room-temperature emission spectra for the InGaN MQW LED before and after sapphire substrate separation measured at 10 mA dc forward current. The measured peak emission at 389 nm with a FWHM of 10 nm showed no measurable degradation in the emission spectra for the InGaN LED membrane compared to the LED on sapphire.

Chapter 8 - Low-temperature Pd-In Metal Bonding and LLO

The intimate integration of thin-film materials with disparate properties is required to enhance the functionality of integrated microsystems. For example, combining laser diodes with low-cost electronics necessitates the integration of III-V semiconductors with silicon. The materials integration can be done simply by direct deposition of the thin film onto the final substrate.[128] In many cases, however, direct deposition involves substantial sacrifices in the microstructural quality, properties and performance of the thin film. In some cases, such as integration of piezoelectric electroceramic thin films with polymer substrates, the processing conditions (*e.g.* temperature and ambient) preclude direct deposition. In these instances, a bonding and lift-off approach may be required.

GaN thin films grown on sapphire substrates exhibit pronounced roughness due in part to the large density of dislocations intersecting the film surface.[129] Hence, direct bonding of the GaN/sapphire structures onto dissimilar substrates presents a formidable challenge. The use of a transient-liquid phase to accommodate surface roughness by spreading laterally to fill voids has been shown to successfully join ceramic materials for high-temperature applications.[130] Of the low melting-point metals, indium is the only metal with a melting point between 100-200°C that permits bonding to a wide range of substrates. It is also known that palladium is adherent to most semiconductors and polymers,[131] thus the Pd-In system is promising for low-temperature bonding in which the compound $PdIn_3$ is the first phase to form at a Pd-In diffusion couple.[132] The resulting $PdIn_3$ phase also has a relatively high melting point of 664°C as shown by the Pd-In phase diagram in Figure 8–1.[133] Consequently, the Pd-In intermetallics are able to

yield a stable high-temperature $PdIn_3$ bond from a low-temperature bonding process. Furthermore, the Pd-In system is an ideal bonding material due to its uniform native-oxide penetration, and limited and uniform semiconductor consumption.[131]

Pulsed UV LLO, in conjunction with wafer bonding, may be used as a direct approach for integration of GaN with other dissimilar substrate materials. The previous chapters have demonstrated the efficacy of bandgap-selective processing to selectively decompose the GaN/sapphire interface into Ga metal and nitrogen gas. By using LLO, GaN thin films were transferred onto epoxy bonded Si receptor substrates without degradation to the GaN thin film quality. In this section, a Pd-In wafer bonding process will be described in conjunction with LLO to fully integrate GaN with dissimilar substrate materials.

8.1 - Pd-In Bonding Process

GaN thin films of thickness 3 μm on double-sided polished sapphire substrates were used as the starting material. A thin bilayer of Ti-Pd (5 nm and 100 nm thickness of Ti and Pd, respectively) was deposited onto the GaN by electron beam (e-beam) evaporation (base pressure ~ 1×10^{-7} Torr). The Ti layer was used to promote adhesion between the GaN thin film and the Pd metal. A 1 μm thick In layer was then deposited by thermal evaporation onto the Pd surface (base pressure ~ 5×10^{-7} Torr). The receptor substrate was separately coated with a 100 nm thick e-beam evaporated Pd film. The Pd and In thickness were chosen such that the ratio of the Pd:In was maintained between 1:3 and 1:1 to ensure complete consumption of the In during the low-temperature bonding process. The GaN/sapphire structures were then bonded at a pressure of ~2.8 MPa onto boron doped p-type Si (001), semi-insulating GaAs (001) or polyimide substrates at

200°C for 30 minutes in a flowing nitrogen ambient. The process flow is shown in Figure 8–2.

During the initial stage of the bonding, as the temperature exceeds the In melting point (T_m = 156°C), molten In flows laterally to fill in any voids and encase submicron particulates and surface asperities. The Pd + 3In $PdIn_3$ reaction begins at room temperature and is completed during the 200°C treatment. The resulting $PdIn_3$ bond is strong enough to withstand the subsequent thermal and mechanical shock from the LLO process.

The wafer-bonding process was performed using a modified heater plate capable of a maximum annealing temperature of 350°C. The plate is equipped with two 300 Watt resistive heaters and a manual screw-down press for pressure bonding. Samples were mounted in the press and a bonding pressure of ~3 MPa was applied to join wafers at 200°C. The temperature of the heater plate was controlled using a solid-state relay switch controlled by a variable-frequency generator. The wafer-bonding tool was able to bond wafers up to four inches in diameter. The entire tool was enclosed in a nitrogen-purged Plexiglas™ case. The nitrogen ambient was used to minimize oxidation of the bonding metals during the 200°C anneal.

8.2 - Pd-In Bonding and Laser Lift-off

The two-step LLO process allowed GaN films up to 10 cm^2 to be successfully transferred by rastering a 0.03 cm^2 beam spot across the entire sample. A thin Ga rich layer on the surface of the exposed interface was easily removed with a 1:1 solution of HCl and de-ionized water. The transferred films were then characterized by XRD, SEM,

and AFM to verify the structural integrity of the GaN film before and after liftoff and transfer.

Formation of $PdIn_3$ from a Pd-In bi-layer structure, deposited onto a 200 nm SiO_2 coated Si substrate, was observed using x-ray diffraction (XRD). The thermally grown oxide layer was used as a barrier to prevent consumption of Pd by the Si substrate to form Pd_2Si. Figure 8–3 shows the $\theta - 2\theta$ normal-coupled XRD pattern for an In (1 μm thick)/Pd (200 nm thick)/SiO_2/Si stack for 0, 5, 30 and 60 minute anneal times at 200°C. The as-deposited Pd-In XRD pattern shows the prominent 111 Pd and 002 In reflections.

After a 200°C, five-minute anneal the 321 and 411 $PdIn_3$ reflections are observed, indicating the development of the $PdIn_3$ compound. The increased 002 In intensity at the 5-minute anneal may be due to texturing of the resolidified residual In in the metal layer. After annealing for 30 minutes, the XRD spectrum shows the near total consumption of elemental Pd and In indicating nearly complete $PdIn_3$ formation. The $PdIn_3$ formation is complete after a 60-minute anneal indicated by the disappearance of the 002 and 110 In reflections along with the 111 Pd peak. In the case of the bonded GaN/sapphire structures, the bonding time was chosen to be 30 minutes as the reaction should be faster given two Pd-In interfaces are reacting to form the $PdIn_3$ compound.

Figure 8–4 shows a cross-sectional SEM micrograph of a successfully transferred GaN film onto a Si substrate. The $PdIn_3$ layer appears to be free of voids, indicating a uniform and complete bond of the GaN on Si. The GaN $\{1\bar{1}00\}$ prismatic planes were aligned to the Si $\{111\}$ inclined planes to allow for the creation of smooth, clean facets on both the GaN and the Si by cleaving the Si substrate. The alignment, bonding, and

LLO technique can thus be used for fabricating parallel cleavage mirror facets for GaN-based laser diodes.

Figure 8–5 shows a $\theta - 2\theta$ normal-coupled XRD spectrum for GaN transferred onto GaAs and Si after liftoff from sapphire using a single pulsed 600 mJ/cm^2 fluence. The 0002 GaN along with the 004 Si and 004 GaAs reflections are evident. In agreement with the XRD data shown in Figure 8–3, the Pd-In metal bi-layer bond was also found to form the compound $PdIn_3$ after a 30 minute 200°C pressure bond.

Analysis of the GaN film transferred onto polyimide substrates by XRC is shown in Figure 8–6. The FWHM of the 0002 GaN reflection showed very little broadening after separation from the sapphire substrate. The measured FWHM increased from 0.18° to 0.20° indicating the film had not suffered significant mechanical damage during the bonding, liftoff and transfer processes. Similar results were obtained for GaN thin films transferred onto GaAs and Si substrates. The surface morphology of the exposed GaN interface, which can be further processed to remove the defective interfacial layer or integrated with another material in a "paste and cut" methodology, showed a relatively smooth surface morphology with a measured 12 nm (rms) surface roughness by AFM.

The Pd-In wafer bonding and LLO process can also be applied to pattern transfer of GaN features from sapphire onto other substrate materials. Figure 8–7 shows an SEM micrograph of several 200 μm GaN mesa features that were fabricated on a sapphire wafer by argon ion milling, and subsequently transferred onto a Si substrate by the LLO process. Such a technique may also be used to transfer an array of GaN-based blue LEDs or lasers for such applications as color displays or optical data communications.

8.3 - Post-processing of LLO GaN

The resulting $PdIn_3$ (T_m=664°C) compound formed by a solid-phase reaction[132] during the Pd-In bonding process creates a stable high-temperature intermetallic bond ideal to withstand a high-temperature post-LLO processes. Additionally, the LLO process offers the advantage of allowing relatively easy access to the interface at the GaN/sapphire junction. This access allows fast sample preparation for GaN interface studies where direct examination of the structural, optical, and chemical properties at the interface is now possible.

In addition, the absence of the sapphire allows the direct modification of the interfacial layer. One can now remove the substrate and the interfacial defects common in the GaN/sapphire system and enhance the quality of the GaN film. Typically, the highest density of defects lies within a few hundred nanometers from the interface.[12,13] These defects can be removed using dry or wet etching, thermal or laser annealing, or chemo-mechanical polishing. After the defect removal process, the films can again be characterized to examine the effectiveness of the etch process.

Following the procedure described above, the bandgap-selective LLO technique, in conjunction with the Pd-In wafer bonding process[134] was utilized to integrate GaN thin films with Si substrates. After lift-off and transfer of the GaN film onto Si, the exposed defective former-interfacial layer was etched away by argon-ion milling using a 1 kV, 1 mA/cm^2 argon ion beam resulting in a 100 nm/minute GaN etch rate.

8.3.1 - Results and Discussion

Low-temperature (4K) PL was measured to characterize the optical quality of the GaN before and after LLO using a 50 mW HeCd laser with a GaN penetration depth of

~150 nm.[99] The PL spectra for the original GaN surface and the exposed GaN/sapphire interface are shown in Figure 8–8. The FWHM of the donor-bound exciton (DX) peak excited from the interfacial layer exposed by LLO was measured to be ~24 meV. PL measurements of the interface prior to lift-off yielded the same peak linewidth when luminescence was excited through the polished sapphire substrate. Thus, the LLO process had no apparent effect on the optical quality of the GaN as assessed by the PL linewidth. In contrast, the DX peak measured from the GaN surface before lift-off was considerably narrower, with a FWHM of ~15 meV. Hence, it was hypothesized that the interfacial-layer linewidth broadening may be solely attributed to the high density of extended defects commonly found at the GaN/sapphire interface[13] and not to damage induced by the LLO process.

To test this hypothesis, the PL measurements were complemented by channeling-Rutherford backscattering spectrometry (c-RBS) analysis using a 1.95 MeV $^{4}He^{+}$ beam in a 165° backscattering geometry. Figure 8–9 shows the c-RBS results for the as-grown 2.5 μm thick GaN film on sapphire. The χ_{min} versus thickness spectrum shows the as-grown GaN to be of high structural quality with a 3% minimum yield at the surface of the film. The figure also shows channeling data plotted for the same GaN sample after 1.5 μm of the GaN was removed by argon-ion milling. Dechanneling, a result of the increased dislocation density near the interface,[135] begins approximately 700 nm below the ion-milled surface and extends down to the film/substrate interface. The measured thickness of the GaN/sapphire defective interfacial region is approximately 350 nm. It should also be noted that the χ_{min} of the ion-milled surface compares very well with that

of the as-grown GaN indicating that the GaN surface suffered no measurable degradation from the argon-ion beam bombardment.

The same ion-milling process was subsequently performed on LLO GaN films bonded onto Si substrates. Figure 8–10 shows the χ_{min} yield as a function of depth for the as-separated and ion-milled GaN on Si. The c-RBS results show a two-fold decrease in the backscattering yield after etching away 50 nm of the interfacial layer, indicating removal of line defects within the GaN. Following a 400 nm etch, the backscattering yield was found to be comparable to the χ_{min} values of the as-grown GaN/sapphire surface. X-ray rocking curve of the as-separated and ion beam processed GaN/Si samples also showed a slight narrowing of the GaN 0002 reflection FWHM from 0.16° to 0.14° after a 400 nm ion mill etch. Atomic force microscopy of the exposed GaN interface showed a decrease in the surface roughness (over a 1×1 μm^2 area) from 24 nm (rms) after LLO to 2.2 nm (rms) after ion milling.

The PL measurements corroborate the c-RBS data. After removal of the defective interfacial layer, the FWHM of the DX peak decreased to ~16 meV, comparable to that of the original GaN film surface as shown in Figure 8–11. A 5.3 meV red-shift in the DX peak indicates relief of a bi-axial compressive stress in the GaN after LLO from the sapphire.[127]

These results demonstrate that i) the LLO process does not degrade the optical or structural quality of the GaN film as assessed by PL and c-RBS, and that ii) removal of the exposed interfacial layer on a LLO GaN film yields a GaN surface of structural and optical quality that is comparable to that of the top surface of an as-grown GaN film on sapphire.

8.4 - Fabrication of Vertical-structure Light-emitting Diodes

As a demonstration of the effectiveness of the metal-bonding and LLO processes, vertical GaN-based blue-LEDs, prefabricated on a sapphire substrate were integrated onto a Si substrate. The InGaN LED structures were fabricated at the Xerox Palo Alto Research Center, in a similar process described in the previous section. The devices were then coated with Ti/Au for the p-contact of the diodes and then metal bonded onto a n^+ Si (001) substrate. LLO was then performed to remove the sapphire substrate and expose the n-type GaN layer. Isolation trenches were then etched into the device layer to isolate discrete LED diodes of ~200 μm × 200 μm. N-metal contacts were subsequently deposited onto the top n-GaN layer completing the vertical structure LED using the n^+ Si as the p-contact.

Figure 8–12 displays an operating vertical-structure blue LED on Si with a single probe contact on the GaN surface. The device performance of the blue LED is almost identical to the devices used for the membrane fabrication with the only exception being the emission wavelength being 470 nm. The turn-on voltages for these devices were ~3.2 volts at 1 mA and ~4.9 volts at a drive current of 25 mA.

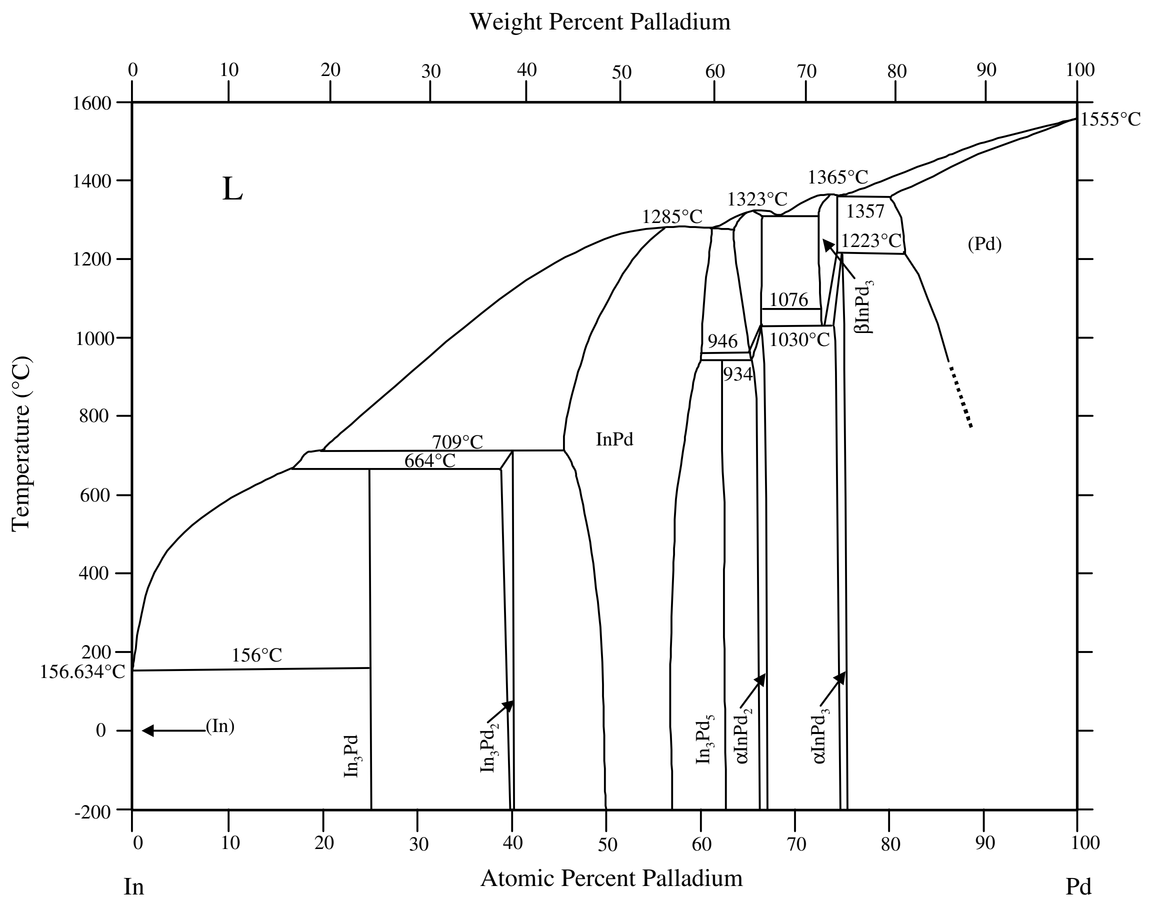

Figure 8–1: Pd-In phase diagram showing the PdIn$_3$ melting point at 664°C.

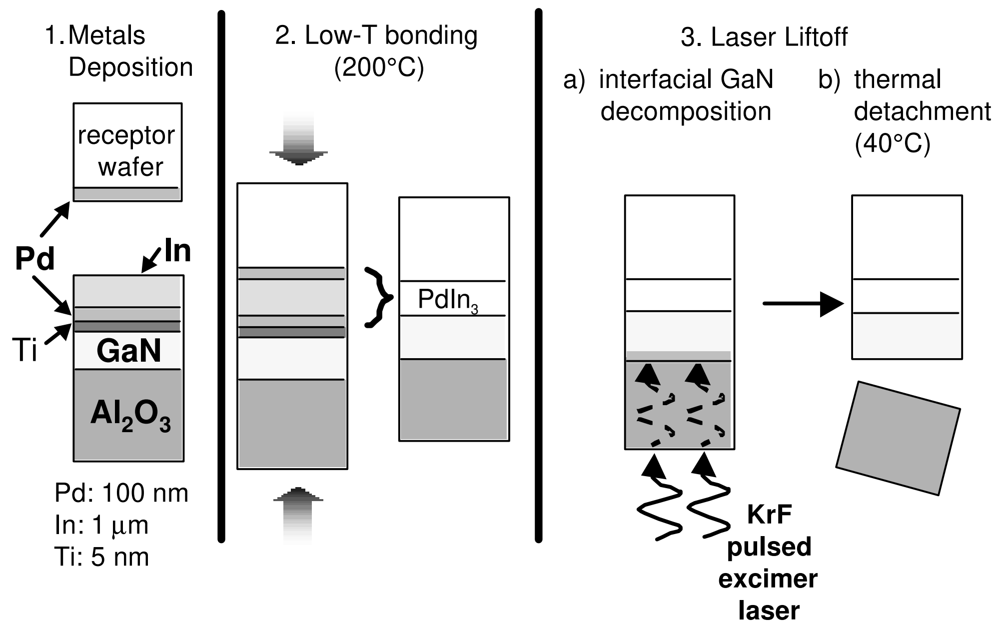

Figure 8–2: Pd-In wafer bonding process and LLO process for transferring GaN thin films.

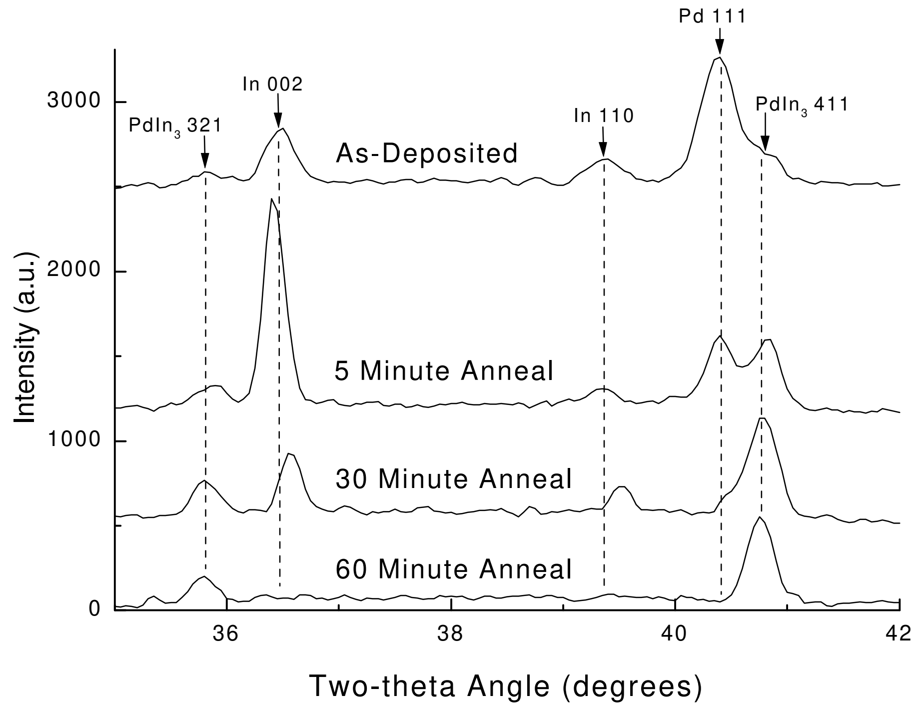

Figure 8–3: X-ray diffraction pattern of Pd-In bi-layers deposited on a SiO_2 coated Si wafer. The as-deposited Pd-In layers show the dominant 002 In and 111 Pd peaks. After a 30-minute anneal at 200°C in a N_2 ambient the 411 and 321 $PdIn_3$ peaks have become dominant. The absence of the 111 Pd peak indicates consumption of the Pd layer to form $PdIn_3$ after 60 minutes.

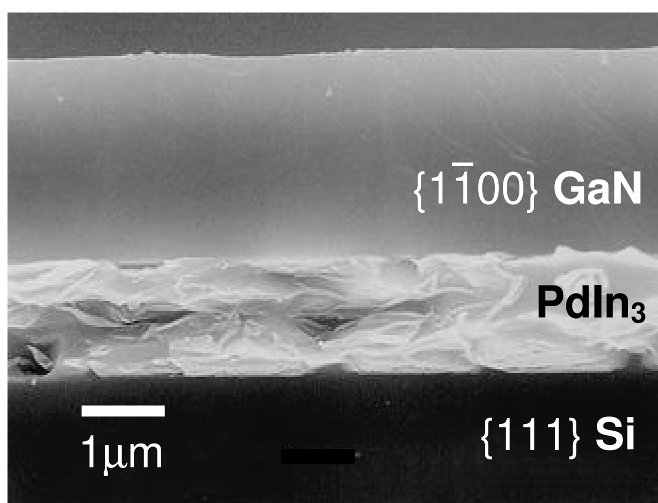

Figure 8–4: Cross sectional SEM micrograph of a transferred GaN film onto a Si substrate. Pd-In metal bilayers were used as bonding material which formed the compound $PdIn_3$ after the low-temperature bonding process. Cleaving the Si substrate was performed to make the cleavage facets on the GaN.

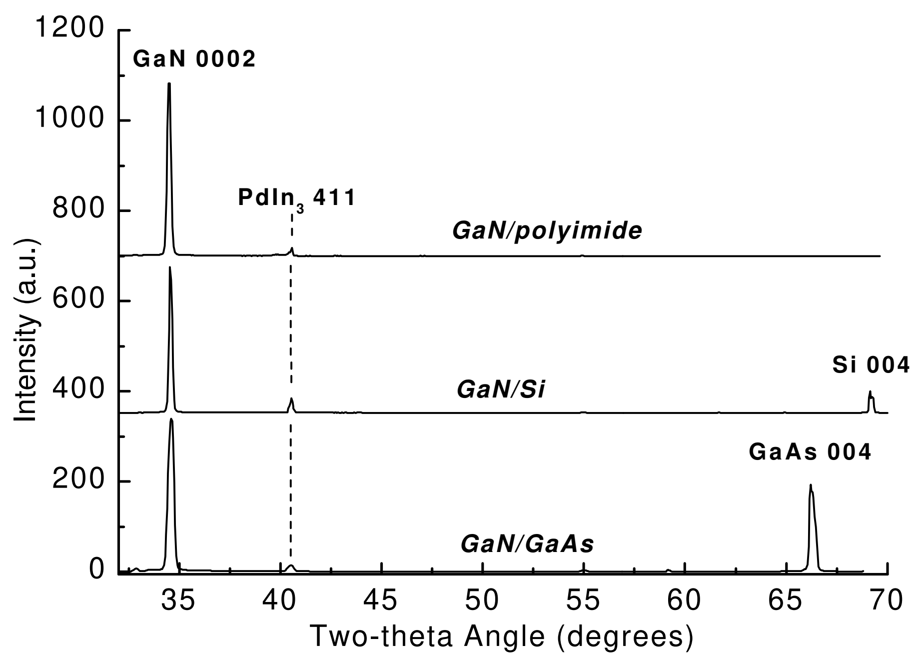

Figure 8–5: Theta-two-theta normal coupled scans of transferred GaN thin films onto GaAs, Si and polyimide substrates. The $PdIn_3$ 411 reflection from the metallic bond is shown along with the 0002 GaN reflection.

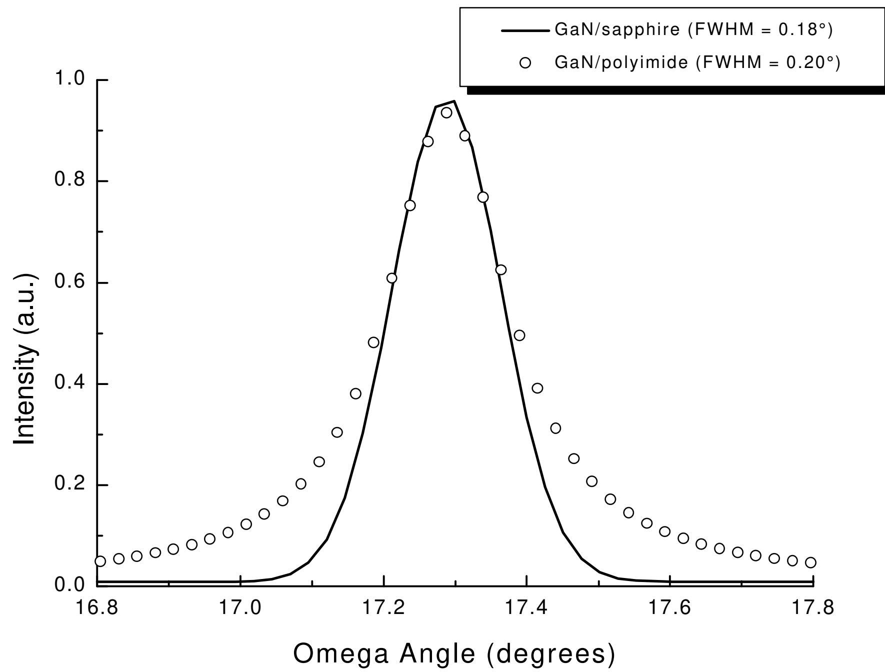

Figure 8–6: X-ray rocking curve of GaN transferred onto polyimide. The full-width at half maximum of the 0002 GaN reflection broadened slightly from 0.18° to 0.20° indicating the structural quality of the transferred film did not degrade significantly after bonding and LLO.

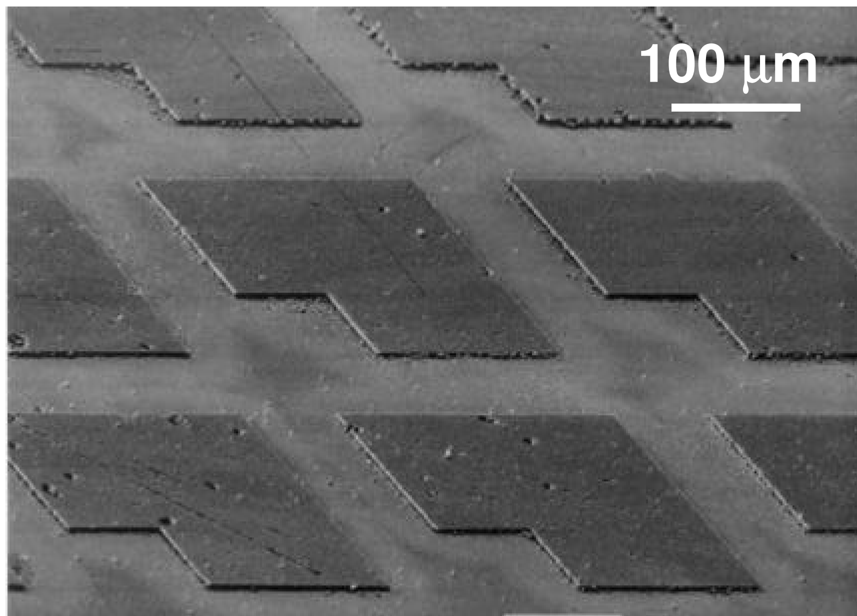

Figure 8–7: SEM micrograph of pattern transferred GaN onto a Si substrate.

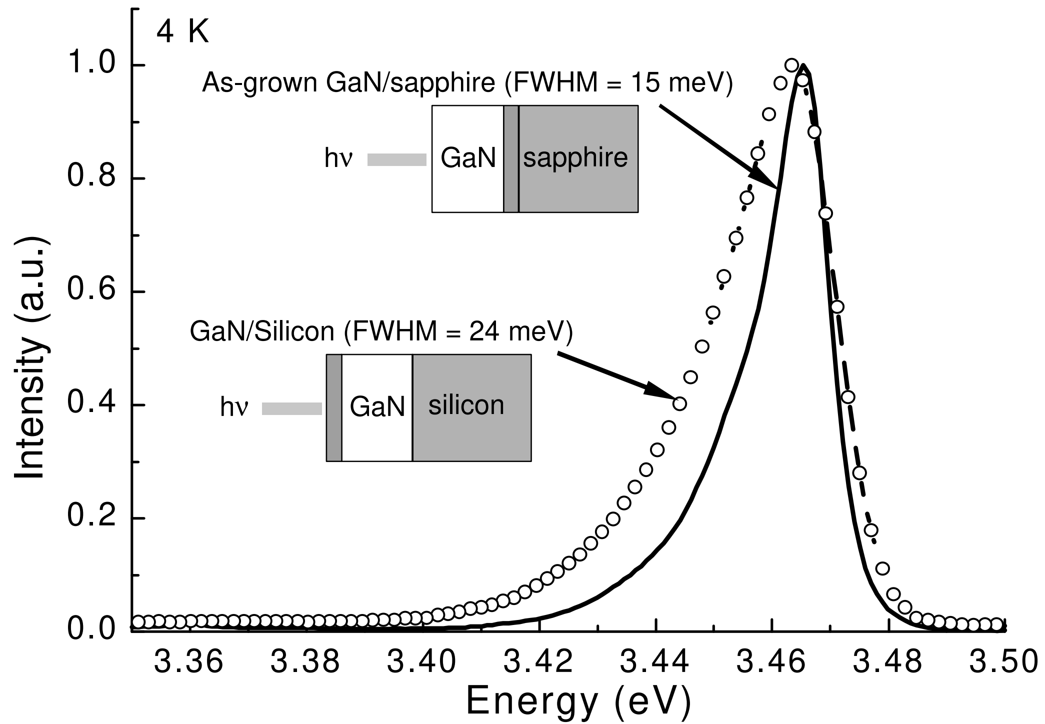

Figure 8–8: Low-temperature (4K) PL of GaN on sapphire and GaN transferred onto Si. The broadening of the GaN/Si DX peak FWHM compared to the as-grown GaN/sapphire is due to the localized defects at the exposed GaN/sapphire interface.

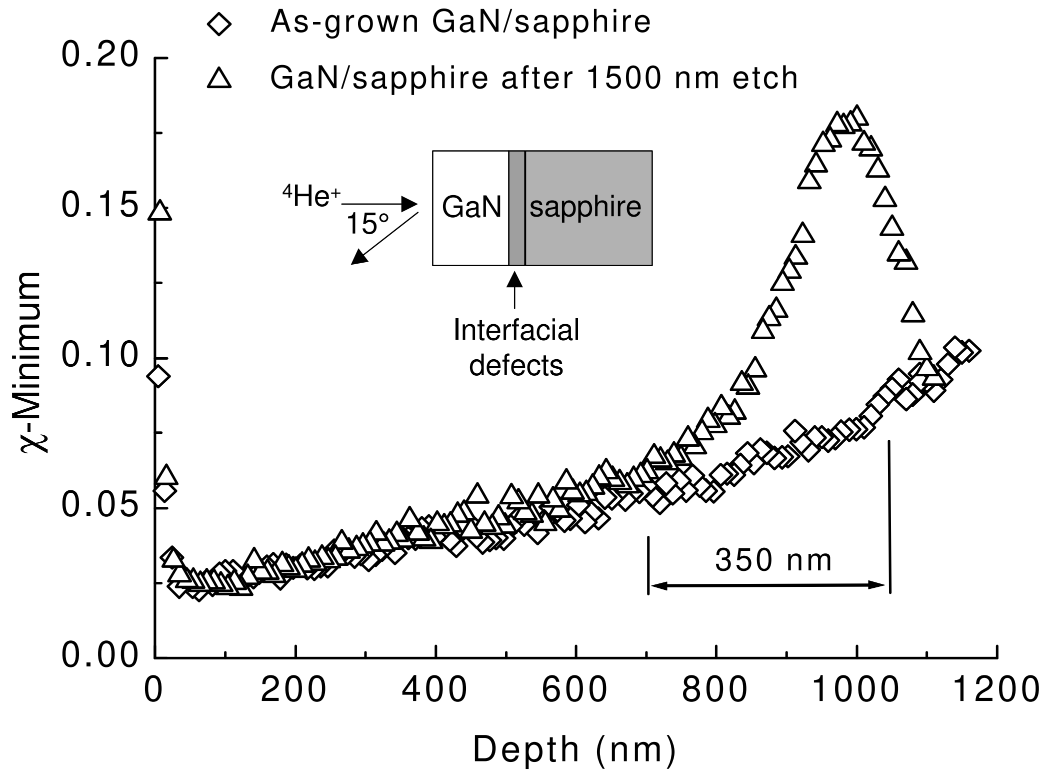

Figure 8–9: C-RBS results for the as-grown GaN on sapphire and after removal of 1.5 μm of GaN by ion milling with a 1 kV Ar ion beam. The spectrum shows the GaN to be of high quality with a minimum yield of approximately 3% at the surface of the film. The defective interfacial region thickness was measured to be approximately 350 nm.

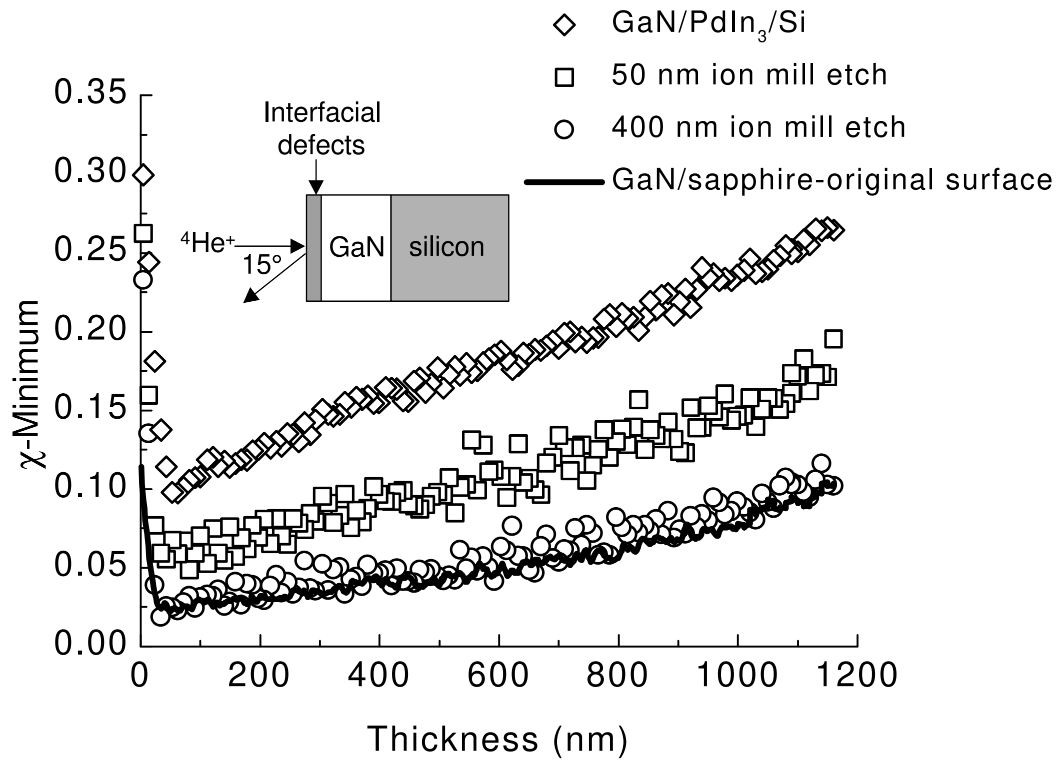

Figure 8–10: Backscattering yield as a function of depth for as-separated GaN on Si and after ion-beam processing. The c-RBS results show that after removal of 400 nm of GaN by ion milling, the backscattering yield returned to the initial χ-minimum values of the original GaN/sapphire surface.

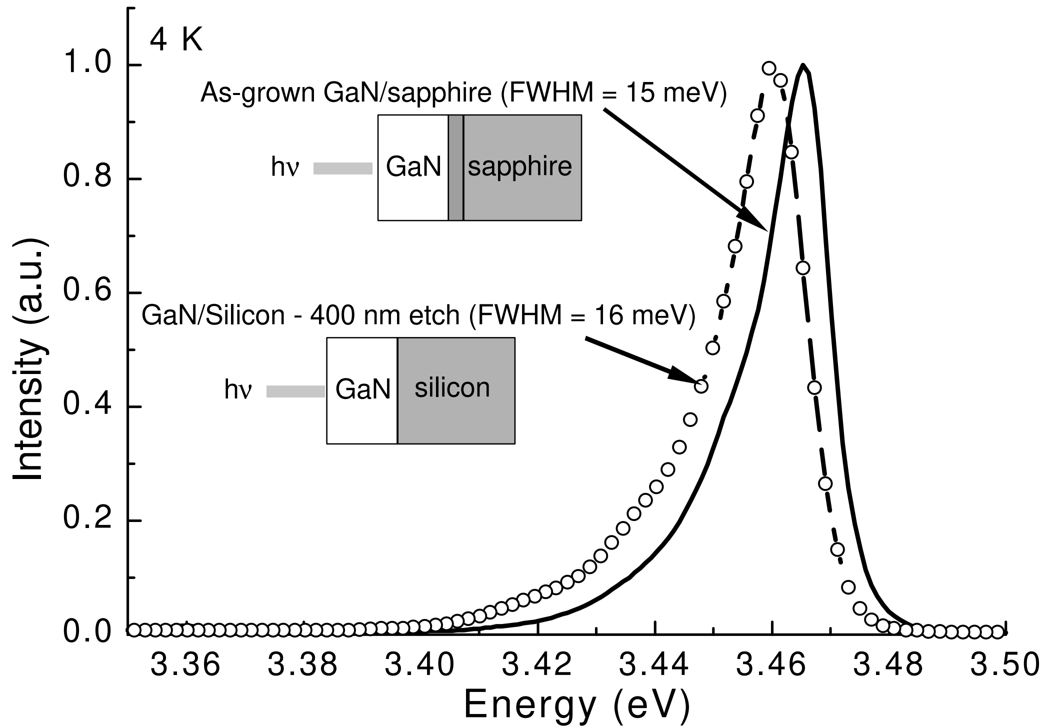

Figure 8–11: Low-temperature PL of the GaN thin film after ion milling. The DX peak FWHM was comparable to that from the original GaN surface after removing 400 nm of the former interface. A slight red-shift is due to release of the compressive stress after removing the sapphire substrate. The relative DX peak intensities have been normalized to better show the change in the FWHM and red shift. The relative peak intensities of the original surface and ion milled interface were within 5% of each other.

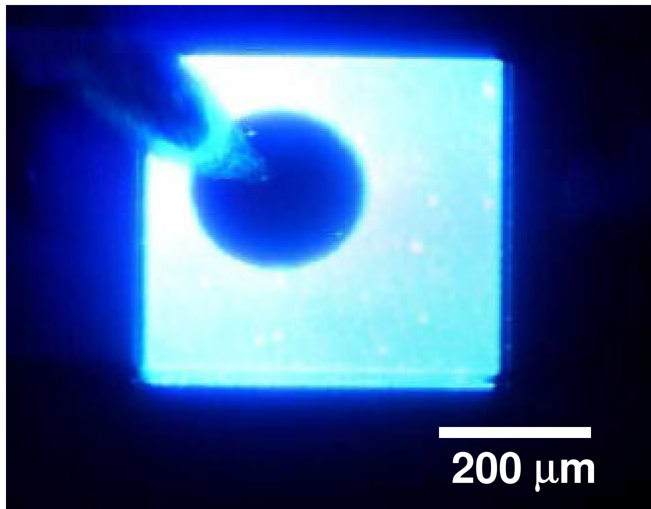

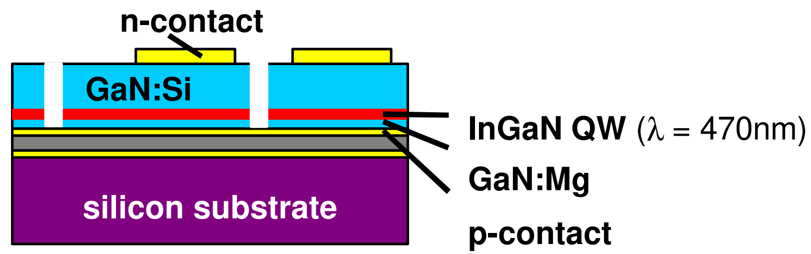

Figure 8–12: Vertical-structure InGaN blue-LED.

Chapter 9 - Conclusion

A review of the integration of GaN-based materials with dissimilar substrates by thin-film layer transfer was presented. A newly developed integration tool, laser lift-off, was shown to effectively separate GaN thin films from sapphire substrates by a thermally decomposing of a thin GaN interfacial layer. The thermal decomposition at the GaN/sapphire interface is accomplished by pulsed-laser irradiation through the transparent sapphire substrate.

Given the high GaN absorption coefficient at the 248 nm KrF laser wavelength, the LLO process induces a highly-localized temperature rise at the thin-film/substrate interface. A simple one-dimensional thermal diffusion model showed this temperature rise, coupled with a steep temperature gradient across the GaN, restricts the decomposition region to within 100 nm below the thin-film/substrate interface for a 600 mJ/cm^2 laser fluence.

Using the information obtained from the theoretical calculations, the LLO process was successfully demonstrated by transferring GaN thin films from sapphire onto epoxy-bonded Si substrates at a ~600 mJ/cm^2 laser fluence. Characterization of the transferred films by XRC, SEM, AFM, and PL showed no degradation to the GaN film quality after LLO. As a further test, free-standing GaN-based light-emitting diode membranes were fabricated by LLO. The GaN-based LED membranes, which were pre-fabricated on sapphire substrates, showed little or no degradation before and after LLO. The measured I-V and eletroluminescence performance of these devices was found to remain unchanged after separation from the sapphire.

To make the integration process complete, the development of a low-temperature transient liquid-phase Pd-In wafer-bonding process was presented to compliment the LLO technique. The Pd-In metal bond was employed to form a thermally and electrically conductive interface between the transferred GaN and the "receptor" substrate. The metal bonding technique, performed at a temperature of 200°C, forms an intermetallic $PdIn_3$ compound from a 1 μm thick Pd-In bilayer. As the bilayer is heated, the In layer melts to fill any voids or asperities at the GaN thin-film/"receptor"-substrate interface while reacting with the Pd to form the intermetallic compound $PdIn_3$ (T_m=664°C). The versatility of Pd-In wafer-bonding and LLO process was demonstrated by successfully joining and transferring GaN onto Si, GaAs, and polymer substrates.

The metal bond and LLO process technique direct processing of the exposed GaN interface. Etching away this exposed interfacial layer by ion beam milling was found to improve the GaN quality. By removing the extended defects, the resulting optical and structural properties of the former interface were comparable to the original GaN surface.

As a final demonstration of the LLO and metal-bonding integration process, a vertical-structure InGaN blue LED was fabricated on Si. The InGaN blue LED, grown and fabricated on a sapphire substrate, was metal bonded onto Si and transferred by LLO. The vertical-structure LED, with a turn on voltage of ~3.2 Volts at 1 mA, dramatically demonstrated the effectiveness of the metal-bonding and LLO process to integrate GaN with other materials substrates.

Further work is still needed to optimize the performance of the transferred optoelectronic devices. The optimization of the metal bond, either by varying the Pd-In ratio or with a different metals system, can be performed to increase the thermal stability

of the bond interface. In addition, shorter pulse-length lasers, such as femto- or pico-second pulses, can be used reduce the required fluence for LLO. These parameters may be adjusted to optimize integration process, thus maximizing and enhancing the performance of transferred GaN-based LEDs, LDs or transistors onto different substrates.

Chapter 10 - Appendix

10.1 - Thermoelastic Stress Wave Propagation

In addition to the thermoelastic stress developed during the laser irradiation, a stress wave is generated during the absorption of the laser light. The thermal expansion following the rapid heating of the GaN sapphire interface will promote a stress wave to propagate into the GaN thin film. The resulting wave may cause the delamination of the bonded interface joining the GaN film to the receptor substrate or film fracture. Various parameters effect the amplitude of the generated stress wave and its reflection at an interface including the pulse duration, velocity of propagation, density of the supporting substrate material, and the acoustic impedance.

The reflection and refraction of an elastic wave as it reaches a slip-free boundary between two media, *a* and *b*, generates four separate waves (Figure 10–1). For these four waves there are four boundary conditions which must be equal: 1) the normal displacement, 2) the tangential displacements, 3) the normal stress and 4) the tangential stress. Assuming the wave has no rotational velocity, consider a dilatation wave travelling parallel to the *x*-*y* plane which creates an angle α_1, with respect to the *x*-axis, and with the reflected and refracted dilatation waves be α_2 and α_3. If a rotational velocity is considered then the wave of distortion makes angles β_2 and β_3 for the reflected and refracted waves, respectively. The boundary condition may be satisfied if the wave front is considered to be an envelope of a series of spherical wavelets and Huygen's principle is applied to get the relationship:[136]

$$\frac{sin\,\alpha_1}{c_1} = \frac{sin\,\alpha_2}{c_1} = \frac{sin\,\beta_1}{c_2} = \frac{sin\,\alpha_3}{c_3} = \frac{sin\,\beta_3}{c_4} \qquad [10.1–1]$$

where c_1 and c_2 are the propagation velocities of the dilatation and distortion waves in the first medium and c_3 and c_4 are the respective velocities in the second medium. In addition, let the amplitude of the incident wave be A_1 while the reflected and refracted dilatation waves are A_2 and A_4, respectively. The corresponding amplitudes for the reflected and refractive distortion waves are then A_3 and A_5, respectively.

The four boundary conditions can then be used to obtain four simultaneous equations. [136] From condition 1):

$$(A_1 - A_2)cos\,\alpha_1 + A_3\,cos\,\beta_2 - A_3\,cos\,\alpha_3 - A_5\,cos\,\beta_3 = 0 \qquad [10.1–2]$$

and from condition 2):

$$(A_1 + A_2)sin\,\alpha_1 + A_3\,cos\,\beta_2 - A_4\,sin\,\alpha_3 - A_5\,cos\,\beta_3 = 0 \qquad [10.1–3]$$

while condition 3 gives:

$$(A_1 + A_2)c_1\,cos\,2\beta_2 + A_3 c_2\,sin\,2\beta_2 - A_4 c_3\left(\frac{\rho_b}{\rho_a}\right)cos\,2\beta_3 - A_5 c_4\left(\frac{\rho_b}{\rho_a}\right)sin\,2\beta_3 = 0 \quad [10.1–4]$$

where ρ_a and ρ_b are the densities of media a and b, respectively. Finally, boundary condition 4) reveals:

$$\begin{aligned}&\rho_a c_2^2\left[(A_1 - A_2)sin\,2\alpha_1 - A_3\frac{c_1}{c_2}cos\,2\beta_2\right] - \\ &\rho_b c_4^2\left[A_4\left(\frac{c_1}{c_3}\right)sin\,2\alpha_3 - A_5\left(\frac{c_1}{c_4}\right)sin\,2\beta_3\right] = 0.\end{aligned} \qquad [10.1–5]$$

Equation 10.1–4-10.1–5 may be solved to retrieve the amplitudes of the reflected and refracted waves as a function of the incident wave amplitude, A_1. For the case where

the wave is normal incidence, $\alpha_1 = 0$, then the amplitudes A_3 and A_5 vanish generating only the dilatation waves. The solutions for the amplitudes of the reflected and refracted waves, respectively, are:[136]

$$A_2 = \frac{A_1(\rho_b c_3 - \rho_a c_1)}{(\rho_b c_3 + \rho_a c_1)} \quad \text{and} \qquad [10.1\text{–}6]$$

$$A_4 = \frac{A_1(2\rho_a c_1)}{(\rho_b c_3 + \rho_a c_1)}. \qquad [10.1\text{–}7]$$

Equation 10.1–6 and 10.1–7 show that the reflected stress wave at the media interface depends on the quantity, $(\rho_b c_3 - \rho_a c_1)$. If the density of the media is equal then no reflected wave will be generated at the interface. The product ρc is sometimes referred to as the *characteristic impedance* of the media. When the characteristic impedance is higher in the second medium, then the amplitudes of the reflection is the same sign as the incident wave but with a change in phase of π due to a reversal in propagation direction. However, when the characteristic impedance of the second medium is less than the first then the amplitude changes sign but the phase remains the same on reflection.

For the GaN system, the characteristic impedance is 4.2×10^7 kg/m^{2}s, assuming the dilatation wave travels at the speed of sound in GaN, which depends on the bulk modulus and the density of the media. If a supporting substrate such as Si is assumed to be at the interface between the then the ratio of the reflected stress wave amplitude of GaN to Si is $A_{GaN}^{refl.} : A_{Si}^{refl.} = 0.48$. The resulting ratio of the refracted wave amplitude is found to be $A_{GaN}^{refr.} : A_{Si}^{refr.} = 1.48$. These results show that the reflected wave at the bond interface is

approximately one half of the incident stress-wave amplitude suggesting good coupling between the GaN and Si interface for an ideal continuous bond at the Si/GaN interface.

The actual interface between the GaN film and the receptor substrate may be an adhesive that will need to have similar properties as Si. Ideally, the bonding material at the interface should be of a higher density in order to minimize the reflected wave effect and improve the coupling between the GaN and receptor substrate. By optimizing the coupling, the reflected wave will be decreased thus minimizing the possibility of degrading the bond interface or the GaN film. Given the ceramic nature of GaN a large reflected tensile stress wave may cause the mechanical fracture of the thin film during laser irradiation.

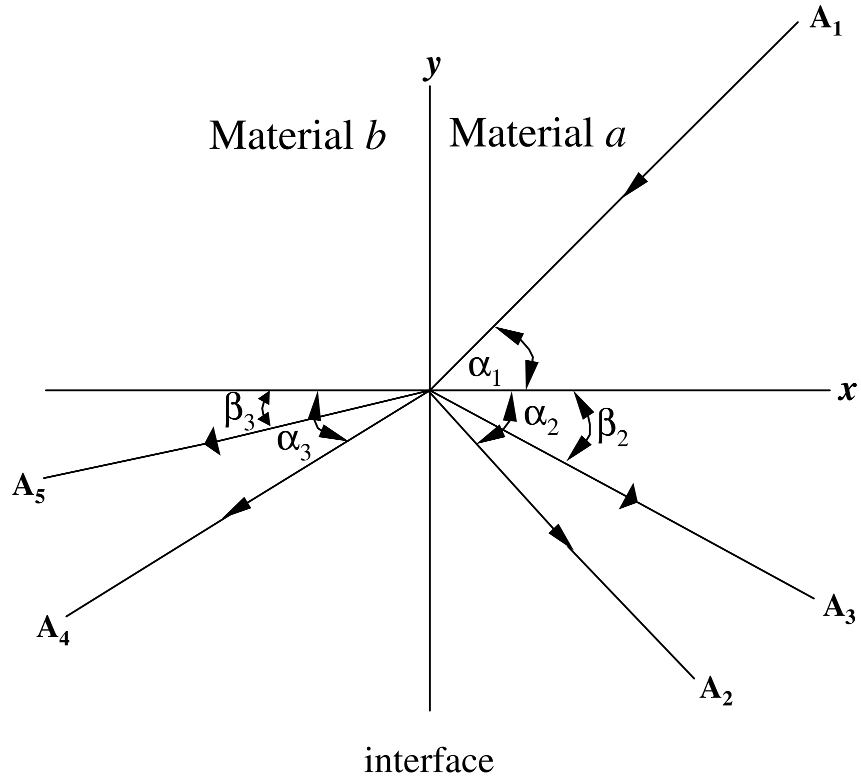

Figure 10–1: Schematic of an incident wave incident onto an interface between materials *a* and *b*.

References

1. Y.-F. Wu, B.P. Keller, D. Kapolnek, P. Kozodoy, S.P. Denbaars, and U.K. Mishra, *Appl. Phys. Lett.* **69**, 1438 (1996).

2. S. Guha, J.M. DePuydt, J. Qiu, G.E. Hofler, M.A. Haase, B.J. Wu, and H. Cheng, *Appl. Phys. Lett.* **63**, 3023 (1993).

3. S. Guha, J.M. Depuydt, M.A. Haase, J. Qiu, and H. Cheng, *Appl. Phys. Lett.* **63**, 3300 (1993).

4. Y. Matsushita, T. Uetani, T. Kunisato, J. Suzuki, Y. Ueda, K. Yagi, T. Yamaguchi, T. Niina, *Jpn. J. Appl. Phys. Part 1* **34**, 1833 (1995).

5. J.D. Brown, J.T. Swindell, M.A.L. Johnson, Yu Zhonghai, J.F. Schetzina, G.E. Bulman, K. Doverspike, S.T. Sheppard, T.W. Weeks, M. Leonard, H.S. Kong, H. Dieringer, C. Carter, J.A. Edmond, *Nitride Semiconductor Symposium, Mat. Res. Soc.,* p. 1179-84 (1998).

6. S. Nakamura, M. Senoh, N. Iwasa, and S.-I.Nagahama, *Appl. Phys. Lett.* **67**, 1868 (1995).

7. S. Nakamura, *J. Cryst. Growth* **170**, 11 (1997).

8. Z.A. Munir, and A.W. Searcy, *J. Chem. Phys.* **42**, 4233 (1965).

9. N. Newman, J. Ross, and M. Rubin, *Appl. Phys. Lett.* **62**, 1242 (1993).

10. S. Nakamura, M. Senoh, and T. Mukai, *Appl. Phys. Lett.* **62**, 2390 (1993).

11. H. Amano, M. Kito, K. Hiramatsu, and I. Akasaki, *Jpn. J. Appl. Phys.* **28**, L21 (1989).

12. S.D. Lester, F.A. Ponce, M.G. Craford, and D.A. Steigerwald, *Appl. Phys. Lett.* **66**, 1249 (1996).

13. I. Akasaki, H. Amano, Y. Koide, K. Hiramatsu, and N Sawaki, *J. Cryst. Growth* **98**, 209 (1989).

14. D.L. Barton, M. Osinski, C.J. Helms, N.H. Berg, B.S. Phillips, *SPIE-Int. Soc. Opt. Eng* **2694**, 64 (1996).

15. A.T. Ping, Q. Chen, J.W. Yang, M.A. Khan, I. Adesida*, IEEE Electron Device Letters* **19**, 54 (1998).

16. W.S. Wong, T. Sands, and N.W. Cheung, *Appl. Phys. Lett.* **72**, 599 (1998).

17. W.S. Wong, J. Krüger, Y. Cho, B.P. Linder, E.R. Weber, N.W. Cheung, and T. Sands, *Proceedings of the Symposium on LED for Optoelectronic Applications and the 28th State of the Art Programs on Compound Semiconductors* **98-2**, 377 (1998).

18. P. Perlin, T. Suski, H. Teissyre, M. Leszczynski, I. Grzegory, J. Jun, S. Porowski, P. Boguslawski, J. Bernholc, J.C. Cherwin, A Polian, and T.D. Moustakas*, Phys. Rev Lett.* **75**, 296 (1995).

19. S. Prowski, M. Bockowski, B. Lucznik, I. Grzegory, M. Wróblewski, H. Teisseyre M. Leszczynski, E. Litwin-Staszewska, T. Suski, P. Trautman, K. Pakula, and J. Barabowski, *Acta Phys. Pol. A* **92**, 958 (1997).

20. O. Knacke, O. Kubaschewski, and K. Hesselmann, editors, *Thermochemical Poperties of Inorganic Substances*, Springer Verlag, Berlin (1991).

21. W.C. Johnson, J.B. Parsons, and M.C. Crew, *J. Phys. Chem.* **36**, 2651 (1932).

22. R.B. Zetterstrom, *J. Mater. Sci.* **5**, 1102 (1970).

23. J. Karpinski, S. Porowski, and J. Jun, *J. Cryst. Growth* **66**, (1984).

24. S. Strite and H. Morkoç, *J. Vac. Sci. Technol B.* **10**, 1237 (1992).

25. M. Mizuta, S. Fujieda, Y. Matsumoto, and T. Kawamura, *Jpn. J. Appl. Phys.* **25**, L945 (1986).

26. S. Guha and N.A. Bojarzuk, Appl. Phys. Lett. **72**, 415 (1998).

27. K.S. Stevens, M. Kinniburgh, and R. Beresford, *Appl. Phys. Lett.* **66**, 3518 (1995).

28. R.C. Powell, N.-E. Lee, Y.-W. Kim, J.E. Greene, *J. Appl. Phys.* **73**, 189 (1993).

29. T. Sasaki and T. Matsuoka, *Appl. Phys. Lett.* **64**, 4531 (1988).

30. T. Detchprohm, H. Amano, K. Hiramatsu, and I. Akasaki, *J. Cryst. Growth* **128**, 384 (1993).

31. H. Amano, N. Sawaki, I. Akasaki, and Y. Toyoda, *Appl. Phys. Lett.* **48**, 353 (1986).

32. S. Nakamura, *Jpn. J. Appl. Phys.* **30**, L1705 (1991).

33. A. Sakai, H. Sunakawa, and A. Usui, *Jpn. J. Appl. Phys. Lett.*, *Part 2* **36**, L899 (1997).

34. Akira Sakai, Harua Sunakawa, and Akira Usui, *Appl. Phys. Lett.* **71**, 2259 (1997).

35. P. Kozodoy, J.P. Ibbetson, H. Marchand, P.T. Fini, S. Keller, J.S. Speck, S.P. Denbaars, and U.K. Mishra, *Appl. Phys. Lett.* **73**, 975 (1998).

36. J.T. Torvik, J.I. Pankove, E. Iliopoulos, H.M. Ng, and T.D. Moustakas*, Appl. Phys. Lett.* **72**, 244 (1998).

37. S. Nakamura, M. Senoh, S. Nagahama, N. Iwasa, T. Yamada, T. Matsushita, H. Kiyoku, Y. Sugimoto, T. Kozaki, H. Umemoto, M. Sano, K Chocho, *Appl. Phys. Lett.* **72**, 2014 (1998).

38. H. Okumura, S. Misawa, and S. Yoshida, *Appl. Phys. Lett.* **59**, 1058 (1991).

39. A. Kikuchi, H. Hoshi, and K. Kishino, *Jpn. J. Appl. Phys.* 33, 688 (1994).

40. T. Lei, M. Fanciulli, R.J. Molnar, T.D. Moustakas, R.J. Graham, and J. Scanlon, *Appl. Phys. Lett.* **58**, 944 (1991).

41. T.D. Moustakas, T. Lei, and R.J. Molnar, *Physica B* **185**, 36 (1993).

42. M.J. Paisley, Z. Sitar, J.B. Posthill, and R.F. Davis, *J. Vac. Sci. Technol. A* **7**, 701 (1989).

43. H. Liu, C. Frenkel, J.G. Kim, and R.M. Park, *J. Appl. Phys.* **74**, 6124 (1993).

44. R.C. Powell, G.A. Tomasch, Y.W. Kim, J.A. Thornton, and J.E. Greene, *Mater. Res. Soc. Symp.* **162**, 525 (1990).

45 . S.A. Nikishin, N.N. Faleev, V.G. Antipov, S. Francoeur, L. Grave de Peralta, G.A. Seryogin, H. Temkin, T.I. Prokofyeva, M. Holtz, and S.N.G. Chu, *Appl. Phys. Lett.* **75**, 2073 (1999).

46. Chuong A. Tran, A. Osinski, R.F. Karlicek, Jr., I Berishev, *Appl. Phys. Lett.* **75**, 1494 (1999).

47. S. Sriram, G. Augustine, A. Burk, R. Glass, H. Hobogood, P. Orphanos, L. Rowland, T. Smith, C. Brandt, M. Driver, and R. Hopkins, *IEEE Electron. Device Lett.* **17**, 369 (19996).

48. P. Bogulslawski, E.L. Briggs, and J. Bernholc, Phys. Rev. B **51**, 17255 (1995).

49. H. Amano M. Kito, K. Hiramatsu, and I Akasaki, Jpn. J. Appl. Phys. **28**, L2112 (1989).

50. H. Amano, M. Kito, K. Hriamatsu, and I Akasaki, Inst. Phys. Conf. Ser. **106**, 725 (1989).

51. S. Nakamura, M Senoh, T. Mukai, Jpn. J. Appl. Phys. **30**, L1708 (1991).

52. S. Nakamura, N. Iwasa, M. Senoh, and T. Mukai, Jpn. J. Appl. Phys., Part 2 **31**, L139 (1992).

53. S. Nakamura, N. Iwasa, M. Senoh, and T. Mukai, Jpn. J. Appl. Phys., Part 2 **31**, L1258 (1992).

54. J.I. Pankove and J.A. Hutchby, J. Appl. Phys. **24**,281 (1974).

55. J.I. Pankove and J.A. Hutchby, J. Appl. Phys. **47**,5387 (1974).

56. J.S. Chan, N.W. Cheung, L. Schloss, E. Jones, W.S. Wong, N. Newman, X. Liu, E.R. Weber, A. Gassman, and M.D. Rubin, Appl. Phys. Lett. **68**, 2702 (1996).

57. W.A. Harrison, *Electronic Structure and Properties of Solids*, Freeman, San Francisco (1980).

58. R. Groh, G. Gerey, L. Bartha, and J.I. Pankove, *Phys. Stat. Sol. A* **26**, 353 (1974).

59. C.J. Sun, P. Kung, A. Saxler, H. Ohsato, E. Bigan, and M. Razeghi, *J. Appl. Phys.* **76**, 236 (1994).

60. M.E. Lin, B.N. Sverdlov, and H Morkoç, *Appl. Phys. Lett.* **63**, 3625 (1993).

61. K. Balasurbramanian, *Chem. Phys. Lett.* **164**, 231 (1989).

62. J.A. Van Vechtan, *Phys. Rev. B* **7**, 9 (1973).

63. W. Class, Contract Rep., NASA-Cr-1171 (1968).

64. J. Karpisnki, J. Jun, and S. Porowski, *J. Cryst. Growth* **66**, 1 (1984).

65. J. Karpisnki and S. Porowski, *J. Cryst. Growth* **66**, 11 (1984).

66. I. Grzegory, S. Krukowski, J. Jun, M. Bockowski, M. Wroblewski, and S. Porowski, *Proc. Of XX AIRAPT Conf.*, Colorado Springs (1993).

67. Landolt-Bornstein, *Numerical Data and Functional Relationships in Science and Technology* **III/17a** and **17d**, Springer-Verlag, Berlin (1982).

68. R.P. Gale, J.C.C. Fan, B-Y. Tsaur, G.W. Turner, and F.M. Davis, *IEEE Electron Dev. Lett.* **EDL-2**, 169 (1981).
69. Y. Shinoda, T. Nishioka, and Y. Ohmachi, *Jpn. J. Appl. Phys.* **22**, L450 (1983).
70. T.H. Windhorm, G.M. Metze, B.-Y. Tsaur, and J.C.C. Fan, *Appl. Phys. Lett.* **45**, 309 (1984).
71. H.K. Choi, B-Y. Tsaur, G.M. Metze, G.W. Turner, and J.C.C. Fan, *IEEE Electron Dev. Lett.* **EDL**, 207 (1984).
72. B.Y. Tsaur, M.W. Geis, J.C.C. Fan, and R.P. Gale, *Appl. Phys. Lett.* **38**, 779 (1981).
73. Yukinobu Shinoda, Takashi Nishioka, and Yoshiro Ohmachi, *Jpn. J. Appl. Phys.* **22**, L450 (1983).
74. Robert M. Fletcher, D. Ken Wagner, and Joseph M. Ballantyne, *Appl. Phys. Lett.* **44**, 967 (1984).
75. G.M. Metze, H.K. Choi, and B-Y. Tsaur, *Appl. Phys. Lett.* **45**, 1107 (1984).
76. E. Yablonovitch, T. Gmitter, J.P. Harbison, and R. Bhat, *Appl. Phys. Lett.* **51**, 2222 (1987).
77. E. Yablonovitch, K. Kash, T.J. Gmitter, L.T. Florez, J.P. Harbison, and E. Colas, *Electron. Lett.* **25**, 171 (1989).
78. J. Fastenau, E. Özbay, G. Tuttle, and F. Laabs, *J. Electron. Mater.* **24**, 757 (1995).
79. K. Hikosaka, T. Mimura, and K. Joshin, *Jpn. J. Appl. Phys.* **20**, L847 (1981).
80. J.C. Fan, C.M. Tsai, K.Y. Chen, S.Y. Wang, G. Lin, and C.P. Lee, *J. Electron. Mater.* **27**, 110 (1998).
81. L. Sugiura, *J. Appl. Phys.* **81**, 1633 (1997).

82. J. Haisma, G.A.C.M Spierings, U.K.B. Biermann, and J.A. Pals, *Jpn. J. Appl. Phys.* **28**, 1426 (1989).

83 . M.K. Kelly, O. Ambacher, R. Dimitrov, R. Handschuh, and M. Stutzmann, *Phys. Stat. Sol. (A)* **159**, R3 (1997).

84. M.K. Kelly, O. Ambacher, R. Dimitrov, H. Angerer, R. Handschuh, and M. Stutzmann, *Mat. Res. Soc. Symp. Proc.* **482**, 973 (1998).

85. P.R. Tavernier, M.C. Hansen, S.P. DenBaars, and D.R. Clarke, presented at the *41st Electronic Materials Conference*, Santa Barbara, CA, June 30-July 2, 1999.

86. Y.-K. Song, M. Diagne, H. Zhou, A.V. Nurmikko, C. Carter-Coman, R.S. Kern, F.A. Kish, and M.R. Krames, *Appl. Phys. Lett.* **74**, 3720 (1999).

87. Y.-K. Song, H. Zhou, M. Diagne, I. Ozden, A. Vertikov, A.V. Nurmikko, C. Carter-Coman, R.S. Kern, F. A. Kish, and M.R. Krames, *Appl. Phys. Lett.* **74**, 3441 (1999).

88. *Compund Semiconductor article*

89. L. Tsakalakos and T. Sands, *Appl. Phys. Lett.* **76**, 227 (2000).

90. L. Tsakalakos and T. Sands, "Excimer Laser Liftoff of Epitaxial Pb(Zr,Ti)O3 Thin Films and Heterostructures, to be published in *Mat. Res. Soc. Sym.* for Fall 1999, Symposium Y, Ferroelectric Thin Films VIII.

91. P.R. Tavernier, P.M. Verghese, and D.R. Clarke, *Appl. Phys. Lett.* **74**, 2678 (1999).

92. I.H. Malitson, *JOSA* **52**, 1377 (1962).

93. Martin Von Allmen and Andreas Blastter, *Laser-Beam Interactions with Materials, Physical Principles and Applications (Second Edition)*, pp 44-48, Springer-Verlag, Berlin (1995).

94. F.P. Incropera, and D.P. De Witt, *Fundementals of Heat and Mass Transfer, 2nd Edition* (John Wiley&Sons, New York, 1985), pp. 43-47.

95. J.M. Poate, James W. Mayer, editors, *Laser Annealing of Semiconductors*, Academic Press, New York, p. 54 (1982).

96. J. Dziewior, and W. Schmid, *Appl. Phys. Lett.* **31**, (1977).

97. H.S. Carlslaw and J.C. Jaeger, *Conduction of Heat in Solids, Second Edition*, Oxford University Press, Oxford (1959).

98. P. Baeri, G. Foti, J.M. Poate, and A.G. Cullis, *Phys. Rev. Lett.* **45**, 2036 (1980).

99. K. Osamua, K. Nakajima, Y. Murakami, *Solid State Commun.* **11**, 617 (1972).

100. G.A. Slack, *J. Phys. Chem. Solids* 38, 330 (1977).

101. S. Bloom, G. Harbeke, E. Meier, I.B. Ortenburger, *Phys. Status Solidi B* **66**, 161 (1974).

102. M.P. Divakar, *Introduction to the COSMOS/M finitel element analysis system*, Structural Reearch and Analysis Corporation, Santa Monica (1994).

103. V.I. Koshenko, A.F. Demidenko, L.D. Sabanova, V.E. Yachmenev, Y.M. Gran, and A.F. Radchenko, *Inorg. Mater.* **15**, 1329 (1979).

104. A. Sheleg, and V.A. Savastenko, Vesti. Akad. Navuk BSSR *Ser. Fiz Mat. Novuk* **1976**, 126 (1976).

105. V.N. Abramov, M.G. Karin, A.I. Kuznetsov, K.K. Sidorin, *Soviet Physics – Solid State* **21**, 47 (1979).

106. D.A. Gryvnak, and D.E. Burch, *J. Opt. Soc. Am.* **55**, 625 (1965).

107. D.H. Auston, J.A. Golovshenko, A.L. Simons, R.E. Slusher, R.P. Smith, C.M. Murko, and T.N.C. Venkatesan, *Appl. Phys. Lett.* **34**, (1979).

108. G.E. Dieter, *Mechanical Metallurgy*, pp. 48-49, McGraw-Hill Book Co., New York (1986).

109. B. Boley and J.H. Weiner, *Theory of Thermal Stresses*, pp. 244-245, John Wiley and Sons Inc., New York (1960).

110. B. Boley and J.H. Weiner, *Theory of Thermal Stresses*, pp. 246-247, John Wiley and Sons Inc., New York (1960).

111. B. Boley and J.H. Weiner, *Theory of Thermal Stresses*, pp. 248-254, John Wiley and Sons Inc., New York (1960).

112. B. Boley and J.H. Weiner, *Theory of Thermal Stresses*, pp. 84-89, 255-258, John Wiley and Sons Inc., New York (1960).

113. Boley and J.H. Weiner, *Theory of Thermal Stresses*, pp. 277-279, John Wiley and Sons Inc., New York (1960).

114. Boley and J.H. Weiner, *Theory of Thermal Stresses*, p. 285, John Wiley and Sons Inc., New York (1960).

115. R. Nowak, M. Pessa, M. Suganuma, M. Leszczynski, I. Grzegory, S. Porowski, and F. Yoshida, Appl. Phys. Lett. **75**, 2070 (1999).

116. C. Kisielowski, J. Krüger, S. Ruvimov, T. Suski, J.W. Ager III, E. Jones, Z. Liliental-Weber, M. Rubin, E.R. Weber, M.D. Bremser, and R.F. Davis, Phys. Rev. BII 54,17745 (1996).

117. E.P. EerNisse and S.T. Picraux, J. Appl. Phys. **48**, 9 (1977).

118. G.E. Dieter, *Mechanical Metallurgy*, p. 352, McGraw-Hill Book Co., New York (1986).

119. M.D. Dory, J.W. Ager III, T. Suski, I. Grzegory, and S. Porowski, Appl. Phys. Lett. **69**, 4044 (1996).

120. C.H. Yun and N.W. Cheung, submitted to IEEE J. Microelectromech. Syst. (1999).

121. A.G Evans and J.W. Hutchinson, Int. J. Solids Structures **20**, 455 (1984).

122. S. Timoshenko and S. Woinowsky-Krieger, *Theory of Plates and Shells*, p. 56, 2nd edition, New York, McGraw-Hill (1959).

123. P. Perlin, L. Mattos, N.A. Shapiro, J. Kruger, W. Wong, T. Sands, N.W. Cheung and E.R. Weber, J. Appl. Phys. **85**, 2385 (1999).

124. J. Kruger, N. Shapiro, Sudhir G. S., Y. Kim, H. Siegle, P. Perlin, E. R.Weber, W. S. Wong, T. Sands, N. W. Cheung, and R. J. Molnar, Mat. Res. Soc. Symp. **572**, 289 (1999).

125. M. Kneissl, D. Hofstetter, D. P. Bour, R. Donaldson, J. Walker, and N. M. Johnson, *J. Cryst. Growth* **189/190**, 846-849 (1998).

126. M. Kneissl, D.P. Bour, B.S. Krusor, L.T. Romano, N.M. Johnson, M. McCluskey, W. Goetz, R.D. Bringans, *SPIE Proceedings* **3279**, 69-76 (1998).

127. C. Kisielowski, J. Krüger, S. Ruvimov, T. Suski, J.W. Ager III, E. Jones, Z. Liliental-Weber, M. Rubin, E.R. Weber, M.D. Bremser, and R.F. Davis*, Phys. Rev. BII* **54**,17745 (1996).

128. S. Guha and N.A. Bojarzuk, Appl. Phys. Lett. **73**, 1487 (1998).

129. B. Heying, E.J. Tarsa, C.R. Elsass, P. Fini, S.P. Denbaars, and J.S. Speck*, J. Appl. Phys.* **85**, 6470 (1999).

130. B. J. Dalgleish, K. Nakashima, M. R. Locatelli, A. P. Tomsia, and A. M. Glaeser, *Ceramics International* **23**, 313 (1997).

131. T. Sands, E.D. Marshall, and L.C. Wang, *J. Mater. Res.* **3**, 914 (1988).

132. L.H. Allen, L.S. Hung, K.L. Kavanagh, J.R. Phillips, A.J. Yu, and J.W. Mayer, *Appl. Phys. Lett.* **51**, 326 (1987).

133. R.P. Elliot, *Constitution of Binary Alloys, First Supplement*, pp.548-549, McGraw-Hill, New York (1965).

134. W.S. Wong, A.B. Wengrow, Y. Cho, N.J. Quitoriano, N.W. Cheung, and T. Sands, *J. of Electron. Mater.* **28**, 1409 (1999).

135. Y. Quére, *J. Nucl. Mater.* **53**, 262 (1974).

136. H. Kolsky, *Stress Waves in Solids*, pp. 31-34, Dover Publications, New York (1952).